3

KAPL-4120
(Nonstandard)

MASTER

KNOLLS
ATOMIC POWER
LABORATORY

Computational Fluid Mechanics Qulification Calculations for the Code TEACH

M.C. DeGrazia
L.B. Fitzsimmons
J.T. Reynolds

November 1979

Operated for the United States
Department of Energy
GENERAL ELECTRIC

KAPL-4120

UC-38, Fluid Mechanics
(TID-4500-R66)
(Nonstandard)

COMPUTATIONAL FLUID MECHANICS QUALIFICATION CALCULATIONS FOR THE CODE TEACH

M. C. DeGrazia, L. B. Fitzsimmons,
and J. T. Reynolds

November 1979

General Electric Company
KNOLLS ATOMIC POWER LABORATORY
Schenectady, New York
Operated for the
United States Department of Energy
Contract DE-AC12-76SN00052

NOTICE

This report was prepared as an account of work sponsored by the United States Government. Neither the United States nor the United States Department of Energy, nor any of their employees, nor any of their contractors, subcontractors, or their employees, makes any warranty, express or implied, or assumes any legal liability or responsibility for the accuracy, completeness, or usefulness of any information, apparatus, product, or process disclosed, or represents that its use would not infringe privately owned rights.

CONTENTS

Blank Page

ILLUSTRATIONS

ABSTRACT

KAPL is developing a predictive method for three-dimensional (3-D) turbulent fluid flow configurations typically encountered in the thermal-hydraulic design of a nuclear reactor. A series of experiments has been selected for analysis to investigate the adequacy of the two-equation turbulence model developed at Imperial College, London, England[1,2,3] for predicting the flow patterns in simple geometries. This report describes the analysis of these experiments with the two-dimensional (2-D) turbulent fluid flow code TEACH.[4] This work qualifies TEACH for a variety of geometries and flow conditions.

ACKNOWLEDGMENT

The authors want to acknowledge the support and helpful advice of M. Lubert during all phases of this work.

COMPUTATIONAL FLUID MECHANICS
QUALIFICATION CALCULATIONS FOR THE CODE TEACH

M. C. DeGrazia, L. B. Fitzsimmons,
and J. T. Reynolds

PROBLEM 1 - DEVELOPING LAMINAR FLOW IN A STRAIGHT PIPE

The first calculation involves developing laminar flow in a straight pipe.* In Figure 1, the velocity distribution in the inlet portion of a pipe is compared with experimental results.[5] The TEACH calculations were performed for air flow through a pipe of radius 0.00225 m for a Reynolds number (RE) of 520. R is the pipe radius, y is the radial distance measured from the centerline, X is the axial distance downstream from the inlet, and $\bar{u}$ is the average velocity. Good agreement is shown. In the entrance region of the pipe (where there is a slight discrepancy between TEACH results and the experiment), TEACH has agreed better with data from other experiments.[6] Part of the discrepancy, however, should probably be attributed to the use of a mesh lacking sufficient resolution in this range. The modeling of this problem involved a 40 x 40 nodal grid.

To test the dependence of the flow development on the RE, the laminar flow in the entrance region was next examined with the use of a spatial mesh fine enough to observe the details of the flow. Our original calculations, using a fairly coarse mesh, demonstrated velocity profiles impervious to the RE, thus indicating the need for a fine mesh for computing entrance-flow structure. A shoulder (peak near the wall) in the velocity profile was observed for REs below 2000 whenever the mesh was sufficiently dense at the inlet of the pipe to extract the detail required to observe this anomaly.

Figures 2 and 3 illustrate the velocity profiles for REs of 40 and 2000. In Figure 2, $\bar{u}$ equals 0.002 m/sec and the radius is 0.01 m. It can be seen that the maximum velocity is displaced from the centerline until a downstream distance of $2X/R/RE = 0.068$ is achieved ($X = 0.0136$ m). This is in good agreement with the results of an alternative method of calculation by Friedman, Gillis, and Liron,[7] based on solutions of the stream function and vorticity function. Table 1 illustrates the maxima in the velocity profile for various positions, X, downstream from the inlet, comparing the TEACH results with Friedman, et al. The variable $u(X,0)$ is

*The geometry description for this and subsequent experiments, together with the pertinent flow parameters, is given in Appendix A.

the centerline velocity and r_{max} is the radius of the maximum velocity. Good agreement is realized at all locations.

TABLE 1. LOCATION OF u_{max}

	$u(x,0)/\bar{u}$		$u_{max}(X)/\bar{u}$		$r_{max}(X)/R$	
X(m)	Friedman, et al	TEACH	Friedman, et al	TEACH	Friedman, et al	TEACH
0.0025	0.048	1.058	1.219	1.191	0.753	0.724
0.0050	1.174	1.241	1.314	1.339	0.596	0.513
0.0075	1.326	1.399	1.405	1.439	0.469	0.410
0.0100	1.466	1.527	1.495	1.534	0.346	0.276
0.0125	1.580	1.578	1.583	1.579	0.194	0.145

In Figure 3, the average velocity, $\bar{u}$, is 0.10 m/sec, resulting in an RE of 2000. Although the kink in the velocity profile away from the centerline is confined to a narrow axial region, it is nonetheless obvious and extends until a distance $2X/R/RE = 0.0219$ ($X = 0.219$) is reached.

These calculations serve to demonstrate the detail that is sometimes required in designing a suitable mesh for a flow calculation and the type of flow fine structure that can be overlooked when sufficient resolution is not realized. Figures 2 and 3 also illustrate the flow details that can be computed reliably with the TEACH code.

PROBLEM 2 - FULLY DEVELOPED TURBULENT FLOW IN PIPES

Fully developed turbulent flow in pipes was studied for the range of REs between 50,000 and 500,000. The first data set involved an experiment measured by Lawn[8] of air flow in a pipe at an RE of 92,000. The pipe had a diameter of 0.1443 m and a length of 8.658 m. All measurements were made at a distance of 8.51 m from the entrance to the pipe. The velocity profiles in Figure 4 illustrate the comparison between the theoretical logarithmic profile [$u/u_\tau = 2.5\ln(Y^+) + 5.45$], the TEACH calculations, and the experimental data points. U^+ is the local velocity divided by the friction velocity, u_τ and Y^+ is a distance measurement. ($Y^+ = yu_\tau/\nu$, where y is the distance from the wall.) Excellent agreement with the experiment is realized. Apparent from Figure 4 is the region in the central flow where there exists deviation from the logarithmic velocity

profile, and accurate modeling with the TEACH formulation. Figure 5 is a plot of the turbulent kinetic energy, k, normalized by the friction velocity, u_τ; R is the radius of the pipe, and y is the radial distance measured from the centerline. Figure 6 shows the turbulent energy dissipation, ε, as a function of distance from the wall. In both Figures 5 and 6, good agreement can be seen. Lawn has measured a wall shear stress, τ, of 0.2948. (The units of shear are SI units, and throughout this report we will be consistent in our use of SI units.) Using the TEACH value of the near wall kinetic energy, k, in the fully developed region, we calculate $\tau = 0.2964$, in good agreement. ($\tau = \rho\sqrt{c_\mu}k$, with $c_\mu = 0.09$, is a TEACH model assumption that relates k and τ near the wall.) Correspondingly, our $u_\tau = 0.477$ ($u_\tau = \sqrt{\tau/\rho}$) is in accord with the measured $u_\tau = 0.476$.

As a consequence of the long channel length, a mesh sized 75 x 60 was used. This allowed for sufficiently small spacing in the inlet region of the channel so that an accurate representation of the developing flow could be actualized.

Comparisons of developing flow in the inlet section of a smooth pipe were made for the Barbin and Jones experiment.[9] The experiment entailed water flow in a pipe of diameter 0.2032 m and length 8.84 m, with an RE of 388,600. The results indicated that fully developed flow was not realized within 40 diam of pipe length, although almost fully developed flow characteristics were evident. Figures 7 through 10 show the velocity profiles at various downstream positions. R is the pipe radius, y is the distance from the pipe center, x denotes the axial measurement, D is the pipe diameter, and U_c is the average velocity. Excellent agreement is demonstrated at all locations. In Figure 11, the wall shear stress profile is compared with experimental results. The wall shear at a given location is τ_w, and the fully developed wall shear is τ_{wd}. (τ_{wd} was calculated at a position 3.048 m downstream. At this location, the turbulent kinetic energy at the first node adjacent to the wall had become fully developed with a constant value of 0.012. Hence, the shear $\tau_{wd} = \sqrt{c_\mu}\rho k = 3.87$ was defined and used in this plot.)

Since the wall shear is proportional to the velocity gradient at the wall, it is anticipated that the shear will be large in regions characterized by a small boundary layer and will decrease as the boundary increases. Comparisons of Figures 7 through 10 and Figure 11 corroborate this.

A 44 x44 nodal matrix was used for the mesh describing this problem. It proved adequate for the comparisons required. As a first attempt, a 16 x 16 sized mesh was used. Discrepancies as large as 15% (particularly in the central flow region) resulted from use of such large cells in the calculations.

The third straight pipe calculation utilized data from an experiment by Laufer.[10] Fully developed flow was obtained in a wind tunnel 0.2469 m in diam and 12.3 m long. The air velocity was varied from 3.048 m/sec to 30.48 m/sec with corresponding REs of 50,000 and 500,000. ($RE = \bar{u}d/\nu$, where d is the pipe diameter and $\bar{u}$ is the average velocity.) The results are seen in Figures 12 through 16 (RE of 50,000) and Figures 17 through 21 (RE of 500,000). The velocity profile is plotted in Figures 12 and 13, Figure 13 portraying the near-wall region. The data correspond to a downstream position of 10.577 m (42.8 diam) where fully developed flow was realized. Good agreement is shown. Figure 13 serves to demonstrate the sensitivity to the model assumptions in the near-wall region. Our first data point (open circle notation) is positioned near the laminar sublayer ($Y^+ \cong 10$) where the high turbulence approximations on which the TEACH model is based are not accurate because of the laminar flow at the wall. Caution must be exercised in devising a mesh for a given problem because multiple mesh points in or near the laminar subregion can result in inaccurate calculations throughout the pipe diameter. Unique to this case is the condition where the refining of the mesh at the wall serves to deteriorate the fit because regions of low flow are treated incorrectly. This indicates the significance of choosing an appropriate mesh.

The kinetic energy is plotted in Figure 14. The author had measured the three components of fluctuating velocity, $\bar{u}'$, $\bar{v}'$, and $\bar{w}'$, such that an experimental k [$k = (1/2)(\bar{u}'^2 + \bar{v}'^2 + \bar{w}'^2)$] was accessible. The plot corresponds to a location 8 m downstream from the pipe entrance where fully developed turbulent energy was realized. The turbulent energy appeared to develop more rapidly than the velocity profile, an effect most likely produced by the input turbulent kinetic energy specification. By imposing a larger initial value of kinetic energy at the entrance, the turbulence seemed to develop more rapidly down the pipe.

The friction velocity, u_τ, and the shear stress, τ, were calculated using two techniques and were compared with the experimental values ($\tau = \rho u_\tau^2$).

Experiment:	$u_\tau = 0.1284$	$\tau = 0.0214$
τ from k as predicted by TEACH:	$u_\tau = (c_\mu)^{1/4}\sqrt{k} = 0.161$	$\tau = 0.0337$
τ from u as predicted by TEACH:	$u = (u_\tau/\kappa)\ln(Eyu_\tau/\nu)$ $u_\tau = 0.157$	$\tau = 0.0320$

where $c_\mu = 0.09$

$E = 9.793$

$\kappa = 0.4187$

y = distance from wall

The discrepancy between the TEACH τ and the experimental τ is most likely due to an erroneous experimental value. The τ calculated by TEACH is consistent with the value deduced from the compilation of data in Reference 5 (Chapter 20). Furthermore, Laufer comments that measurements of turbulence levels and shearing stress are less accurate for this RE.

The dissipative rate of turbulent kinetic energy, ε, normalized by (R/u_τ^3) where R is the pipe radius, is displayed in Figures 15 and 16. The agreement in Figure 15 is seen to be very good. Figure 16 is a further illustration of the current limitations in the TEACH model as applied to regions of low turbulence. At the mesh points adjacent to the wall, TEACH calculates a large dissipation rate in contrast to the experiment, which indicates a maximum value for ε, followed by an abrupt loss in energy dissipation as the wall is approached. The maximum ε, a distance of 0.0095 m from the wall, denotes proximity to the laminar sublayer. At this point the turbulent kinetic energy is also at a maximum, illustrating the balance between the production of energy and the dissipation of energy. The necessity for a TEACH model with a variable mesh that can correctly calculate the laminar sublayer values is apparent.

The next four figures reflect a TEACH calculation differing only in the value of the RE. In Figures 17 and 18, good agreement is again seen in the velocity profiles, particularly in the near-wall region. Figure 19 indicates an accurate calculation of the kinetic energy. The shear stress and friction velocity values are as follows:

Experiment:	$u_\tau = 1.098$	$\tau = 1.566$
TEACH:	$u_\tau = (c_\mu)^{1/4}\sqrt{k} = 1.217 \rightarrow$	$\tau = 1.928$
TEACH:	$u = (u_\tau/\kappa)\ln(Eyu_\tau/\nu) \rightarrow u_\tau = 1.215 \rightarrow$	$\tau = 1.919$

Improved agreement is seen in each instance. Utilizing a parametric representation of the compiled data for τ (Reference 5, Chapter 20) yielded a value of 1.961, in closer agreement with the TEACH result than with the experimental value. The value of u_τ was extracted from the experimental data by equating y/R and Y^+ from the Laufer plots, such that some error

in the value of u_τ could have occurred because of inaccuracies in these plots. The dissipation rate is plotted in Figures 20 and 21. For high RE flow, the laminar sublayer decreases to a more narrow region. Thus, our first mesh point did not encompass this region, and the calculated dissipation of energy, seen to monotonically increase as the wall is approached, is in agreement with the experiment. The experimental plots likewise lacked the detail to include this region. Good agreement was obtained for all the energy comparisons.

PROBLEM 3 - FULLY DEVELOPED TURBULENT FLOW BETWEEN PARALLEL WALLS

Fully developed turbulent flow between parallel walls was analyzed.[11] The problem involved air flow with an average velocity of 15.6 m/sec through a channel 0.0635 m in diameter with an aspect ratio of 18:1. The RE, based on the channel diameter, was 64,600. Calculations were performed at a location 100 diameters downstream from the channel entrance to ensure fully developed flow. The velocity profiles are shown in Figures 22 and 23, Figure 23 being an amplification of the near-wall region. Excellent agreement is seen. Figure 24 illustrates the turbulent kinetic energy, k, normalized by the friction velocity u_τ. The turbulent velocity fluctuation in the streamwise direction $\overline{u}'$ was the only fluctuating velocity component measured by the authors. Thus, a kinetic energy, k, was obtained by utilizing data from a straight pipe measurement.[10] The ratio $[\overline{u}'^2/(\overline{u}'^2 + \overline{v}'^2 + \overline{w}'^2)]$ was derived as a function of radial height and the total kinetic energy value was defined at each location based on this ratio. In Figure 24, the agreement with TEACH is shown. Again, good agreement is realized. The value of the friction velocity was also compared. The authors cite a value of $u_\tau = 0.658$ for the RE of 64,000. The term u_τ was calculated using three different relationships:

Experiment:	$u_\tau = 0.658$
$u_\tau = \sqrt{\frac{r}{\rho}\frac{\partial p}{\partial x}}$	$u_\tau = 0.665$
$u_\tau = (c_\mu)^{1/4}\sqrt{k}$	$u_\tau = 0.679$
$u = (u_\tau/\kappa)\ln(Eu_\tau y/\nu)$	$u_\tau = 0.677$

where r = radius of channel
p = average pressure
$c_\mu = 0.09$
$E = 9.793$
$\kappa = 0.4187$
y = distance from the wall

As can be seen, the results were in good agreement with the experiment.

A comparison of turbulent kinetic viscosity [$\nu_T = (c_\mu k^2)/\epsilon$, where k is the turbulent kinetic energy and ϵ is the turbulence dissipation] in the near-wall region and across the channel width is indicated in Figures 25 and 26. Agreement is good in the vicinity of the wall but tends to degrade toward the centerline region. In this region $\partial u/\partial y$ approaches zero, the Reynolds stresses are small, and the constant c_μ becomes inadequate. The modeling of c_μ is based on experimental results in the wall vicinity such that this inaccuracy at the centerline is an anticipated result. The smallness of the Reynolds stresses in this region, however, ensures marginal inaccuracies in the flow calculation.

PROBLEM 4 - ABRUPT AXISYMMETRIC EXPANSION

Turbulent flow at an abrupt axisymmetric expansion was studied for the case of air flow through a pipe at an RE of 200,000.[12] ($RE = \bar{u}D_o/\nu$, where D_o is the diameter of the pipe prior to the expansion.) The expansion ratio, D_1/D_o, was 2 and the average velocity, $\bar{u}$, at the pipe entrance was 27.61 m/sec. Figures 27 through 31 demonstrate the agreement between the TEACH velocity profile calculations and the experimental data. R_1 is the downstream radius (0.108 m), D_o is the upstream diameter (0.108 m), x is the axial distance measured from an origin at the expansion, and y is the radial measurement with the origin located at the centerline. It should be noted that the experimental plots reflect "corrected" values of velocities. In essence, the data points were adjusted to conform to a smooth curve. This served to eliminate experimental scatter and/or the inconsistencies of successive readings. This is of significance in that the recirculating region of flow, reflecting a linear profile as the wall is approached, is the result of data presentation rather than physical measurements at the specified points. This, in part, explains the discrepancies between TEACH results and those of the authors near the wall in the region of recirculating flow. In general, the agreement is fair, although there are sizeable disagreements that cannot be explained. It is hoped that in the future the use of a modified turbulence model will improve the comparisons in the low velocity recirculating region. Better agreement is realized for the varying x locations downstream from the step.

Comparisons of the turbulent kinetic energy are shown in Figures 32 and 33. The authors had measured the three components of turbulent intensity: $\bar{u}'$, the longitudinal component, $\bar{v}'$, the radial component, and $\bar{w}'$, the component in the θ direction, for all locations, such that $k = (1/2)(\bar{u}'^2 + \bar{v}'^2 + \bar{w}'^2)$ was computed directly from the experimental data.

Qualitatively the results were in good agreement and the TEACH kinetic energy profiles were predictive of the developing kinetic energy. In Figure 34, the pressure in the central flow region is plotted as a function of the axial distance downstream. Again, fair agreement is realized.

An indication (though not exact) of the extent of an eddy behind the expansion was studied by plotting the contour of the location of zero axial velocity as shown in Figure 35. The TEACH results are in close approximation with the experimental data, as is illustrated. The reattachment point was calculated by TEACH to lie betwen 0.453 m and 0.541 m from the step. The experiment predicts 0.4984 m, in close agreement with the analysis.

The TEACH calculation utilized a grid mesh sized 55 x 60. The density of mesh points peaked in the region spanning the step, resulting in an adequate mesh for the geometry.

PROBLEM 5 - PLANE SUDDEN EXPANSION — LAMINAR FLOW

Air flow through a plane symmetric sudden expansion[13] was also calculated. The duct contained a 9.2:1 aspect ratio downstream from the expansion with a 3:1 expansion in height from 0.004 m in the upstream region to 0.012 m downstream. The RE was 56, based on an average velocity and the duct height. Figures 36 through 38 show the comparison with experiment for various positions before and after the step face. H is the step height (0.004 m), X is the axial distance as measured from an origin at the step, D is the half height of the downstream duct (0.006 m), y is the height as measured from the centerline, and u_{ℓ} is the centerline velocity at a point 0.001 m before the step. Excellent agreement is demonstrated. It may also be noted that the experiment indicates that for an RE of 56, symmetry exists throughout the duct. (At higher REs, asymmetric flow was observed.)

TEACH predicted a reattachment length of 0.020 m, in excellent agreement with the experiment. For this particular problem, 38 x-mesh points and 42 y-mesh points were sufficient, a reflection of the small RE employed.

PROBLEM 6 - PLANE SUDDEN EXPANSION — TURBULENT FLOW

Another experiment involving an abrupt change in radius is that of Abbott and Kline[14], whose experimental apparatus is sketched in Figure 39. The flow is in an open-surface water table 0.3048 m deep with movable side walls that can be separated as much as 0.6096 m. As can be seen, the flow is complicated by the fact that it is not symmetric about the centerline (the Coanda effect). The reattachment points on either side, ℓ_1 and ℓ_2,

are at different distances from the step. In addition, there are zones of 3-D flow immediately downstream from the step that extend distances n_1 and n_2 from the step. There is some vertical flow in these zones due to the finite depth of the channel. The lengths ℓ_1 and ℓ_2 were measured as a function of h/R_0, the ratio of the radius increase to the radius itself. The calculated reattachment lengths are compared with those in Figure 40. In the range of REs covered by the experiment and calculations (20,000 to 50,000), neither the reattachment lengths nor the velocity profile shapes had a significant dependence on RE. It is seen that for $h/R_0 > 1$, the calculated values are consistent with the average of ℓ_1 and ℓ_2 — the most that can be expected. For $h/R_0 < 1$, the disagreement (theory is too small) is due to the presence of the 3-D zones. In addition to these measurements, for a ratio of $h/R_0 = 1$, velocity profiles at various distances downstream from the step were measured. In order to compare these asymmetric distributions with theory, the velocity profiles on both sides of the centerline were plotted (Figure 41). It can be seen that the data points bridge the TEACH results and that TEACH would agree well with the average of the profiles on the two sides of the centerline. The curves correspond to an R_0 value of 0.0254 m, an average entrance velocity of 1.0 m/sec ($\bar{u}$), and an RE, based on a diameter of 0.0508 m, of 63,500. The term u_0 is the centerline velocity at the expansion (x = 0).

A single step geometry (the centerline now becomes a wall) was also measured by Abbott and Kline. In the TEACH calculation, the entrance diameter, D_0 (represented by R_0 in Figure 39), was 0.0254 m and the step height, h, was equal to 0.0127 m, resulting in an h/D_0 ratio of 0.5. The RE ($RE = \bar{u}D_0/\nu$) was 31,700 with an average velocity of 1.0 m/sec in the entrance section. Figure 42 displays the comparison between the TEACH velocities and the experiment. There is a small but systematic difference in the central flow shapes, with the experimental peak being higher. Also, the TEACH velocity is higher in the expansion region. (This is where any 3-D effects on the flow would be most pronounced.) The TEACH model calculated a reattachment length of 0.056 m compared with the experimental value of 0.074 m (which would be smaller without the 3-D flow region). In Figures 43 and 44, the turbulent kinetic energy is plotted. The experimental plot reflects a quantity that although denoted by the authors as the turbulent intensity, in essence represents merely the longitudinal component, $\bar{u}'$, of the fluctuating velocity. Effectively, this reduces to approximately one third the total turbulent kinetic energy. Drawing from the data of Hsu,[15] an approximate ratio of the longitudinal component and turbulent kinetic energy can be established. Directly beyond the expansion, the remaining two components, $\bar{v}'$ and $\bar{w}'$, exercise a more dominant role and form a peak translated away from the $\bar{u}'$ peak toward the wall. As the turbulence becomes fully developed, the three components reduce to

about the same shape and approximately the same magnitude away from the wall. Analysis of the TEACH results and the experimental plots shows discrepancies conforming to what is anticipated based on the definition of the quantities plotted. Some of the differences in profile shape for small x/D and in magnitude for large x/D,as seen in Figures 43 and 44, can certainly be attributed to this rationalization. However, a serious discrepance remains because this cannot account completely for the difference in peak values for small x/D. The extent to which the 3-D flow zone might account for some of the discrepancies in flow and turbulent energy is unknown. A somewhat judicious choice of the mesh resulted in improved accuracy of the calculation. For the double step problem, a 48 x 28 mesh was successfully implemented. In order to extract the detail necessary for the kinetic energy plot (single step calculation), a 74 x 28 mesh was utilized. An attempt was also made to increase the y mesh points to a value of 48, but little change in the answers was found.

The last data set was that of Hsu[15] involving air flow through a channel with a backward facing step. The entrance diameter, D_0, was 0.814 m and the downstream diameter, D_1, was 1.221 m, resulting in an h/R_0 ratio of 0.5. The aspect ratio was 1.5 and the RE, based on the diameter D_0 and the mean velocity, was 501,000. The mean flow and turbulence characteristics were measured at various downstream positions, x, the origin of x being defined at the step. In Figures 45 through 52, the velocity profiles are compared for the TEACH calculation and the experimental data. The overall agreement is seen to be poor. Figures 53 through 56 display the turbulent kinetic energy profiles normalized by the dynamic head. The agreement is poor in the area directly behind the step, but improves as the location of measurement moves downstream. In Figure 57, the distribution of wall pressure is illustrated. Qualitative agreement is seen. The contour of zero u was derived by plotting the position of zero axial velocity for each location downstream from the step. In Figure 58, y is the distance from the top wall to the point of zero velocity. The agreement again is unsatisfactory. TEACH calculated a reattachment point of 2.12 m, in reasonable agreement with the experimental value of 2.43 m. In the TEACH calculation of the Hsu experiment, 42 axial mesh points and 50 transverse mesh points were used.

The discrepancies in the kinetic energy profiles between TEACH and the experiment appear consistent with the discrepancies seen in the velocity profiles. TEACH, as compared with the Hsu data, calculates significantly more kinetic energy in the region immediately following the step increase. Physically, this corresponds to larger velocity fluctuations

and this leads to greater spreading of the central flow into the channel expansion. Examining the velocity profiles, one observes that TEACH does indeed predict a more rapid spreading, a lower peak velocity, and less recirculating flow just beyond the step than the experimental results indicate. Further downstream, the experimental profile is less peaked than that of TEACH.

Part of the discrepancy could be due to experimental conditions. The aspect ratio of the test section is 1.5, a value sufficiently low so that 3-D effects are present. Furthermore, at the downstream end of the wind tunnel, the air speed is adjusted by a "bank of louvers" at a location corresponding to $x/D_1 = 4.25$. This corresponds to an imprecisely known velocity and pressure exit boundary condition inconsistent with that in TEACH. This is probably the cause of the decrease in the experimental velocity profile peak relative to TEACH at large x/D_1, since the additional frictional resistance of the louver has a flattening effect on the profile.

In the TEACH calculation, as specified by Hsu in the description of the experiment, the plenum is preceded by an inlet section 0.710 m long with diameter D_0. At the beginning of the inlet, the TEACH flow conditions conformed to the published flow conditions. However, in Figures 45 and 53, it is seen that this results in the conditions at the position of the step not being closely approximated by the TEACH calculation. This could also account for some of the TEACH-experiment discrepancies. However, additional calculations in which the entrance length and flow conditions were varied indicate that this has a minor effect.

The lack of agreement between TEACH and experiment cannot be totally explained by these effects. The present model of TEACH is probably the major contributing factor. Discrepancies, showing the same characteristics, were seen in the TEACH calculation of the Abbott and Kline experiment, further substantiating this conclusion. Further analysis of flow situations with the absence of 3-D effects or imprecise boundary conditions and with measurements of all relevant experimental quantities can help to determine the seriousness of this problem, and modifications of the model constants or of the model itself can be made to improve the reliability of TEACH for this geometry.

CONCLUSIONS

The data in the two problem sets involving laminar flow were reproduced very well by TEACH. Problem 1 involved developing laminar flow profiles in a pipe, and Problem 5 involved measurement of velocity profiles and the reattachement length for flow in a channel with a sudden symmetric

expansion in diameter. The good agreement for these two quite different geometries represents a significant further qualification of TEACH for KAPL applications. Although not very common, there do exist reactor problems involving regions of laminar or near laminar flow.

Problems 2 and 3 involved fully developed turbulent flow in straight pipes and between parallel walls, respectively. The quantities measured and analyzed included profiles for velocity, turbulent kinetic energy, turbulence dissipation, turbulent viscosity, and wall shear stress. The results were generally very good and in all cases the TEACH calculations were adequate. (The calculations were accurate everywhere except for details near the laminar sublayer. Here the turbulence model was known beforehand to be inadequate and we see further need for the improved low RE model also developed at Imperial College.) The results certainly increase the confidence one can have in the model for calculating flow in such simple geometries.

Problem 4 involved turbulent flow in a pipe with a sudden expansion in radius. The data available for analysis showed the development of the pressure and the velocity and turbulent kinetic energy profiles downstream from the expansion. The TEACH predictions for Problem 4 did not match the experimental data as accurately as did the results for Problems 1, 2, 3, and 5. However, the differences between TEACH and experiment mainly involved the flow details, and the quality of the TEACH description of the overall flow development is probably adequate for most applications for flow in this or similar geometries.

Problem 6 involved developing turbulent flow in channels with both symmetric and asymmetric sudden expansions in diameter. The experimental quantities measured were velocity and turbulent kinetic energy profiles, the static pressure, and the reattachment length. Here, unfortunately, the experimental results are affected by 3-D flow regions and imprecisely known boundary conditions that partly obscure the theoretical and experimental comparisons. However, these factors probably do not account for all the discrepancies between TEACH and experimental results, and it appears that part or most of the disagreement is due to the model itself. Not only are there differences in detail in all cases, but the magnitudes of the kinetic energy profiles are discrepant. However, even with these problems, the current TEACH code description of flow in such geometries is probably adequate for some applications. Future modifications to the model can be made to significantly improve the description. Furthermore, we know of no general model of similar complexity that does a better job of describing the flow.

The overall agreement with all six problem sets was good despite the obvious problems mentioned above.

REFERENCES

1. Jones, W. P. and B. E. Launder. Int. J. Heat Mass Transfer. 15. 1972. P. 301.
2. Launder, B. E. Imperial College, Mechanical Engineering Department. Report No. HTS/73/26. 1973.
3. Hanjalic, K. PhD Thesis. University of London. 1970.
4. The original TEACH code was documented by A. D. Gosman and W. M. Pun at Imperial College (Department of Mechanical Engineering Report Numbers HTS/73/2 and HTS/73/3). The calculations reported here were done with a KAPL code of the same name that was obtained by extensively modifying and extending the range of applicability of the original TEACH code.
5. Nikuradse, J. Reported by H. Schlicting in Boundary Layer Theory. 6th edition. McGraw-Hill. New York. 1968. P. 232.
6. Campbell, W. D. and J. D. Slattery. "Flow In The Entrance of a Tube." J. Basic Engineering. March 1963.
7. Friedman, M, J. Gillis, and N. Liron. "Laminar Flow in a Pipe at Low and Moderate Reynolds Numbers." Applied Scientific Research. 19. 1968. Pp. 426-438.
8. Lawn, C. J. "The Determination of the Rate of Dissipation in Turbulent Pipe Flow." J. Fluid Mechanics. 48. 1970. Pp. 477-505.
9. Barbin, A. R. and J. B. Jones. "Turbulent Flow in the Inlet Region of a Smooth Pipe." J. Basic Engineering. 85. 1963. P. 29.
10. Laufer, J. "The Structure of Turbulence in Fully Developed Pipe Flow." NACA Report 1174. 1954.
11. Hussain, A. K. M. F. and W. C. Reynolds. "Measurements in Fully Developed Turbulent Channel Flow." Trans. ASME, Series I. J. Fluids Engineering. 97. 1975. Pp. 568-580.
12. Chaturvedi, M. C. "Flow Characteristics of Axisymmetric Expansions." Proceedings ASCE. J. Hydraulics Division. 89. HY3. May 1963. Pp. 61-92.

13. Durst, F., A. Melling, and J. H. Whitelaw. "Low Reynolds Number Flow Over a Plane Symmetric Sudden Expansion." J. Fluid Mechanics. 64. 1973. P. 111.

14. Abbott, D. E. and S. J. Kline. "Experimental Investigation of Subsonic Turbulent Flow Over Single and Double Backward Facing Steps." J. Basic Engineering. 84. 1962. P. 317.

15. Hsu, H. C. "Characteristics of Mean Flow and Turbulence at an Abrupt Two-Dimensional Expansion." PhD Thesis, University of Iowa. February 1950.

APPENDIX A. GEOMETRY DESCRIPTION

Problem 1 — NIKURADSE (air flow in a pipe)
RE = 520

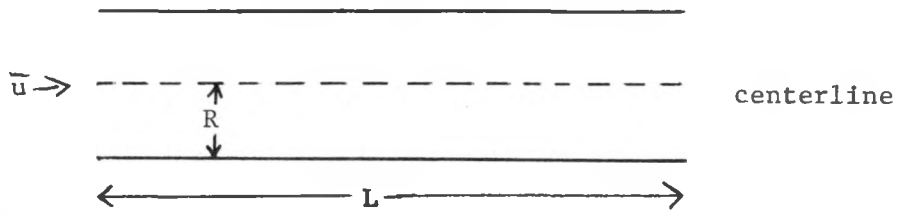

R = 0.00225 m
$\bar{u}$ = 1.6 m/sec
L = 1.805 m

Problem 2 — LAWN (air flow in a pipe)
RE = 50,000 to 500,000

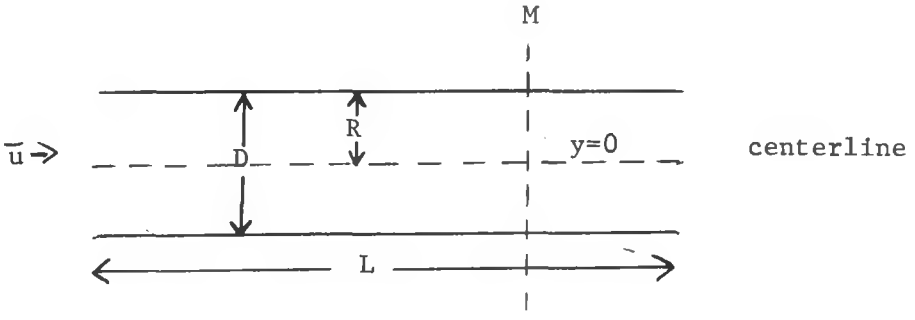

D = 0.1443 m
L = 8.658 m
M = 8.514 m (point of measurement)
R = 0.7215 m
$\bar{u}$ = 1.0 m/sec to 10 m/sec

Problem 2 — BARBIN AND JONES (water flow in a pipe)
RE = 388,600

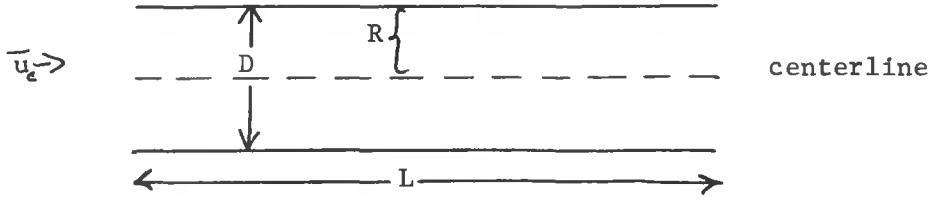

D = 0.2032 m
R = 0.1016 m
L = 8.84 m
u_c = 1.53 m/sec (average velocity)

Problem 2 — LAUFER (air flow in a pipe)
RE = 50,000 to 500,000

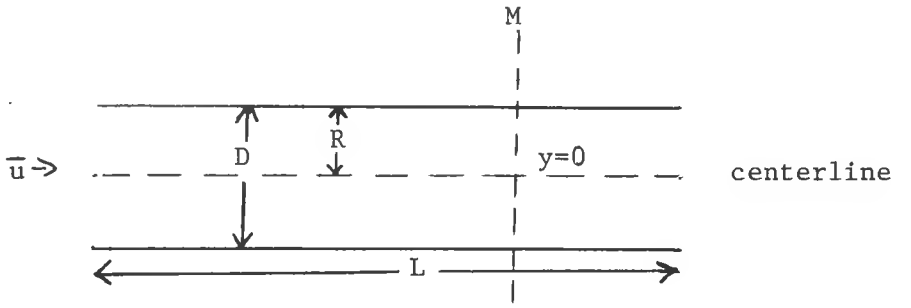

D = 0.2469 m
L = 12.3 m
M = 10.577 m (point of measurement 42.8 diameters downstream)
$\bar{u}$ = 3.048 m/sec to 30.48 m/sec
R = 0.1235 m

Problem 3 — HUSSAIN AND REYNOLDS (air flow in a channel)
RE = 64,600

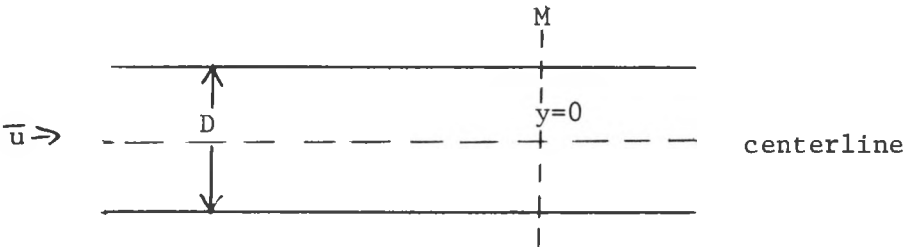

$\bar{u}$ = 15.6 m/sec
D = 0.0635 m
M = 6.35 m (point of measurement 100 diameters downstream)

Problem 4 — CHATURVEDI (air flow in a pipe)
RE = 200,000

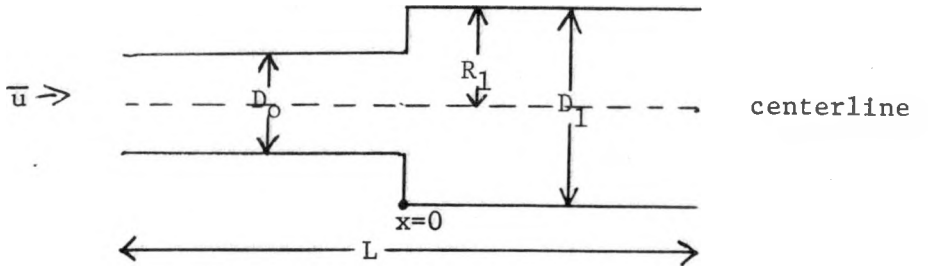

$\bar{u}$ = 27.61 m/sec
L = 2.304 m
D_o = 0.108 m
R_1 = 0.108 m
D_1 = 0.216 m

Problem 5 — DURST (air flow in a channel)
RE = 56

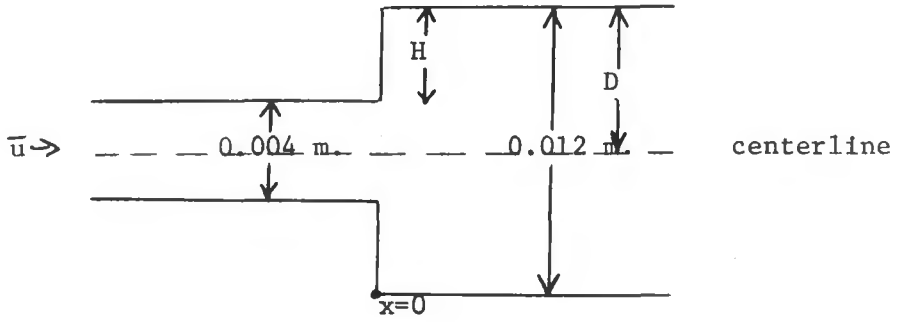

$\bar{u}$ = 0.118 m/sec
H = 0.004 m
$u_{\mathfrak{C}}$ = centerline velocity at point 0.001 m before the step
D = 0.006 m

Problem 6 — ABBOTT AND KLINE (water flow in a channel)
RE = 63,500

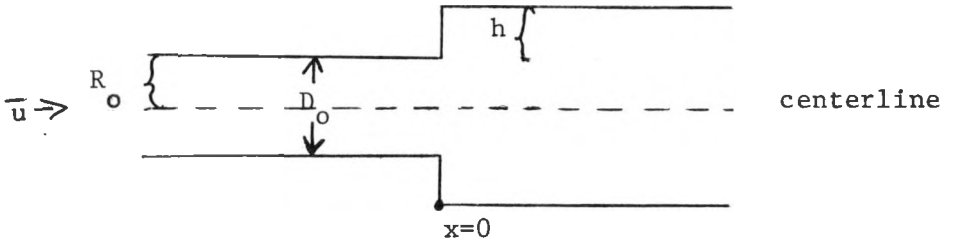

$\bar{u}$ = 1.0 m/sec
R_o = 0.0254 m
D_o = 0.0508 m
u_o = centerline velocity at the expansion (x=0)
h = 0.0254 m

Problem 6 — ABBOTT AND KLINE (water flow in a channel)
RE = 31,700

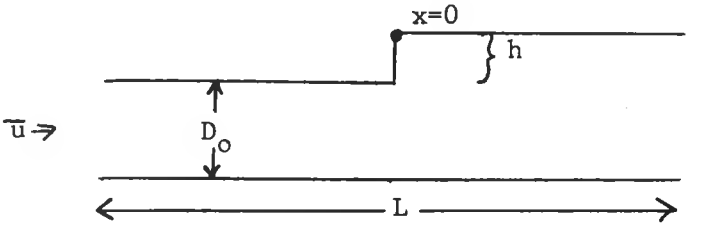

$\bar{u}$ = 1.0 m/sec
D_o = 0.0254 m
h = 0.0127 m
L = 3.657 m

Problem 6 — HSU (air flow in a channel)
RE = 501,000

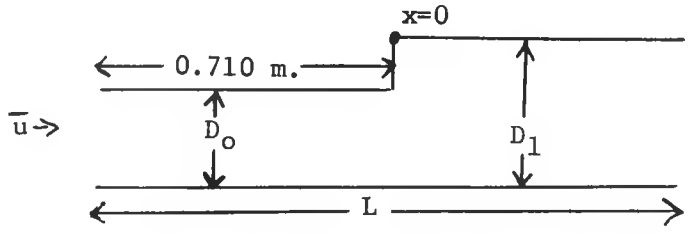

$\bar{u}$ = 9.144 m/sec
D_1 = 1.221 m
D_o = 0.814 m
L = 5.892 m

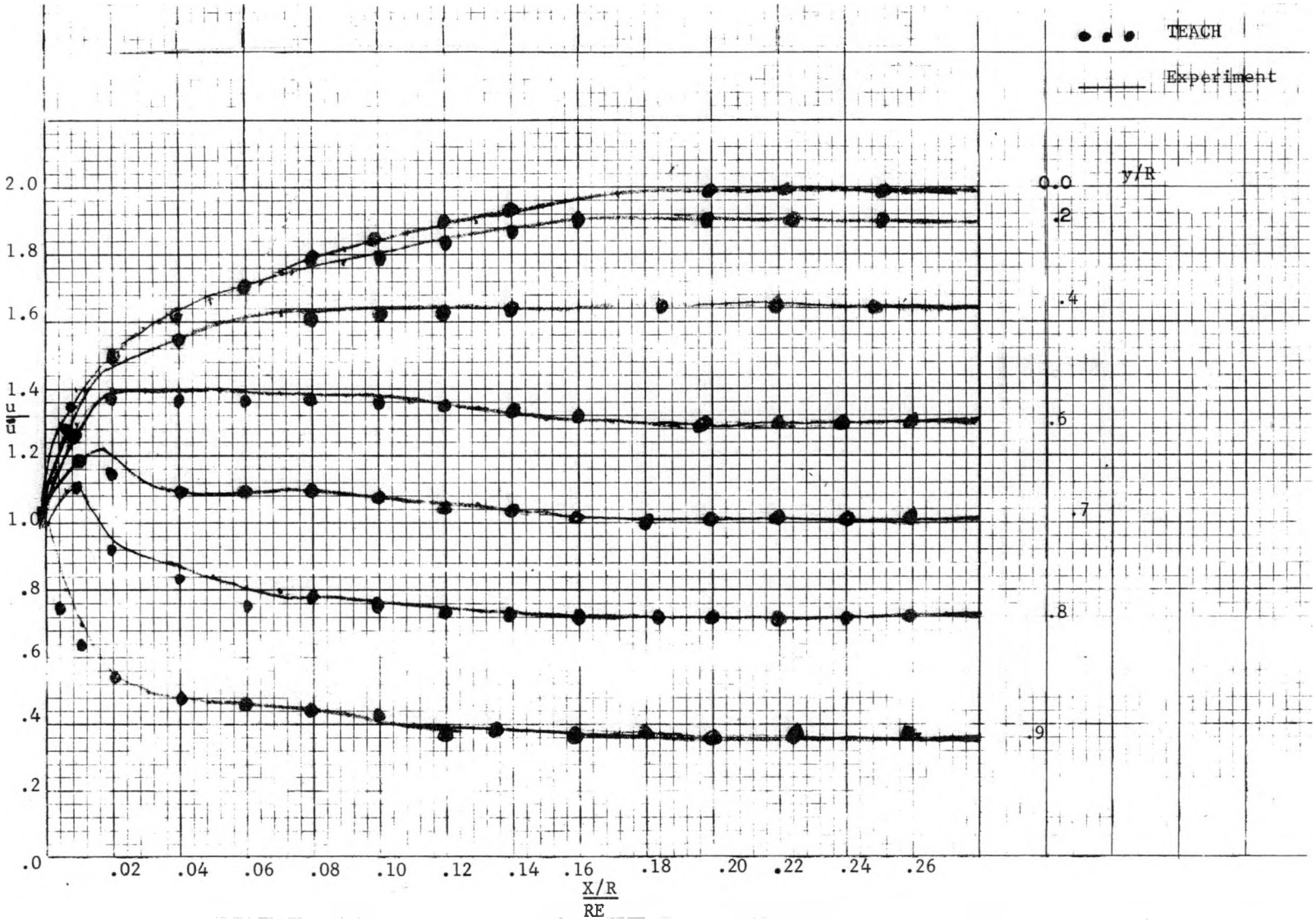

FIGURE 1. Velocity Profile (Nikuradse). RE = 520.
KS-76165

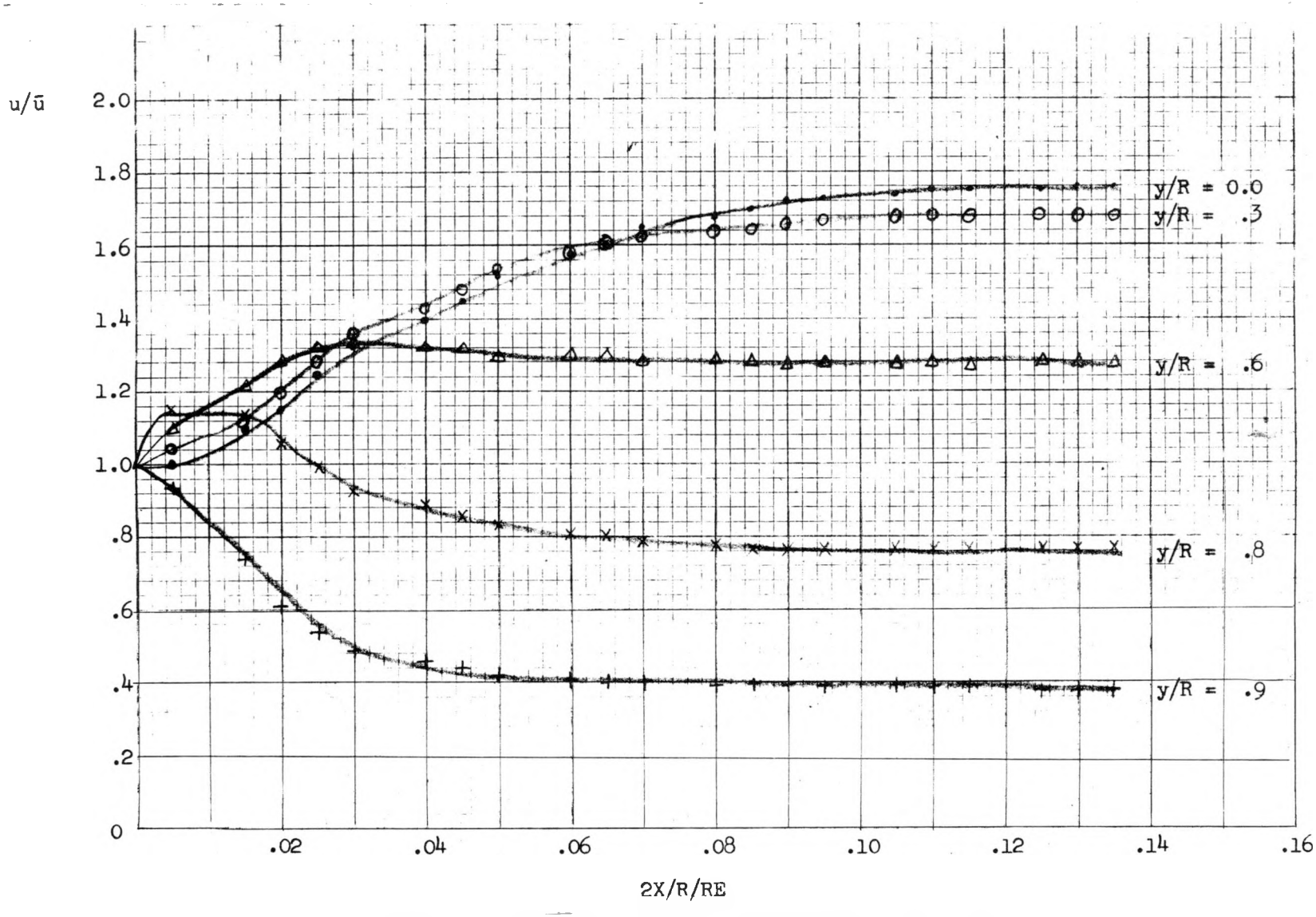

FIGURE 2. Velocity Profile (Nikuradse). RE = 40.
KS-76166

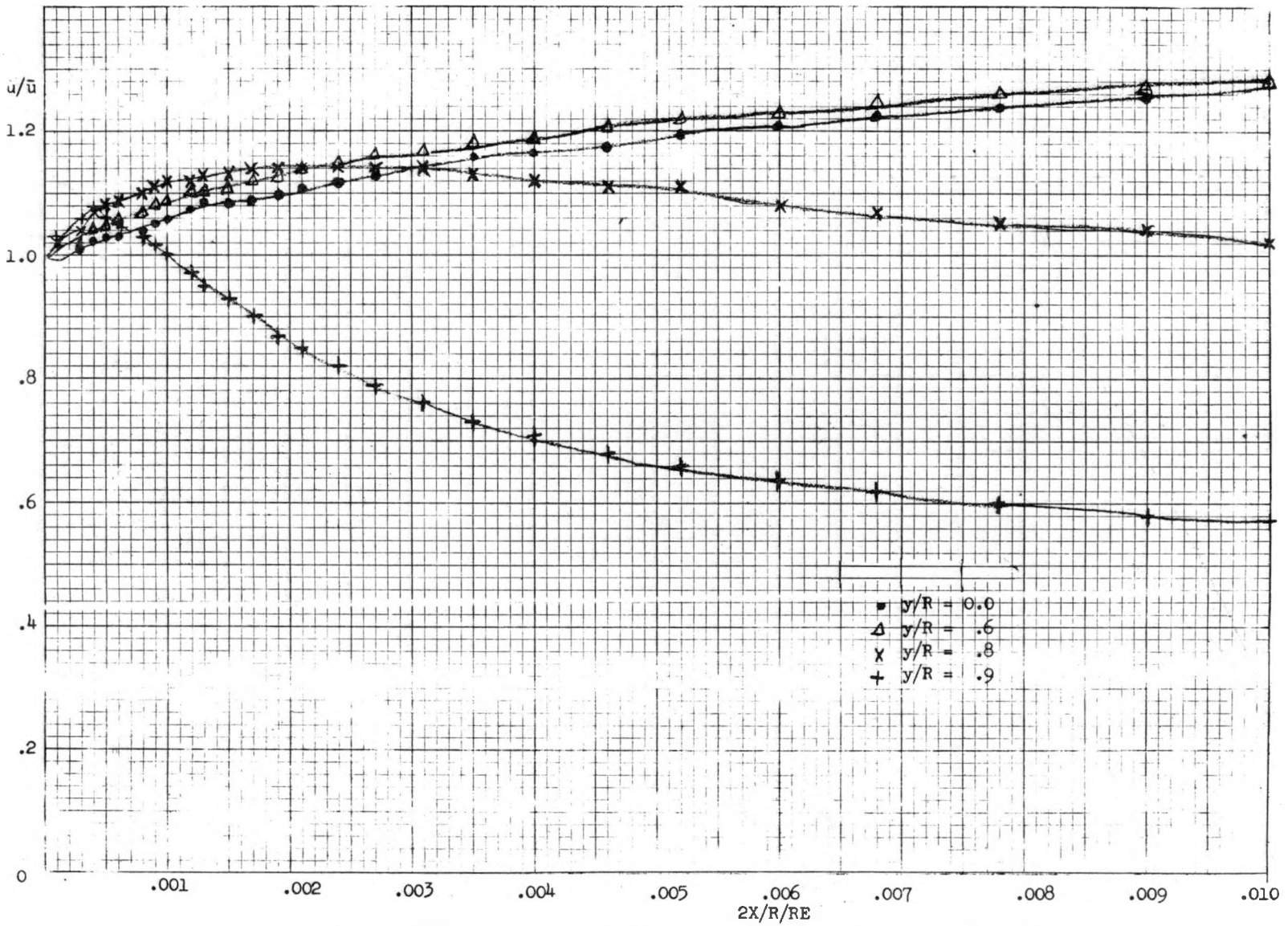

FIGURE 3. Velocity Profile (Nikuradse). RE = 2000.
KS-76167

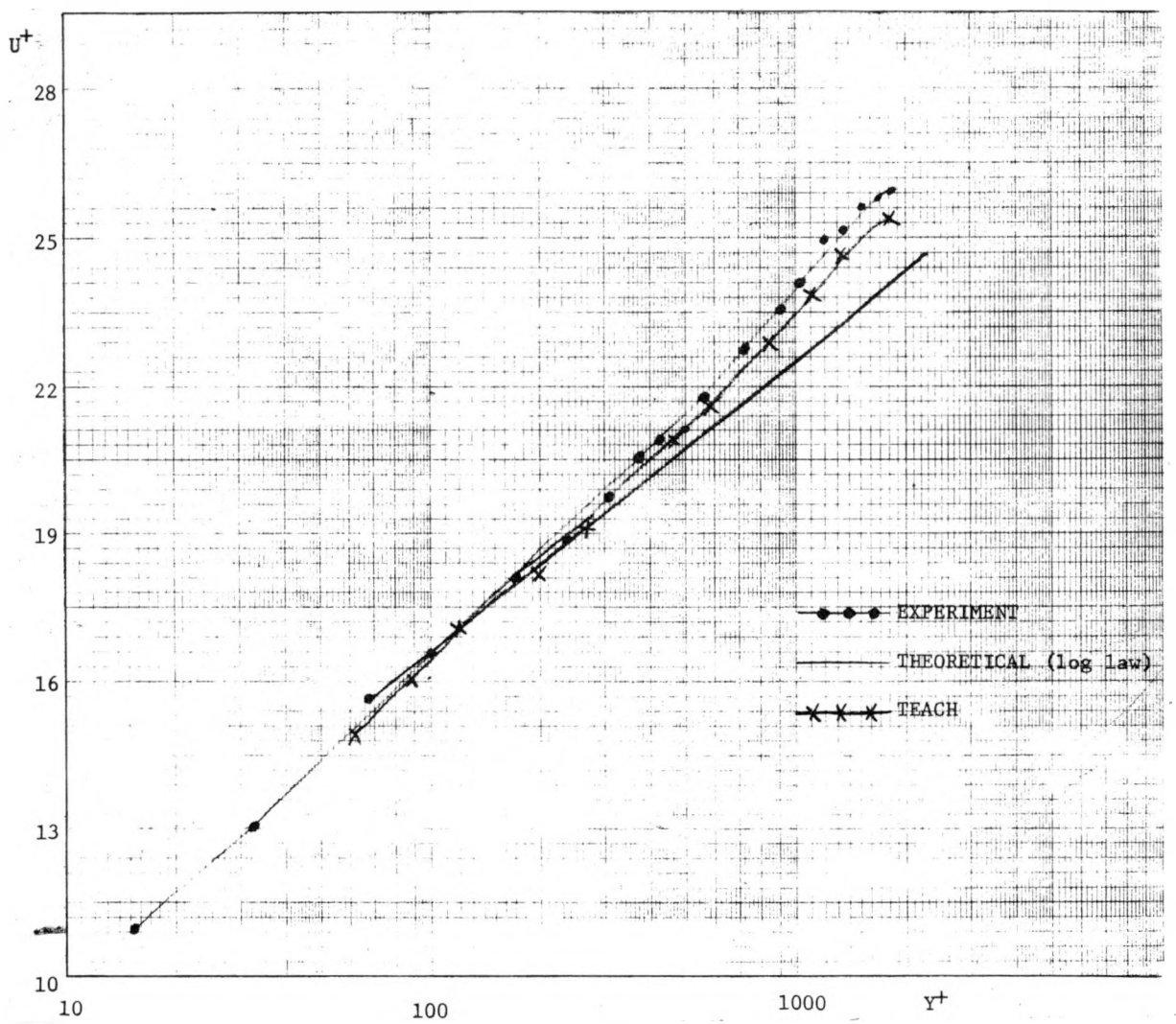

FIGURE 4. Velocity Profile (Lawn). RE = 92,000.
KS-76168

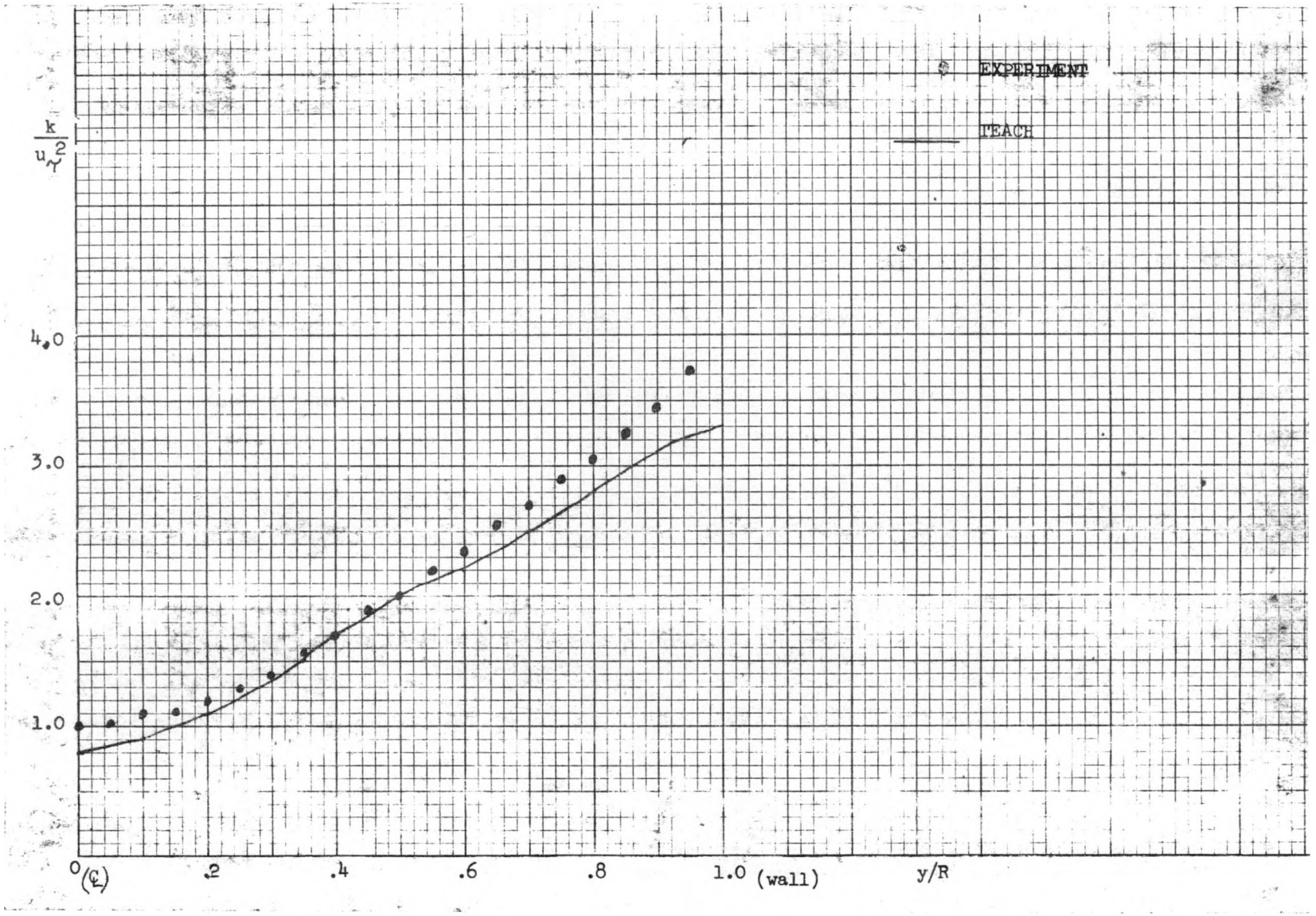

FIGURE 5. Turbulent Kinetic Energy (Lawn). RE = 92,000.
KS-76169

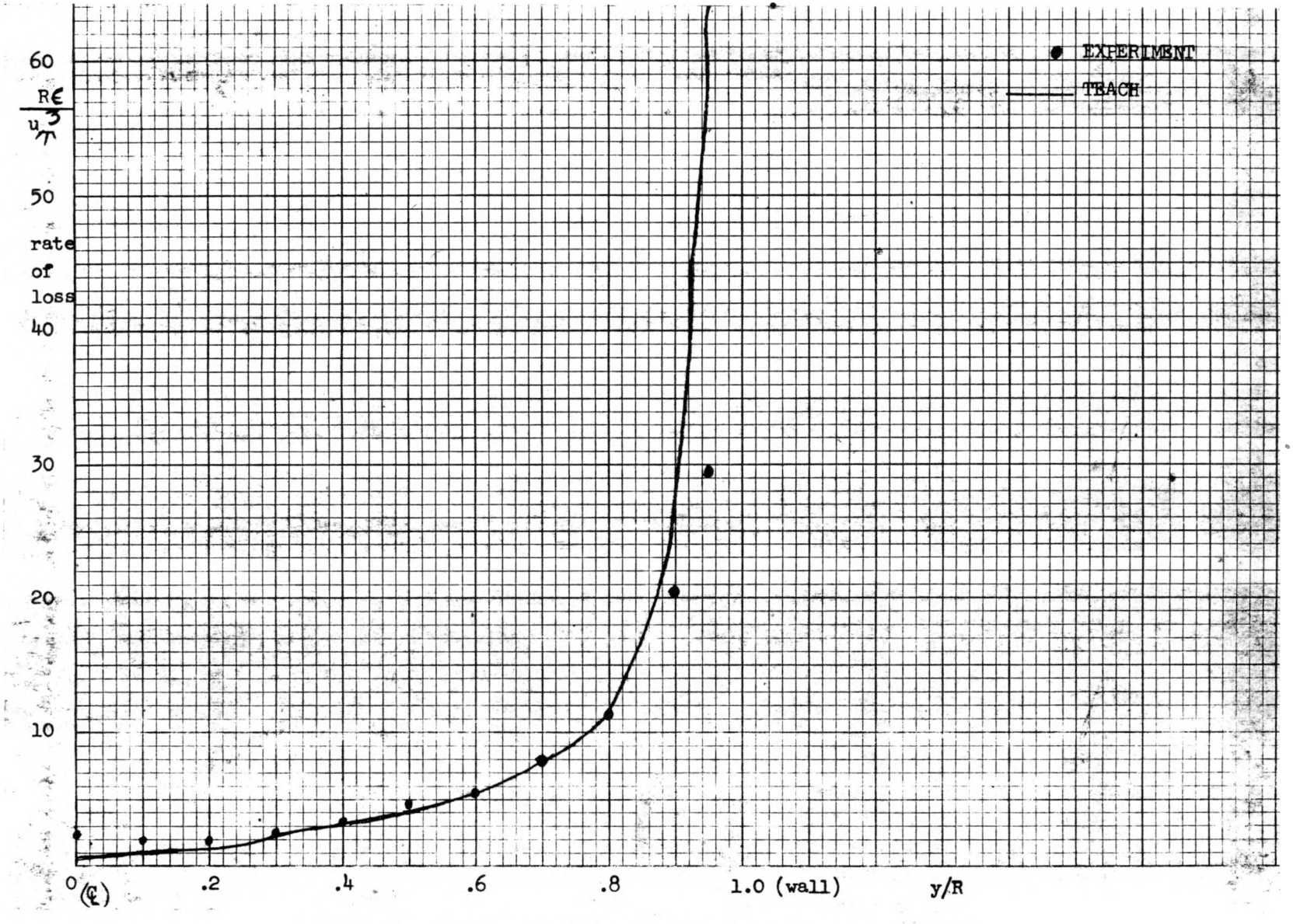

FIGURE 6. Turbulence Dissipation (Lawn). RE = 92,000.
KS-76170

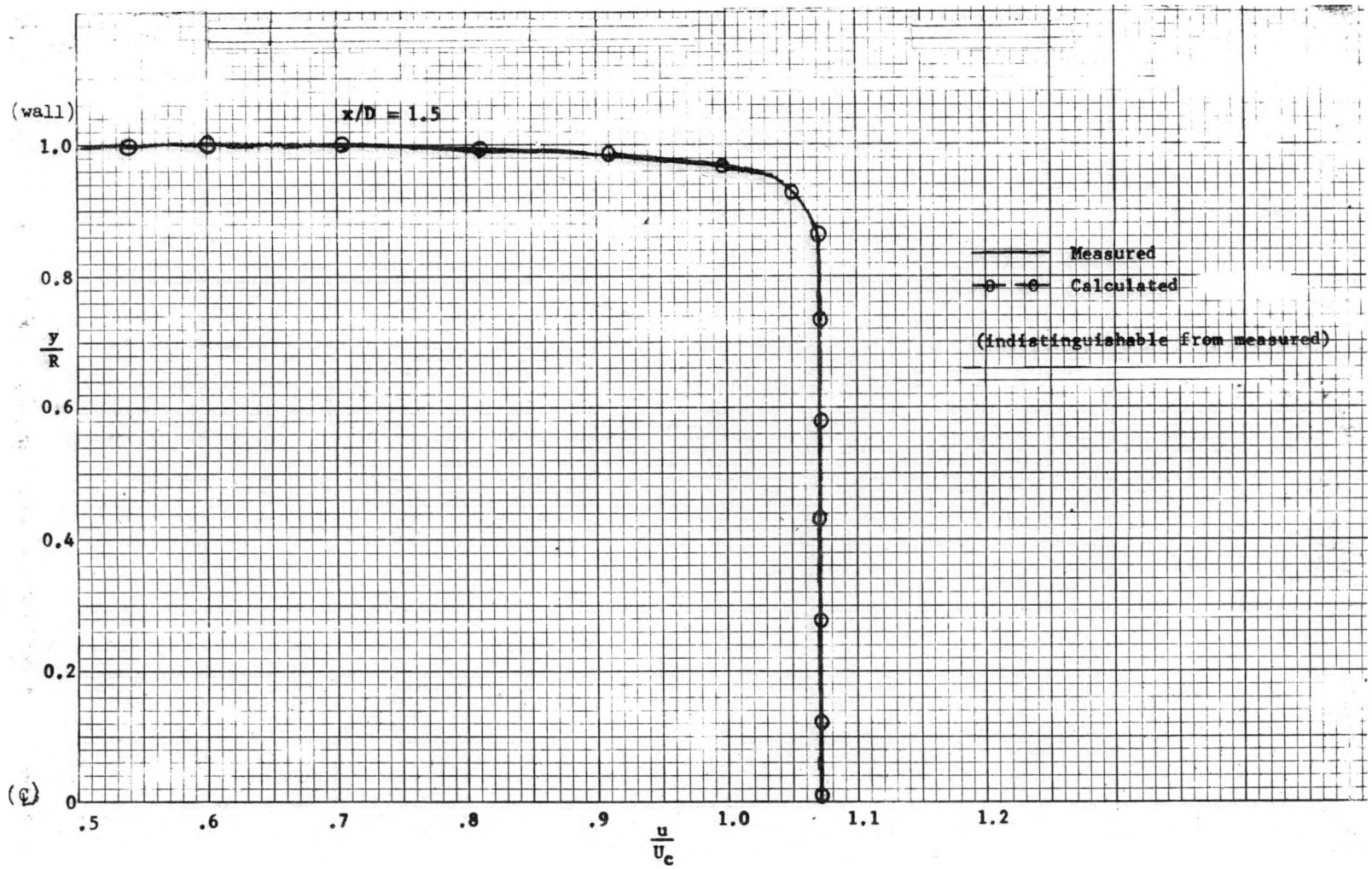

FIGURE 7. Velocity Profile (Barbin-Jones). RE = 388,000.
KS-76171

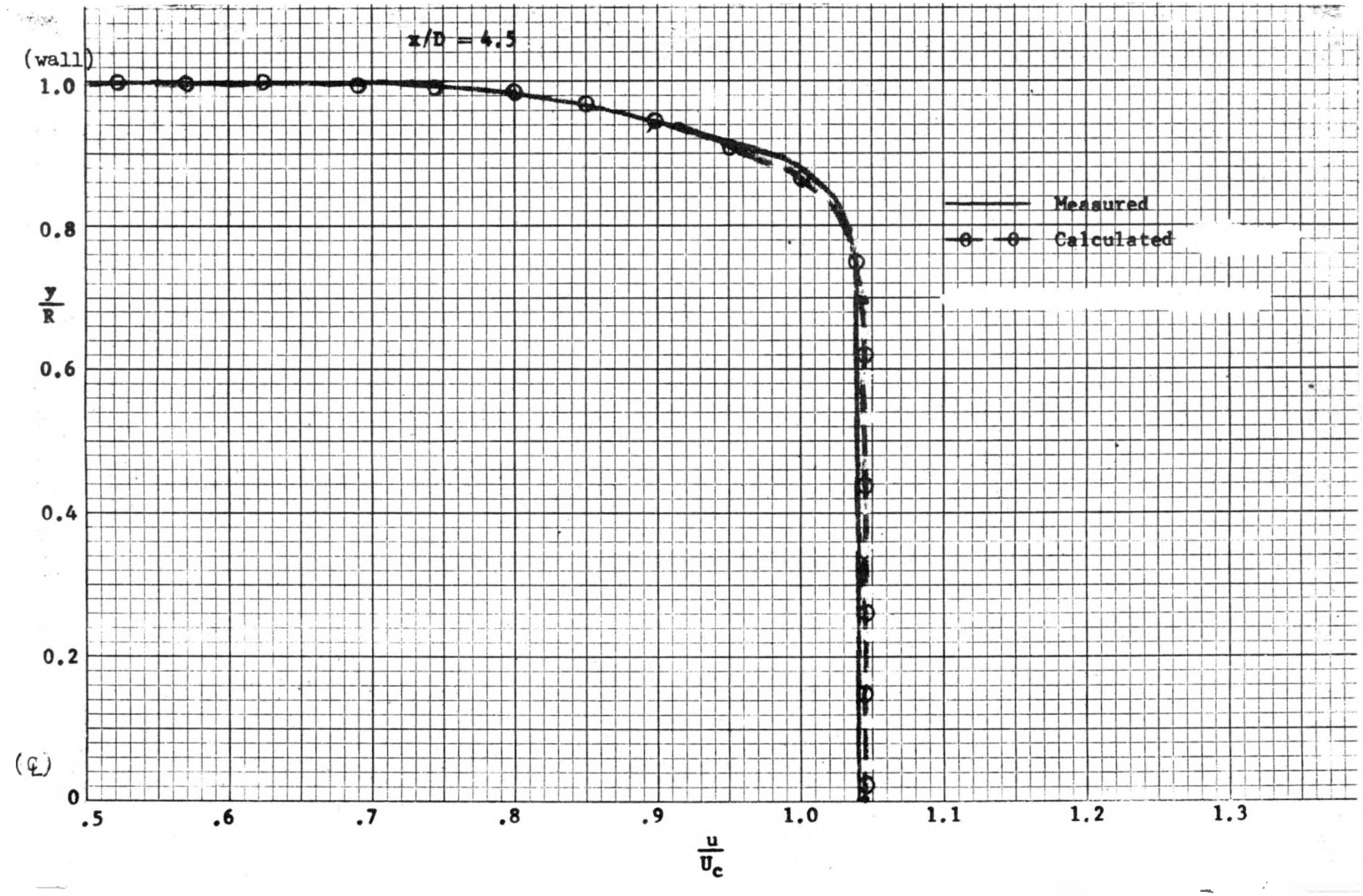

FIGURE 8. Velocity Profile (Barbin-Jones). RE = 388,000.
KS-76172

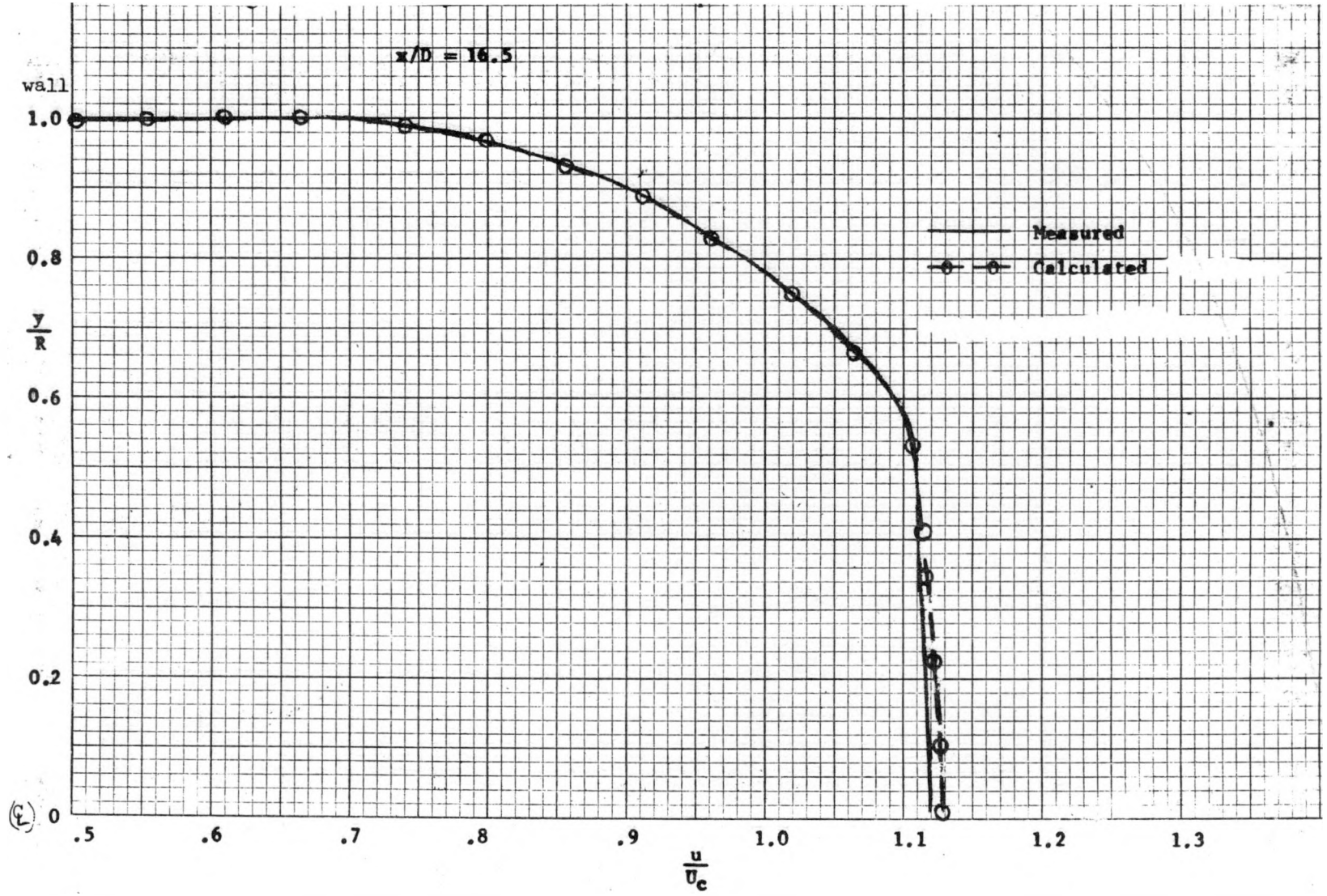

FIGURE 9. Velocity Profile (Barbin-Jones). RE = 388,000.
KS-76173

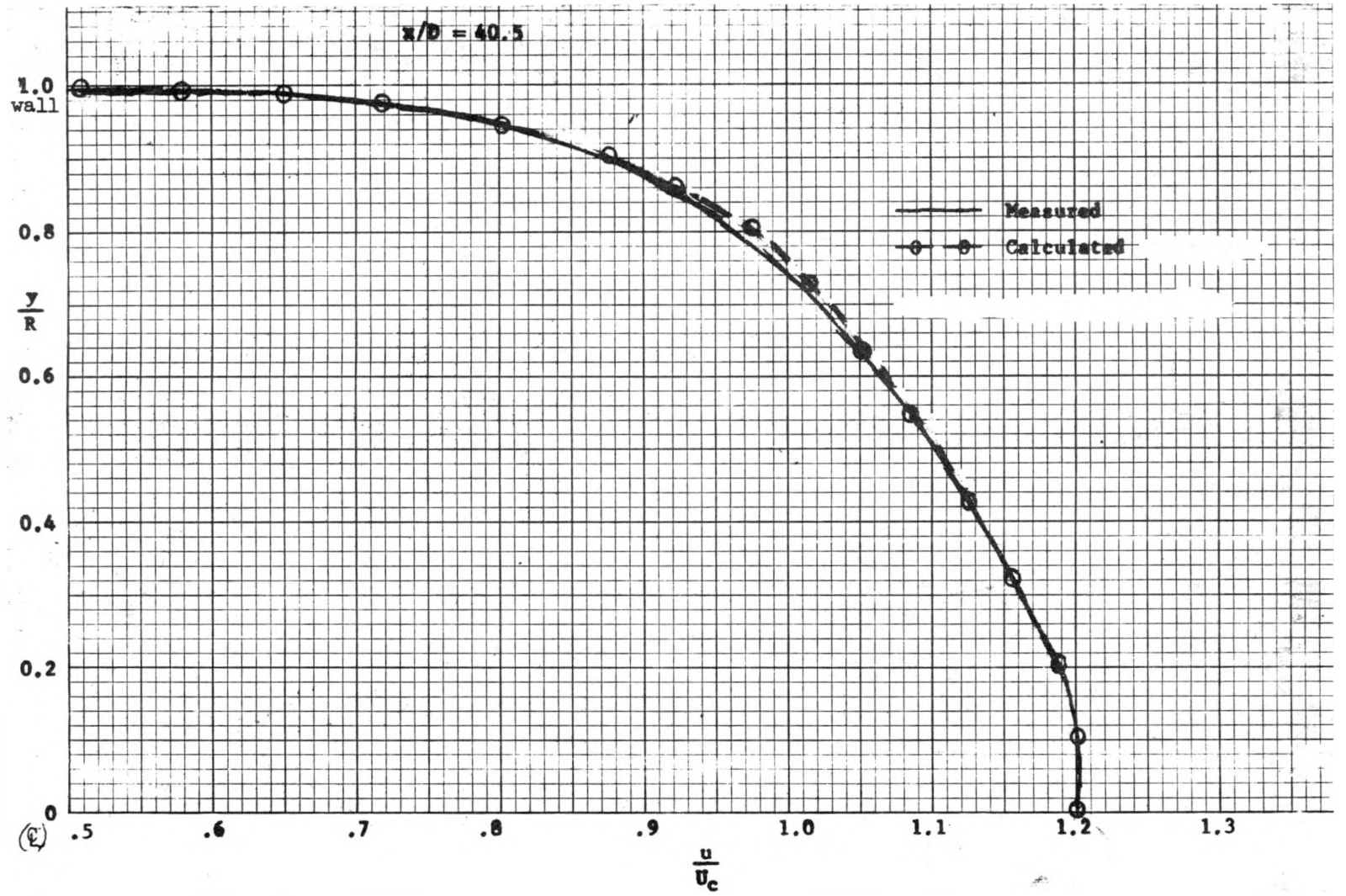

FIGURE 10. Velocity Profile (Barbin-Jones). RE = 388,000.
KS-76174

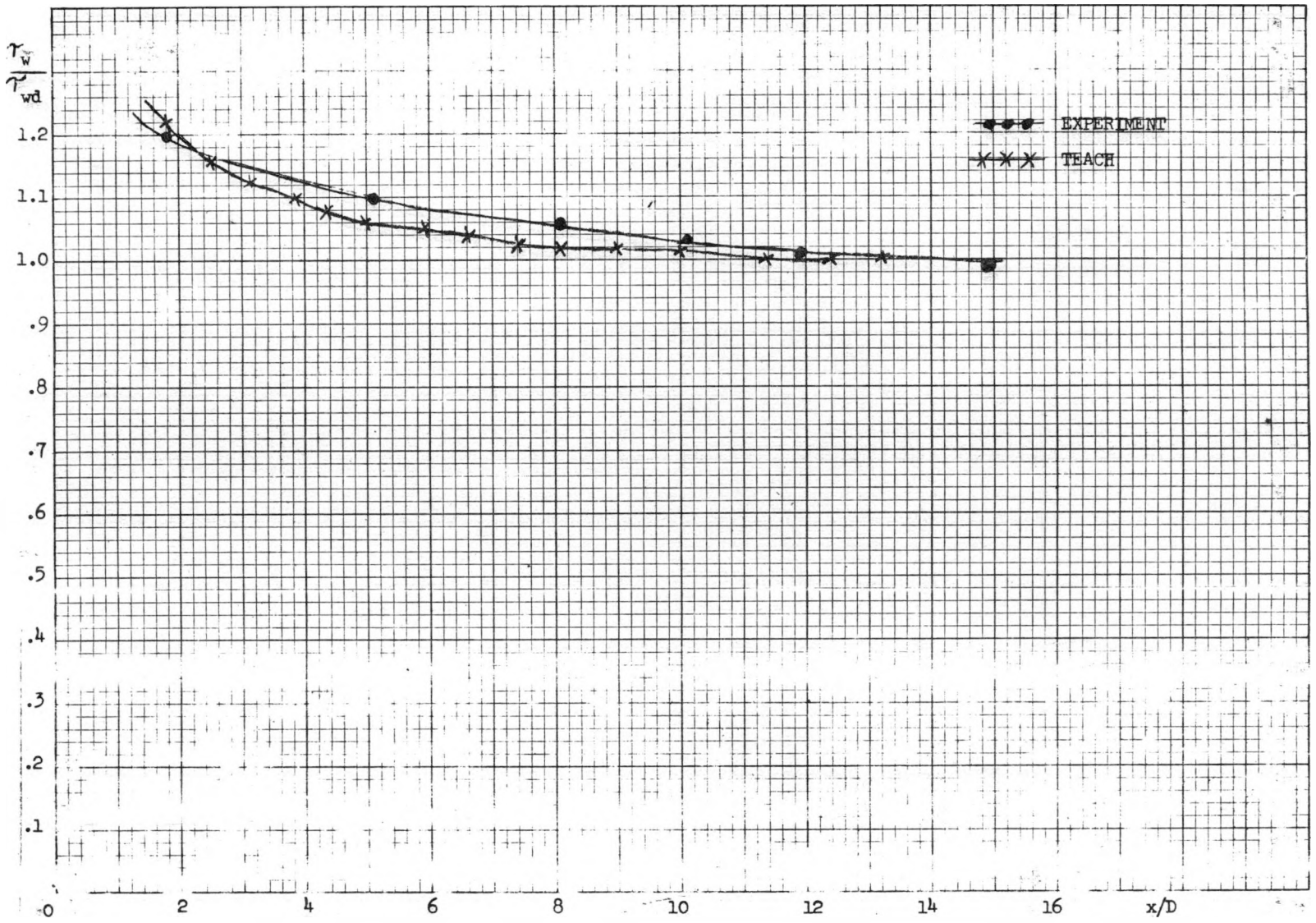

FIGURE 11. Shear Stress (Barbin-Jones). RE = 388,000.
KS-76175

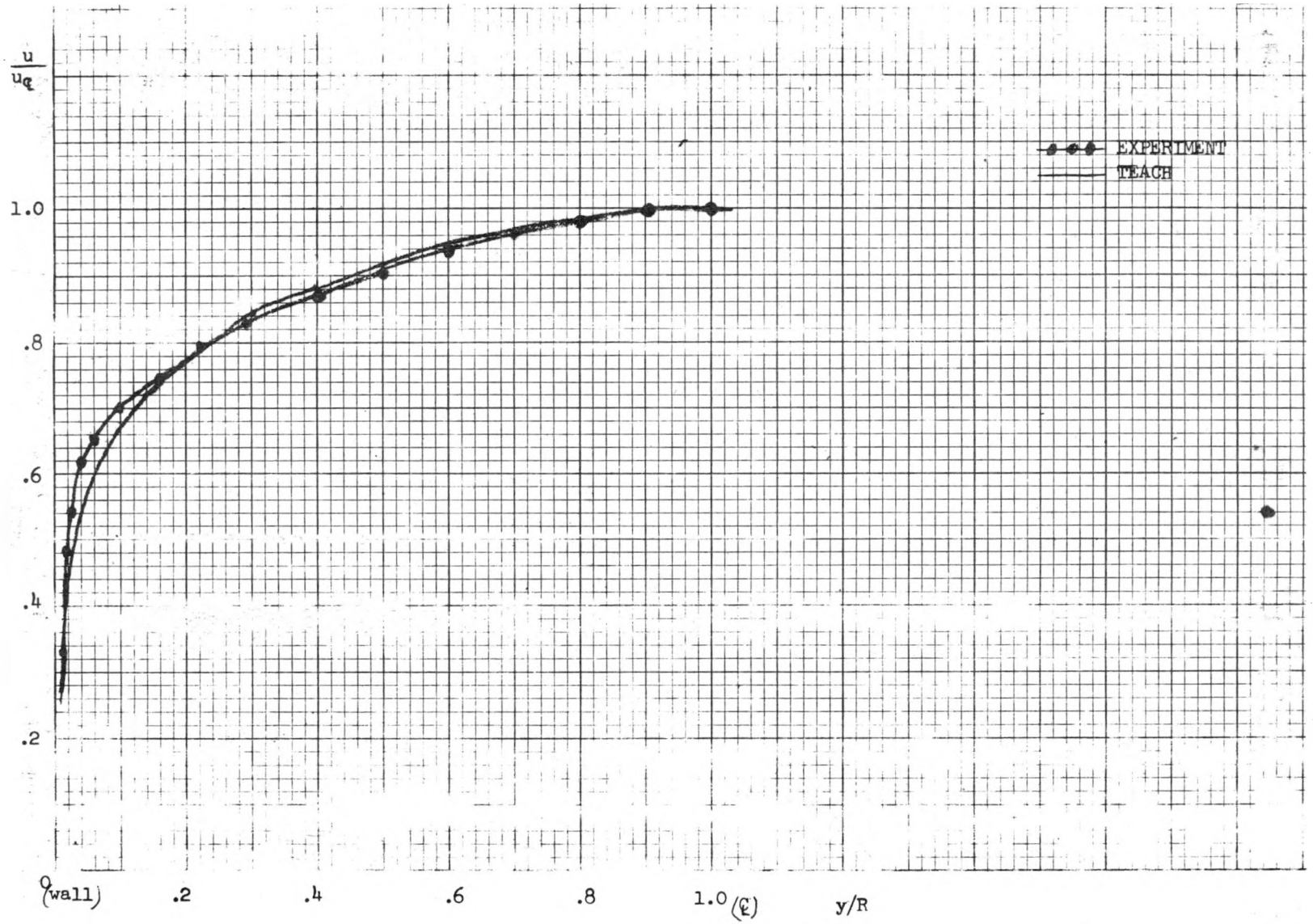

FIGURE 12. Velocity Profile (Laufer). RE = 50,000.
KS-76176

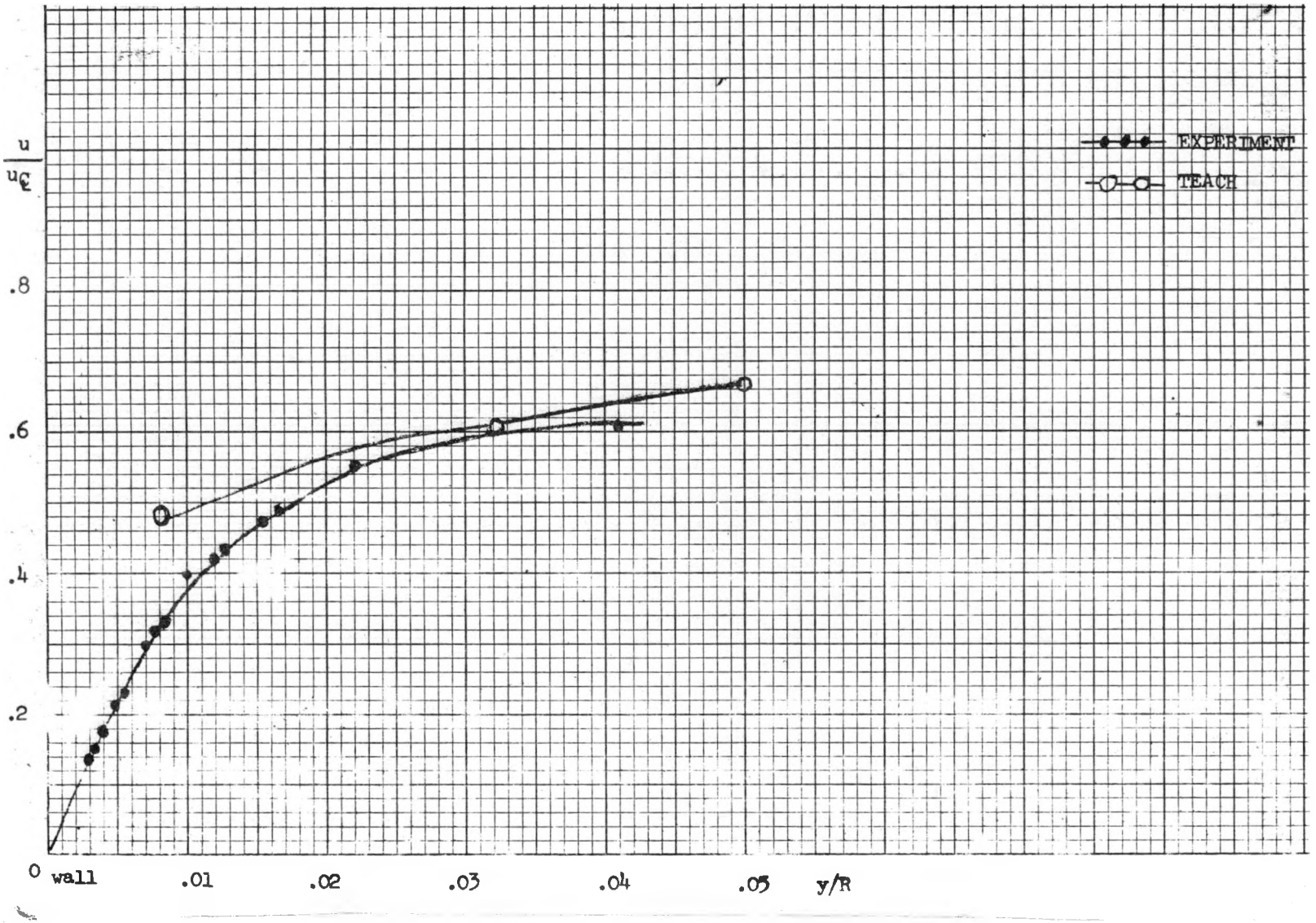

FIGURE 13. Velocity Profile (Laufer). RE = 50,000.
KS-76177

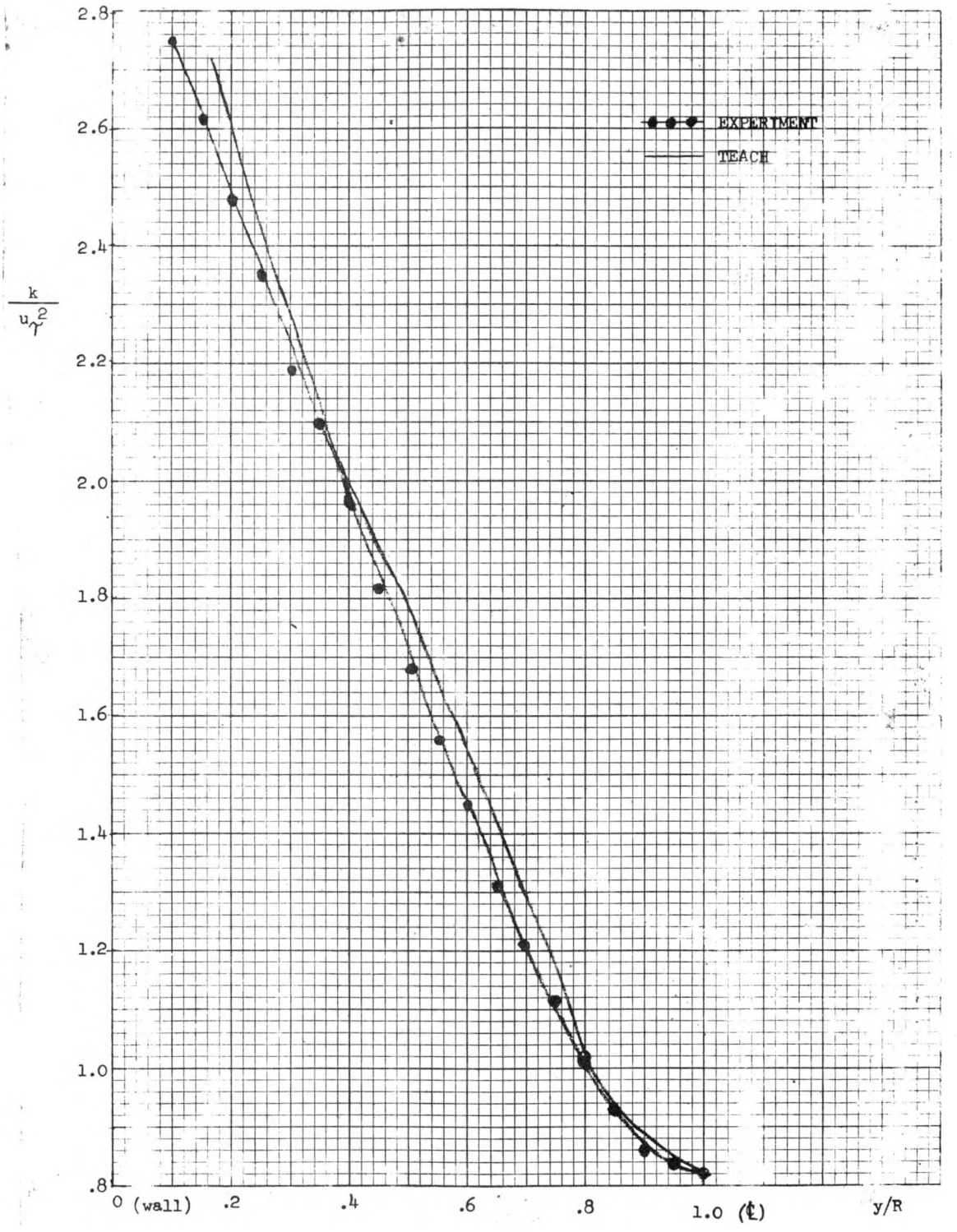

FIGURE 14. Turbulent Kinetic Energy (Laufer).
RE = 50,000.

KS-76178

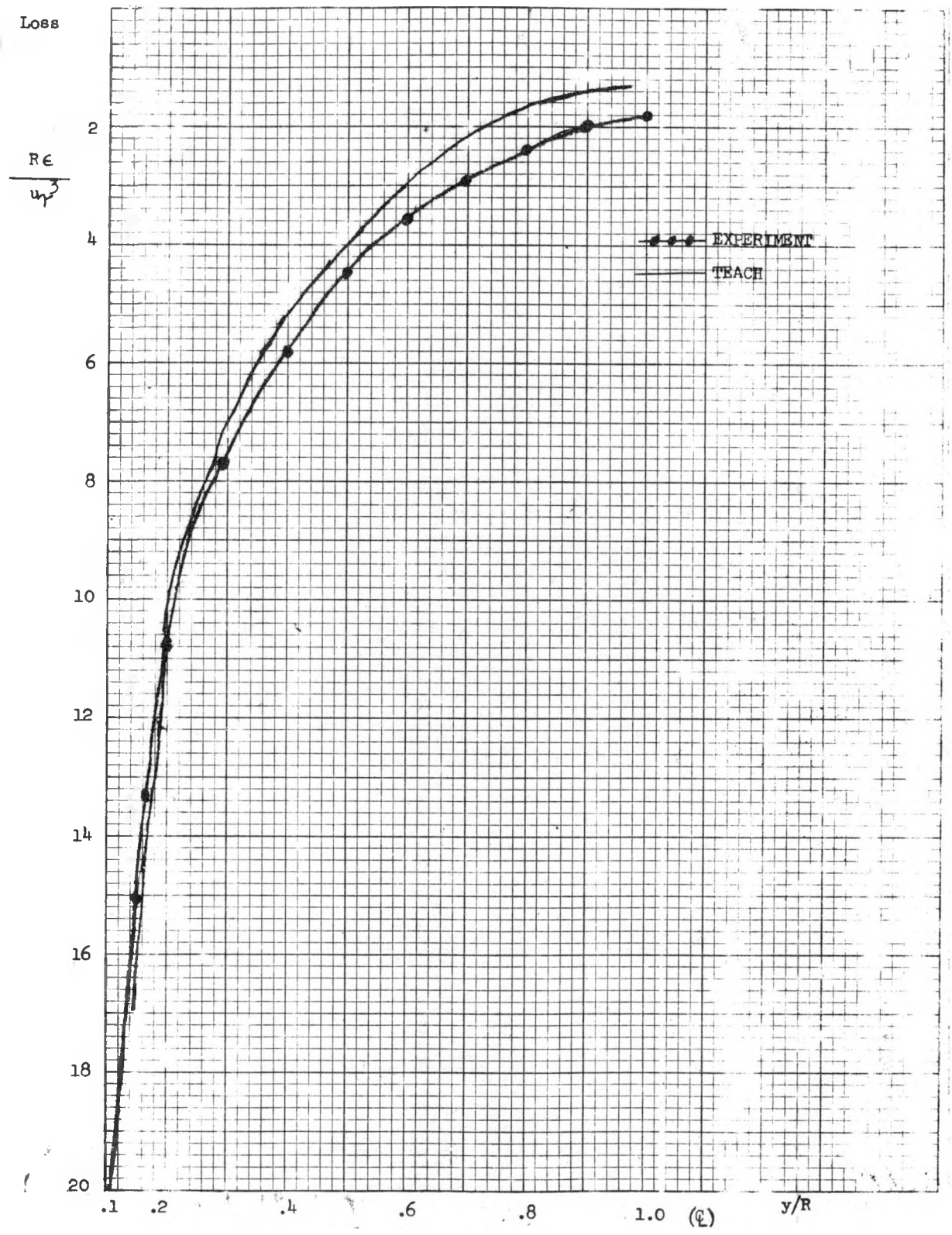

FIGURE 15. Turbulence Dissipation (Laufer). RE = 50,000.
KS-76179

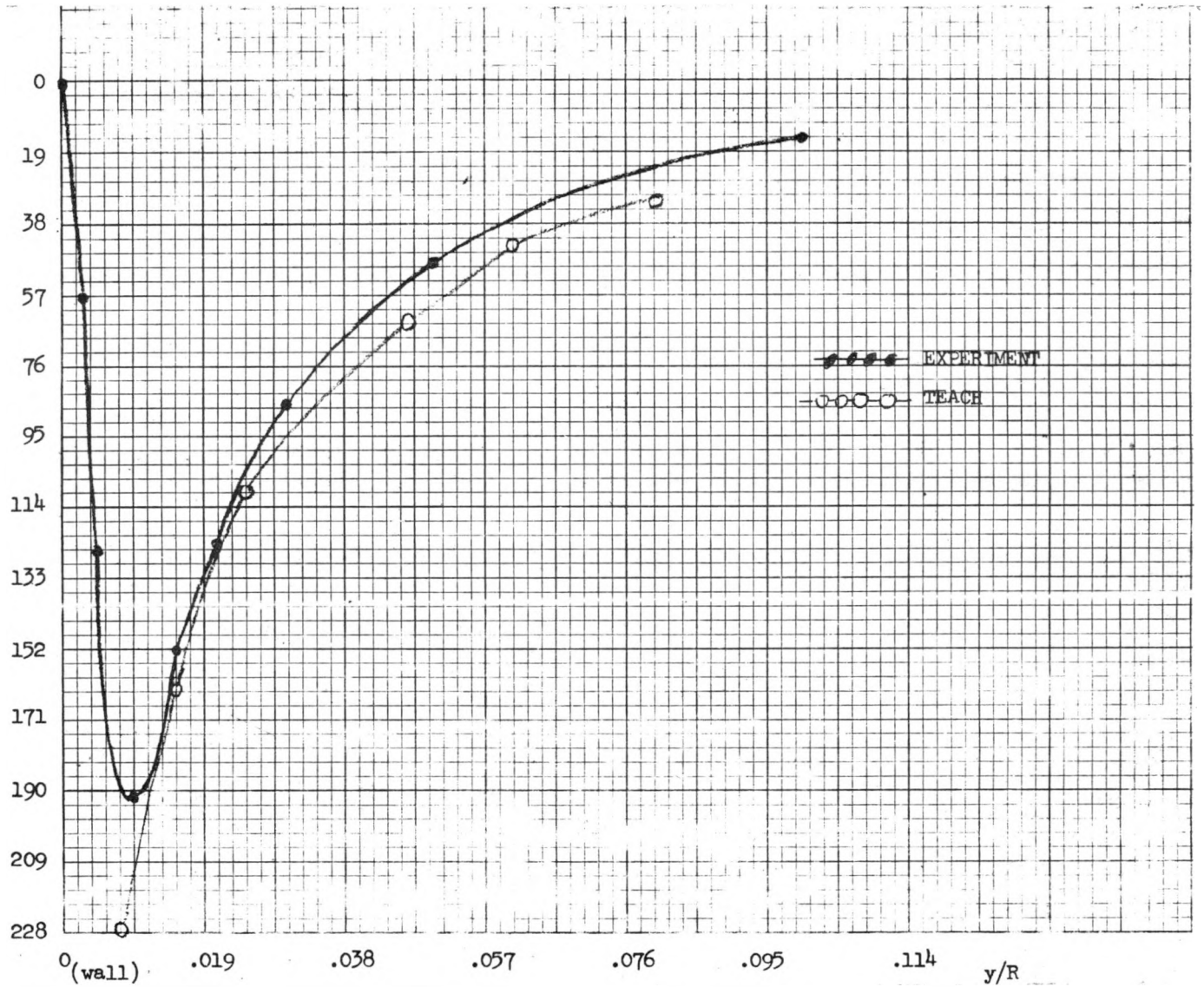

FIGURE 16. Turbulence Dissipation (Laufer). RE = 50,000.
KS-76180

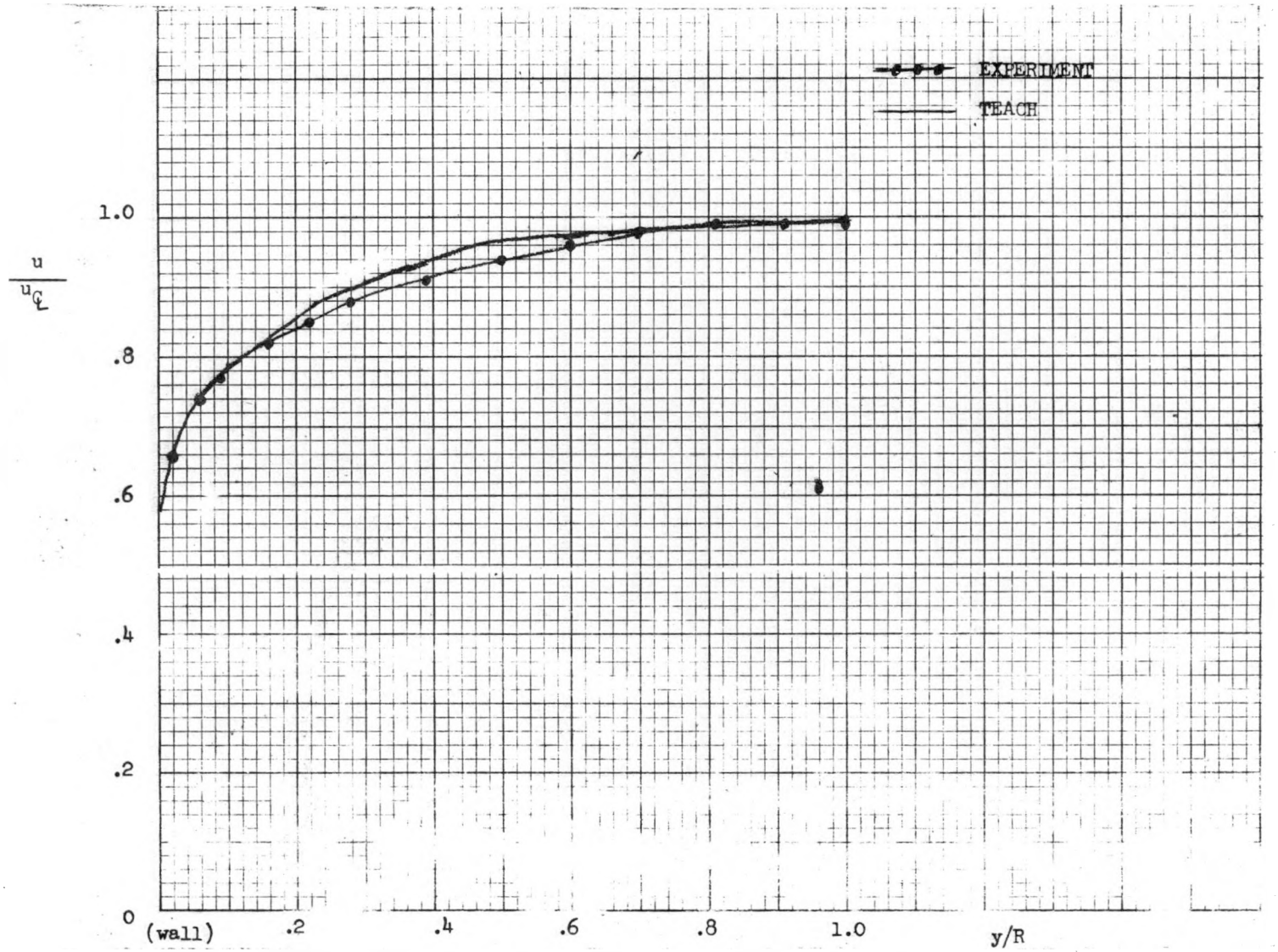

FIGURE 17. Velocity Profile (Laufer). RE = 500,000.
KS-76181

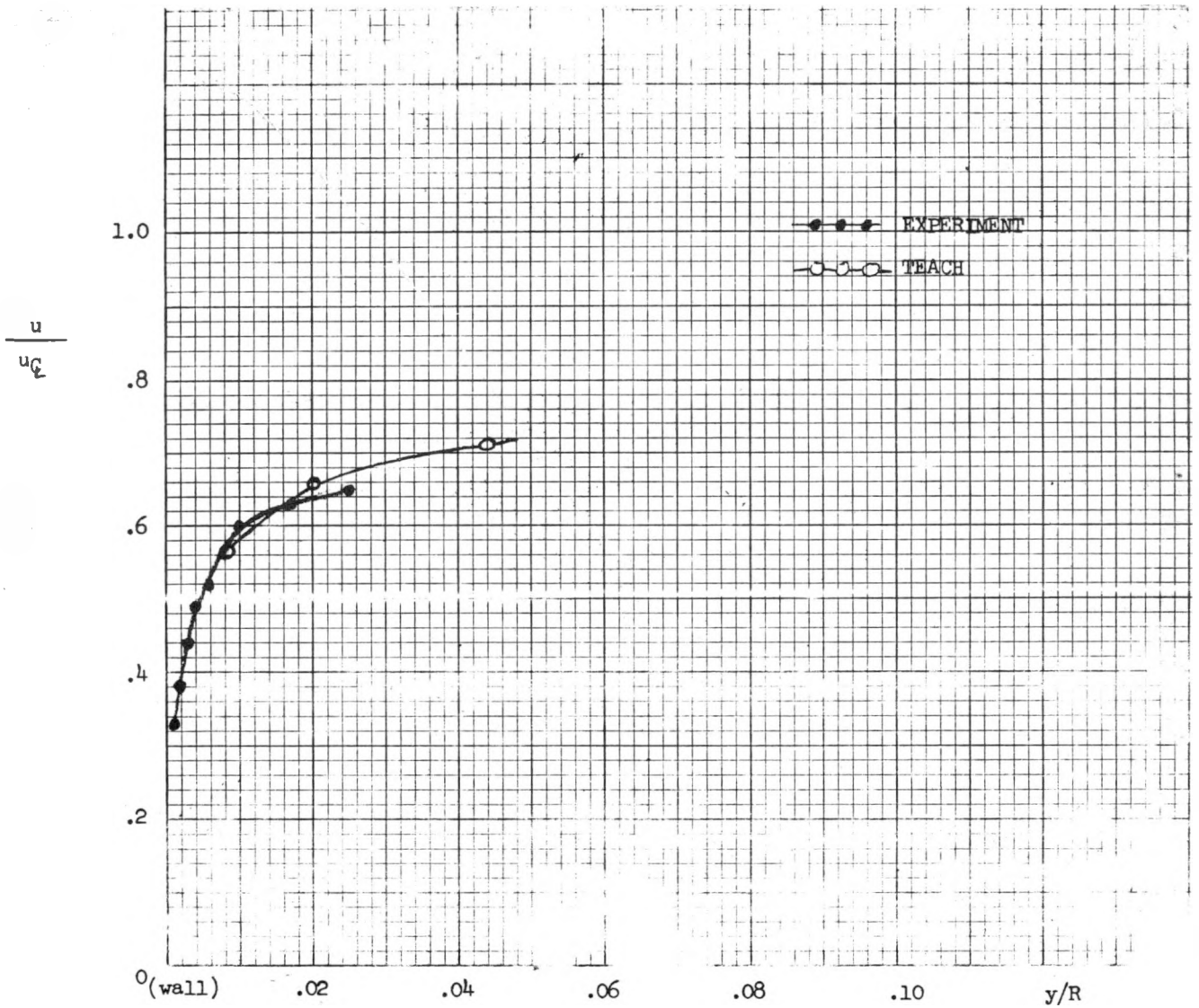

FIGURE 18. Velocity Profile (Laufer). RE = 500,000.
KS-76182

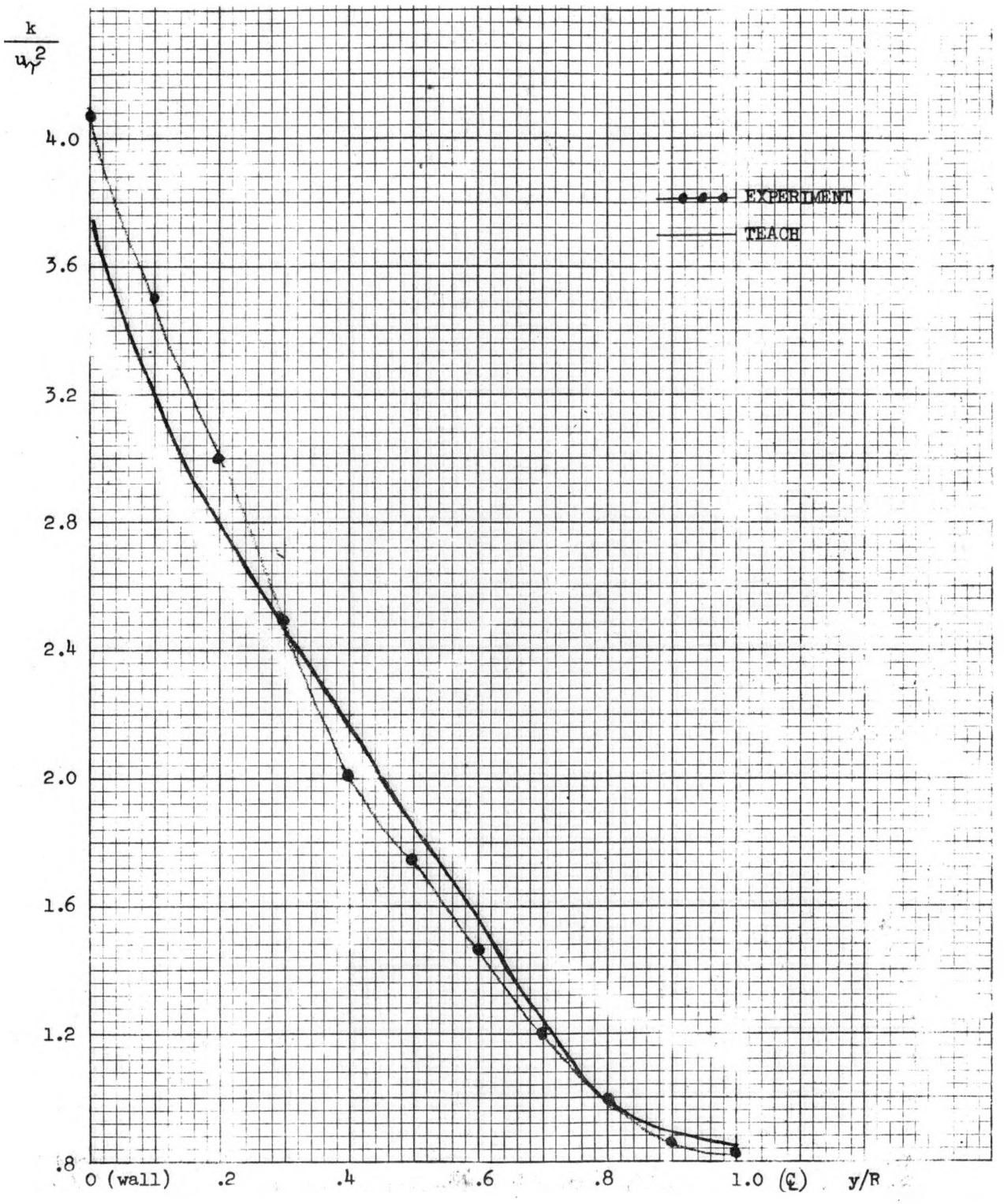

FIGURE 19. Turbulent Kinetic Energy (Laufer). RE = 500,000.
KS-76183

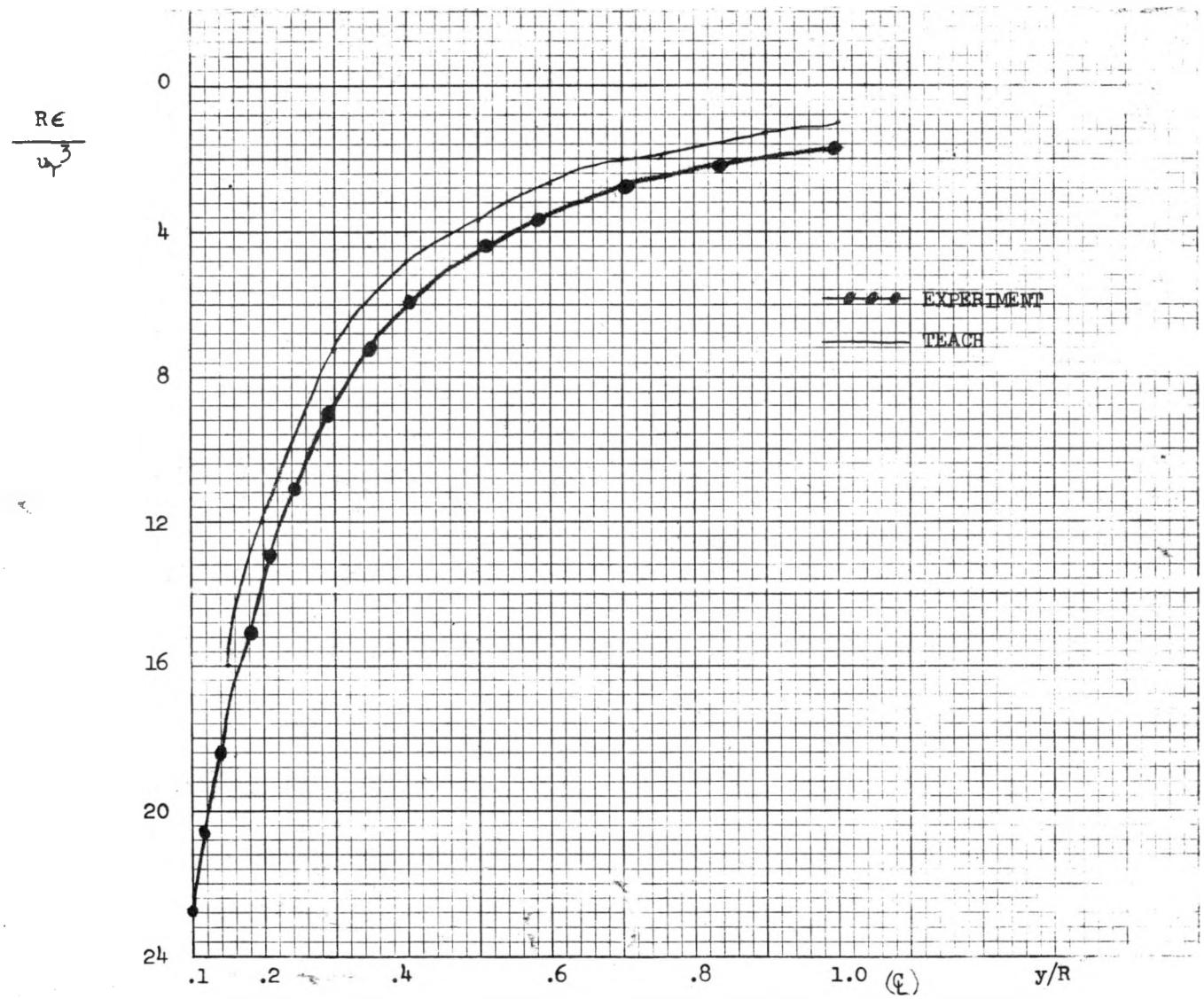

FIGURE 20. Turbulence Dissipation (Laufer). RE = 500,000.
KS-76184

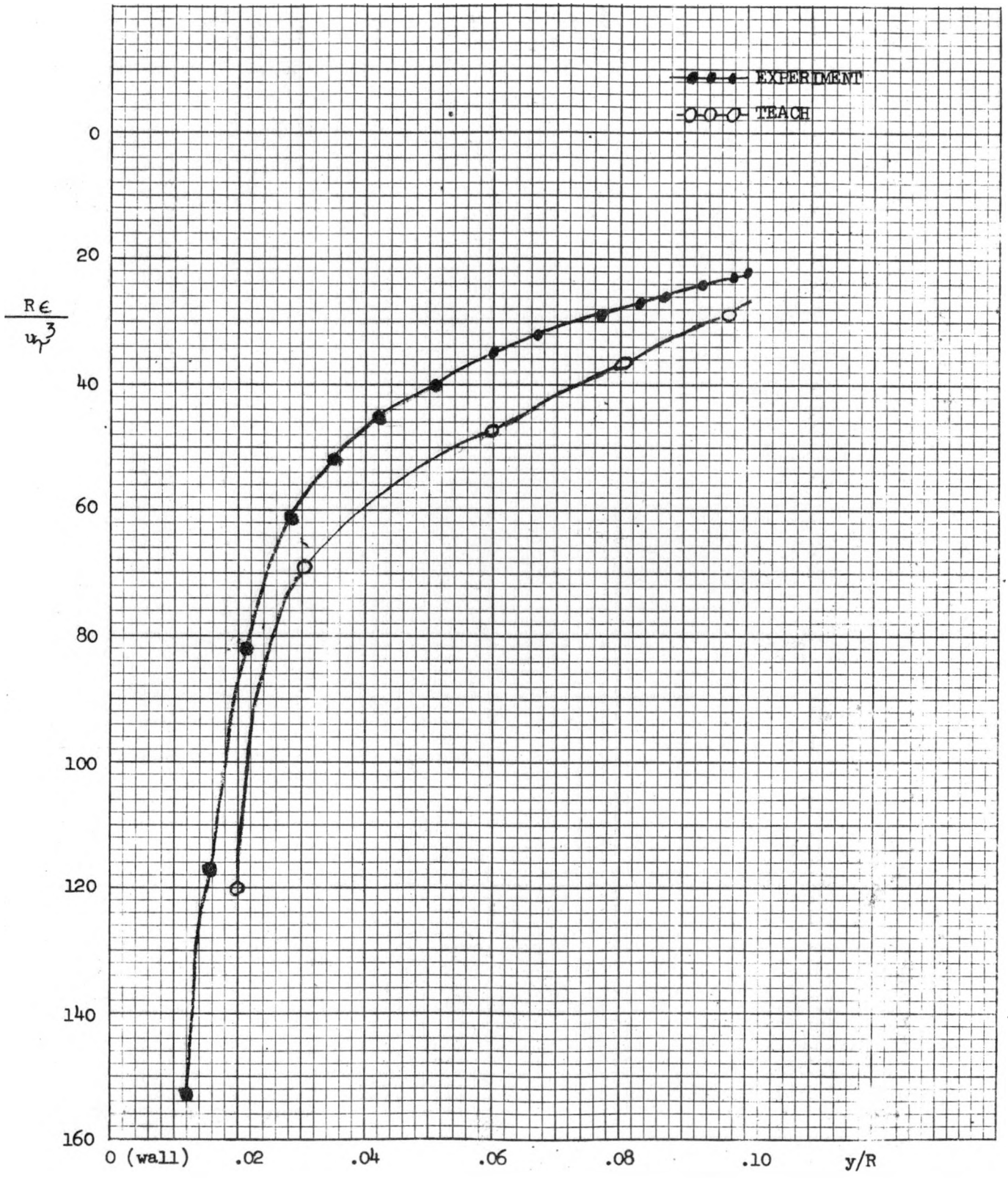

FIGURE 21. Turbulence Dissipation (Laufer). RE = 500,000.
KS-76185

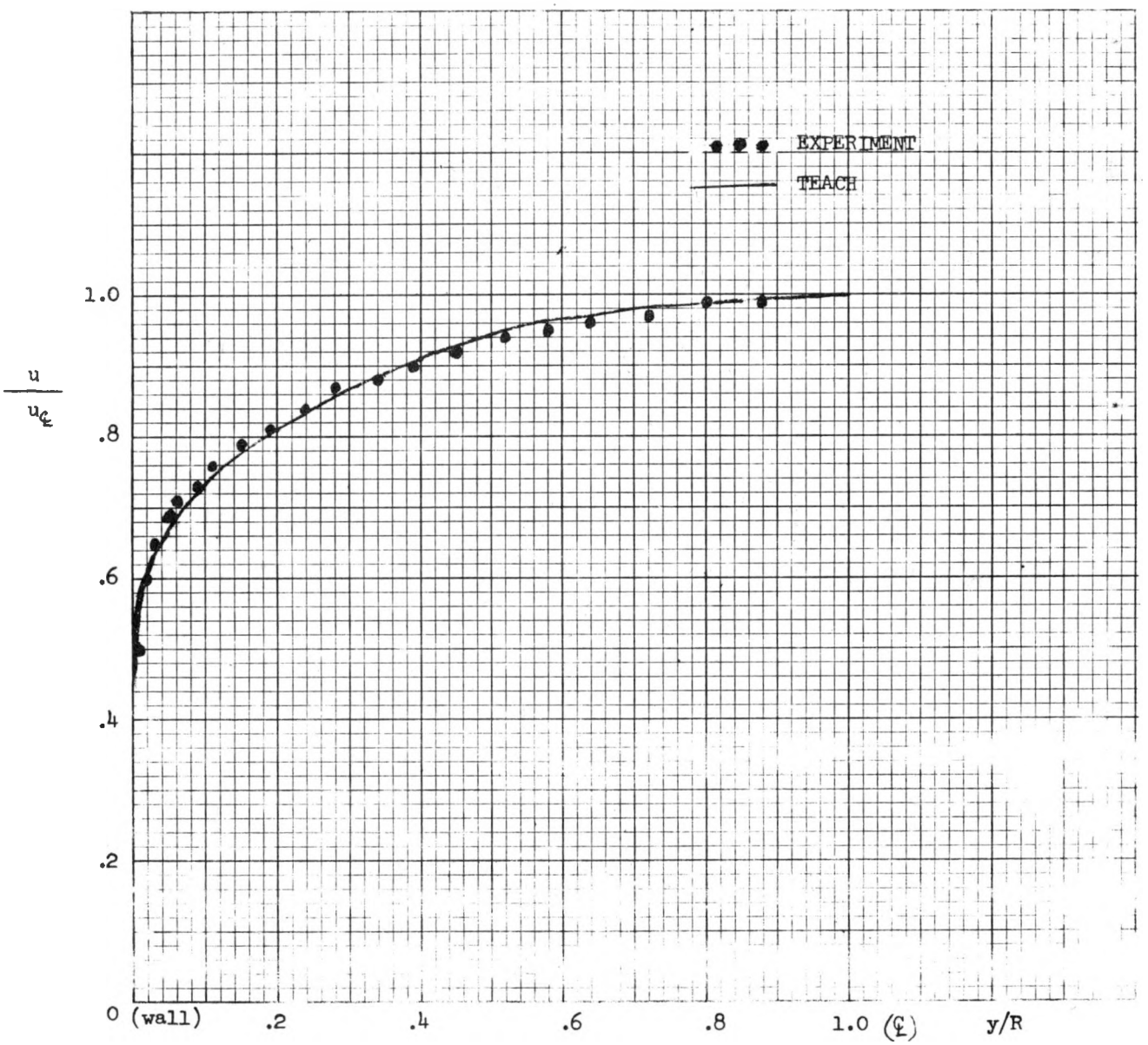

FIGURE 22. Velocity Profile (Hussain-Reynolds). RE = 64,600.
KS-76186

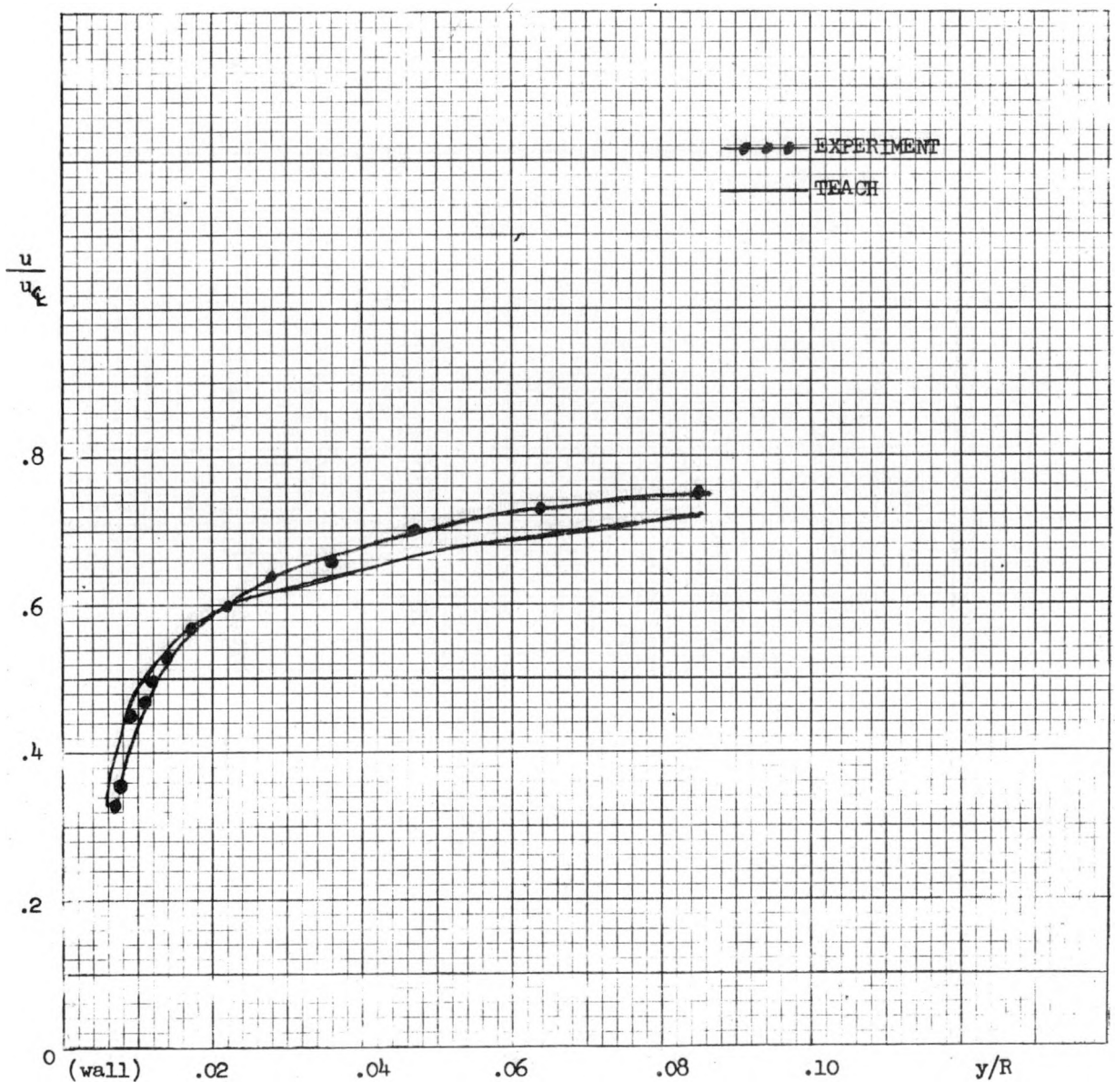

FIGURE 23. Velocity Profile (Hussain-Reynolds). RE = 64,600.
KS-76187

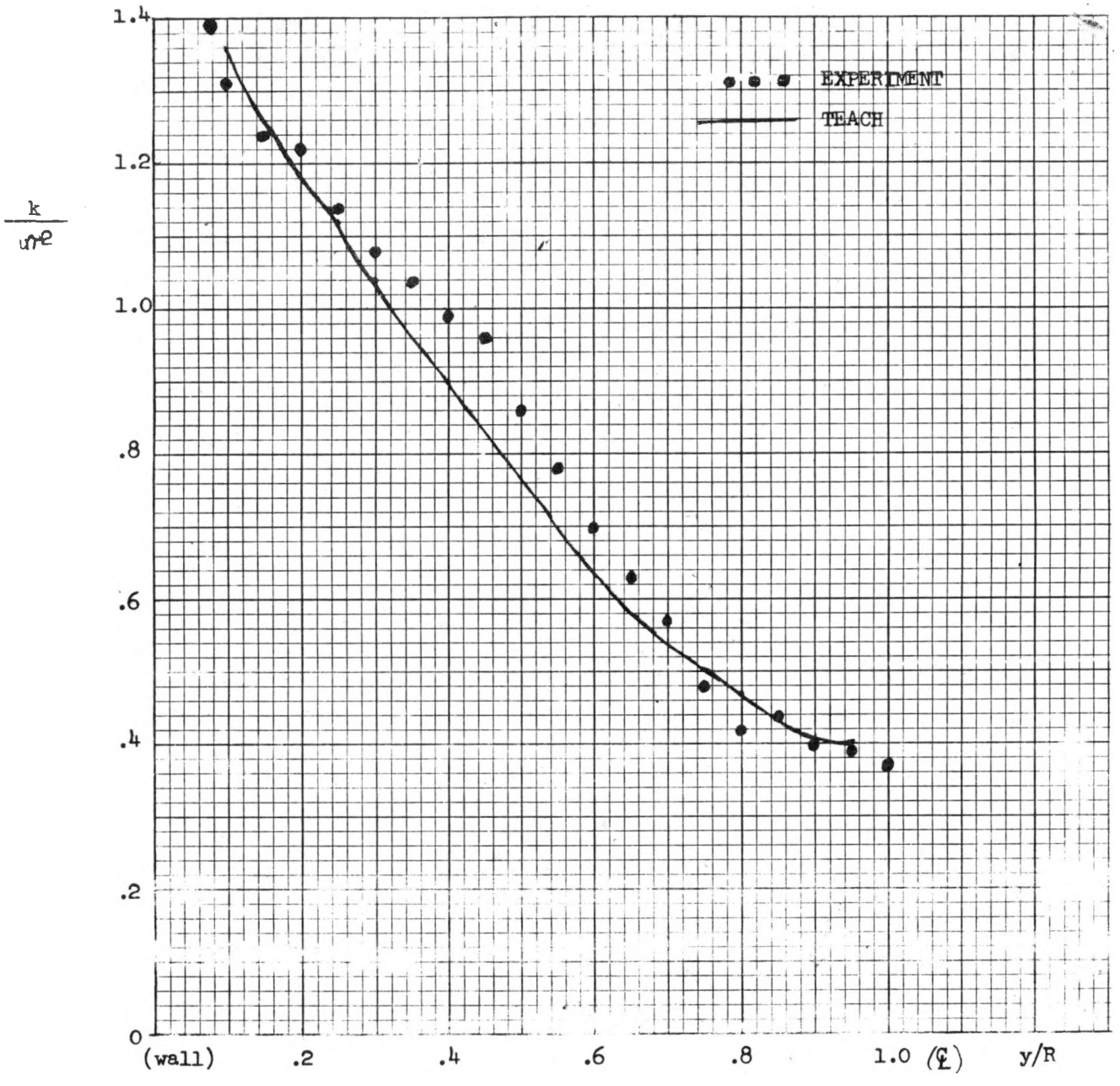

FIGURE 24. Turbulent Kinetic Energy (Hussain-Reynolds). RE = 64,600.
KS-76188

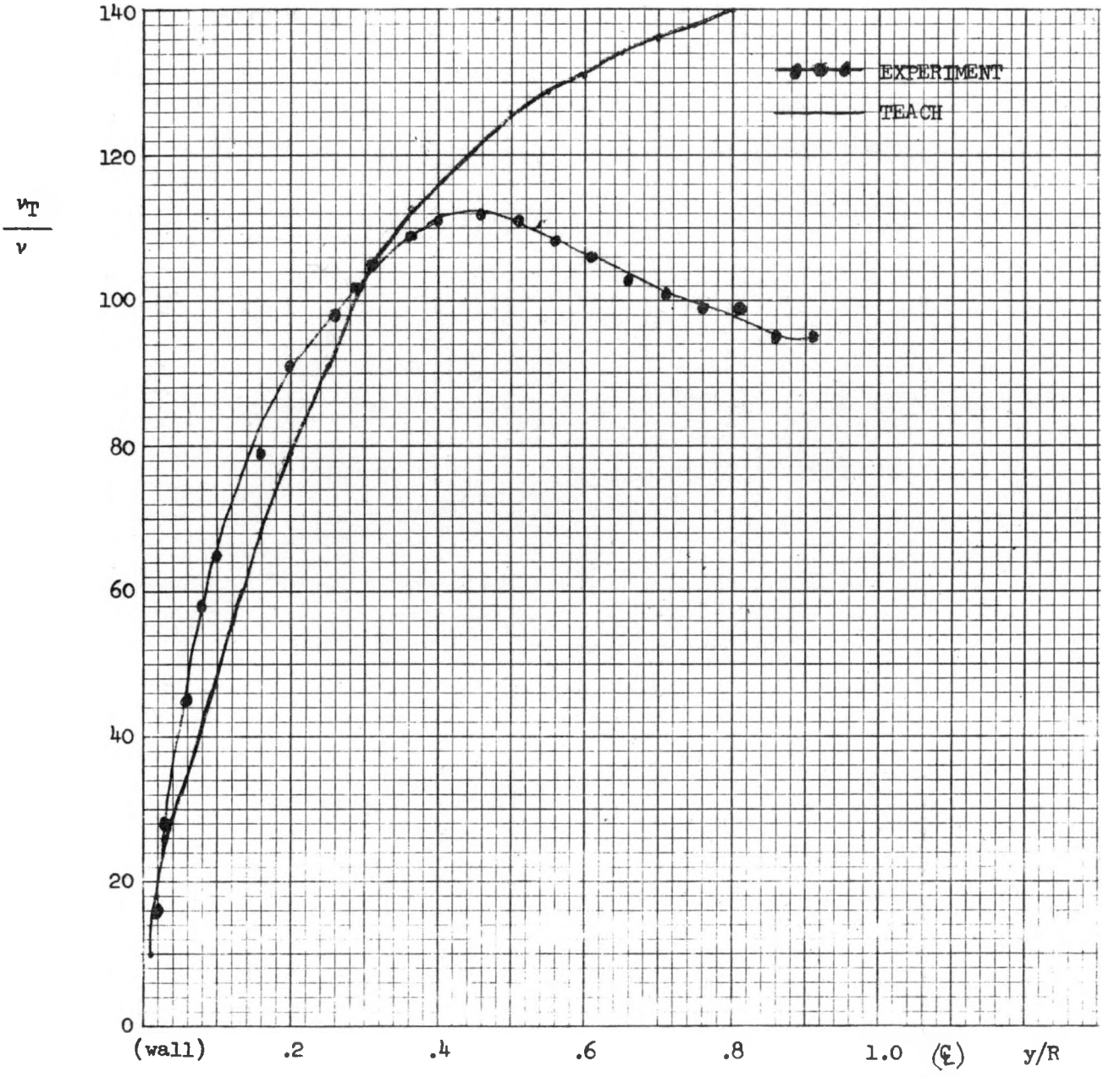

FIGURE 25. Turbulent Viscosity (Hussain-Reynolds). RE = 64,600.
KS-76189

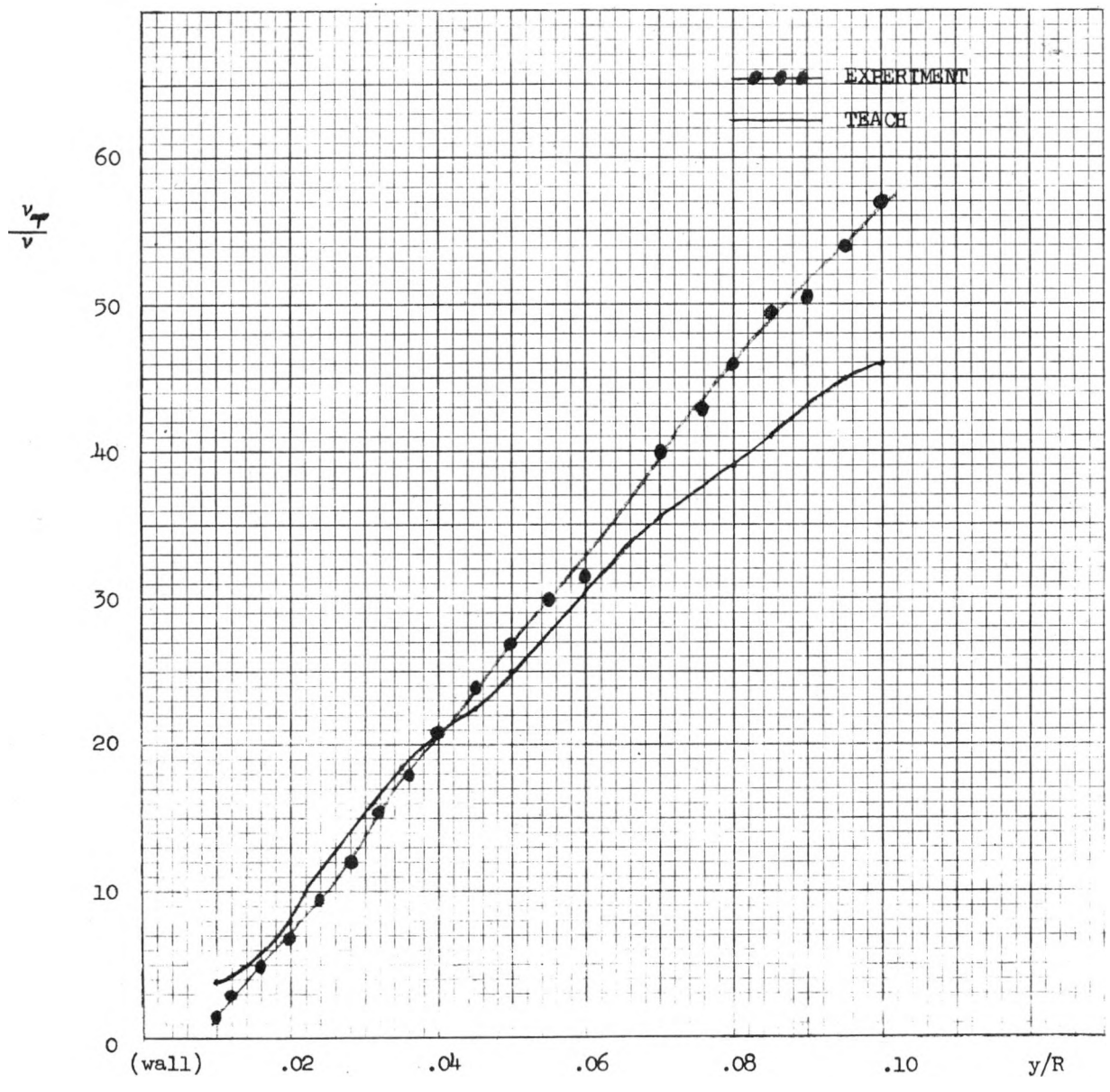

FIGURE 26. Turbulent Viscosity (Hussain-Reynolds). RE = 64,600.
KS-76190

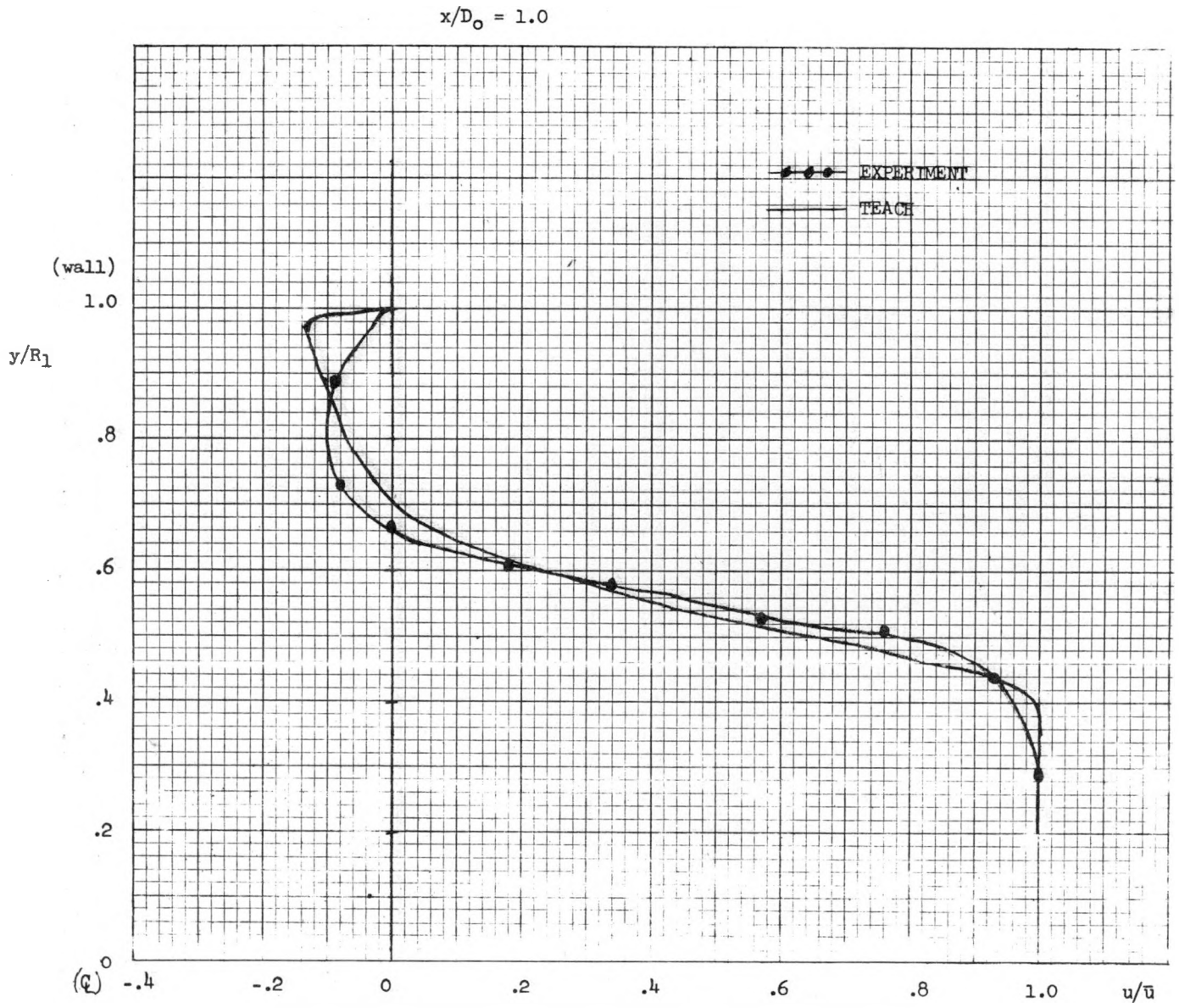

FIGURE 27. Velocity Profile (Chaturvedi). RE = 200,000.
KS-76191

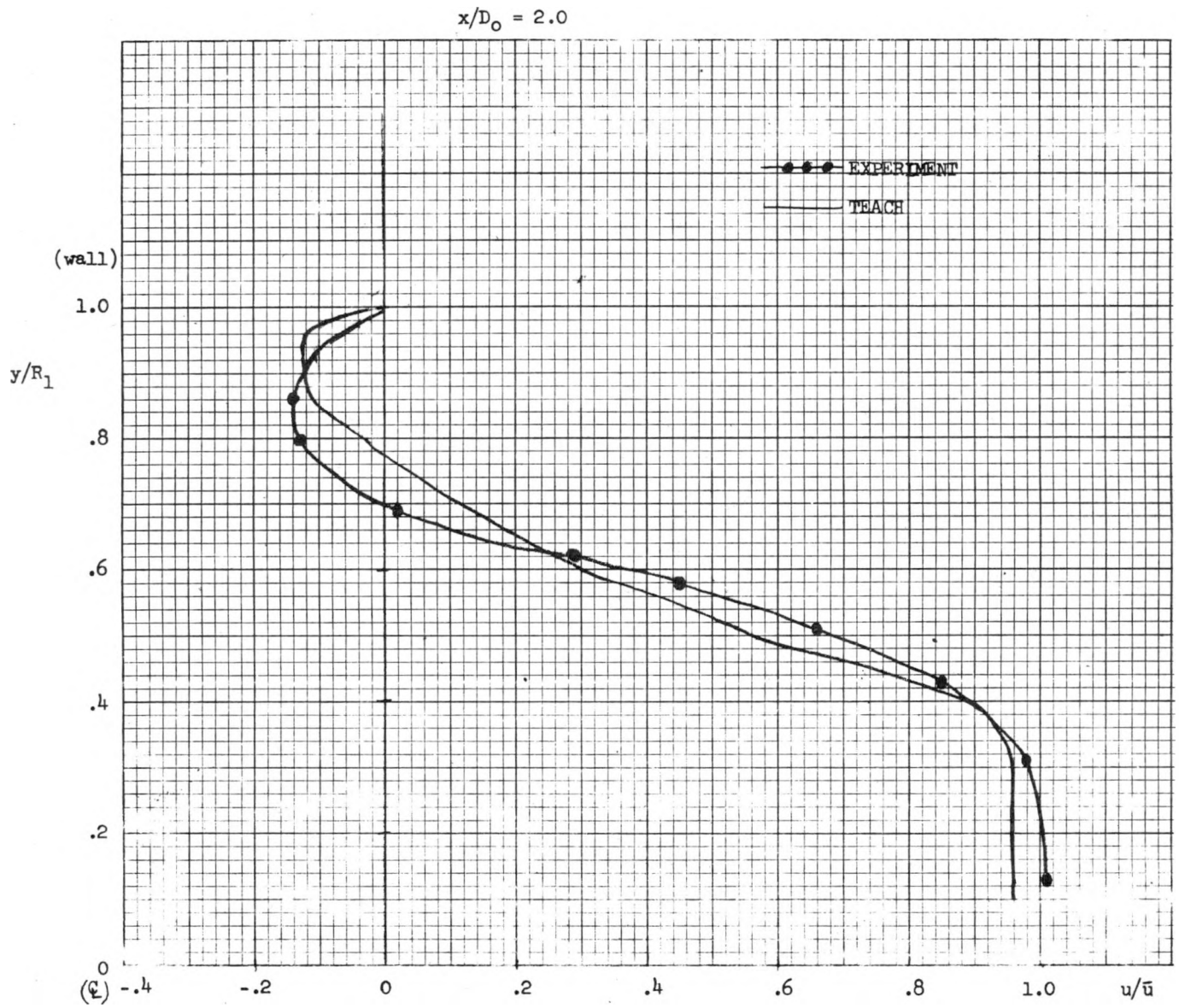

FIGURE 28. Velocity Profile (Chaturvedi). RE = 200,000.
KS-76192

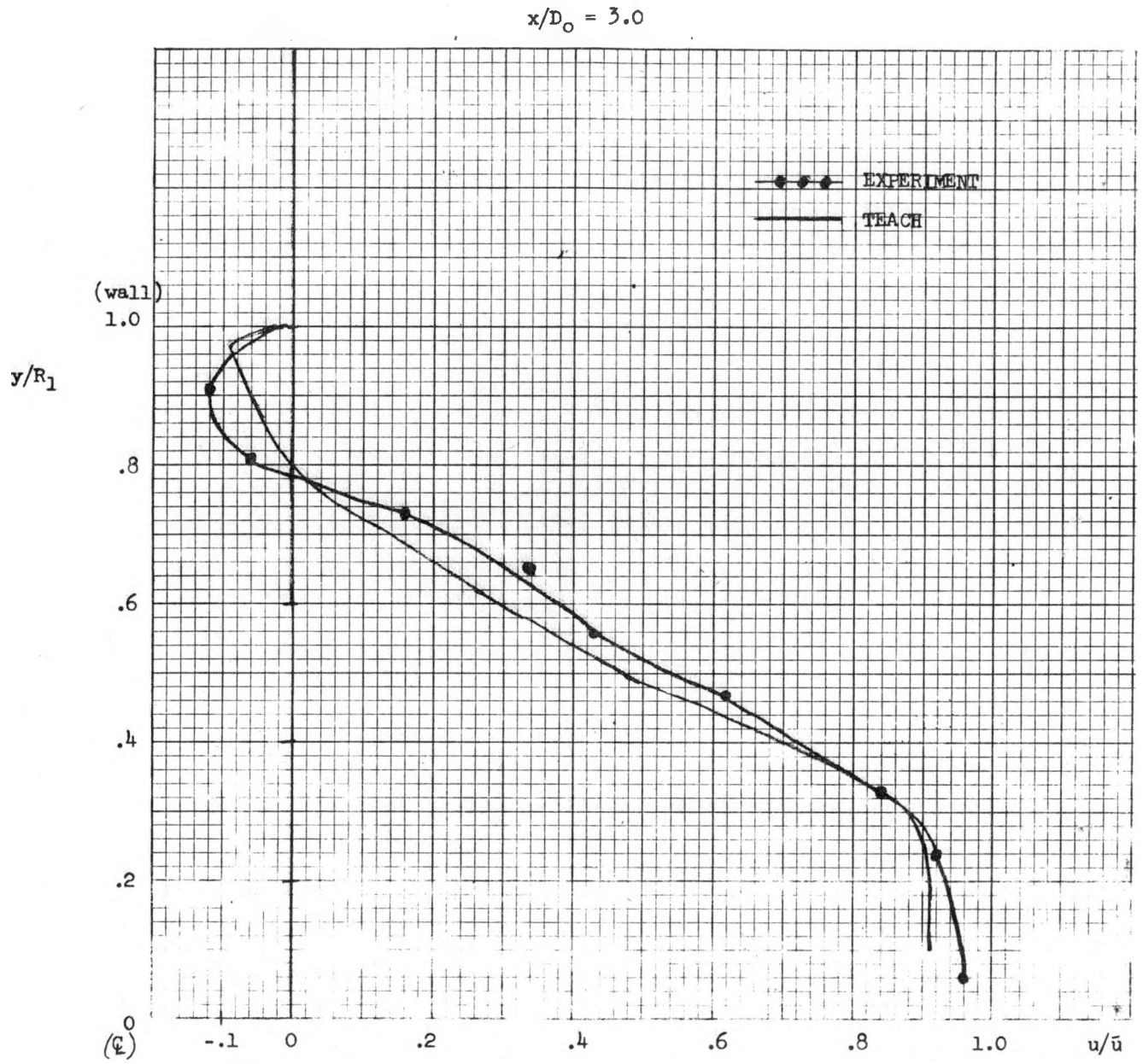

FIGURE 29. Velocity Profile (Chaturvedi). RE = 200,000.
KS-76193

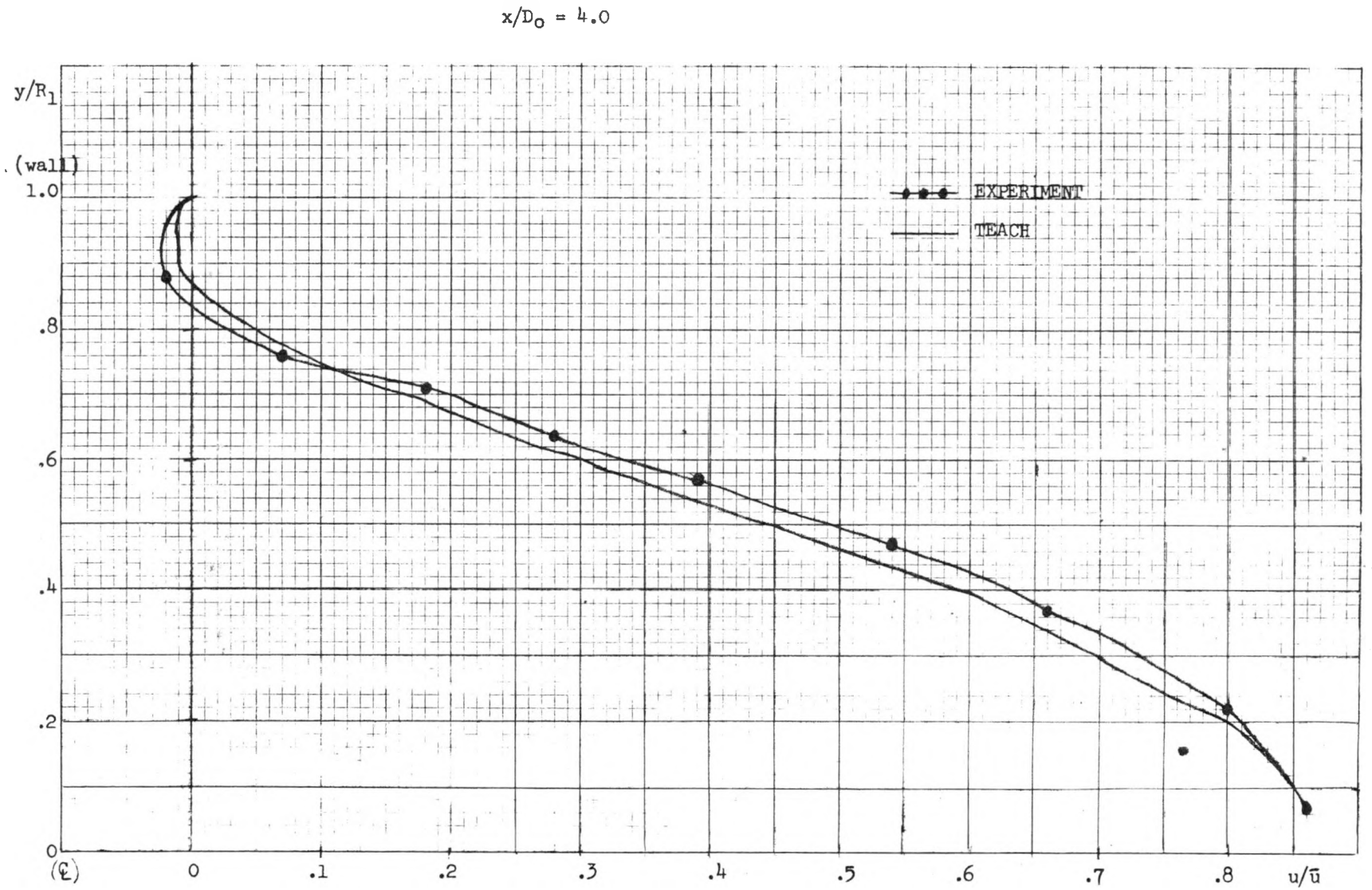

FIGURE 30. Velocity Profile (Chaturvedi). RE = 200,000.
KS-76194

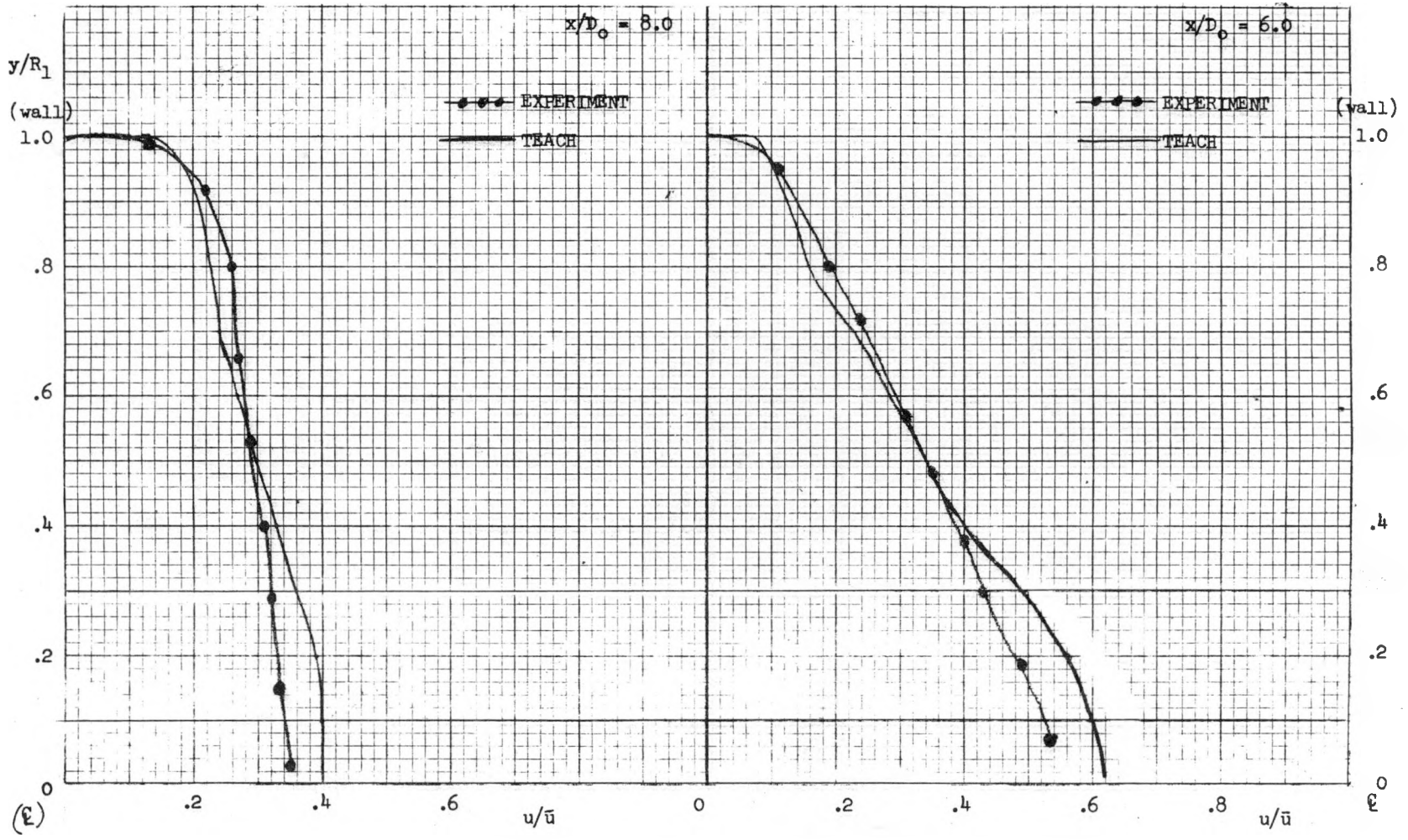

FIGURE 31. Velocity Profile (Chaturvedi). RE = 200,000.
KS-76195

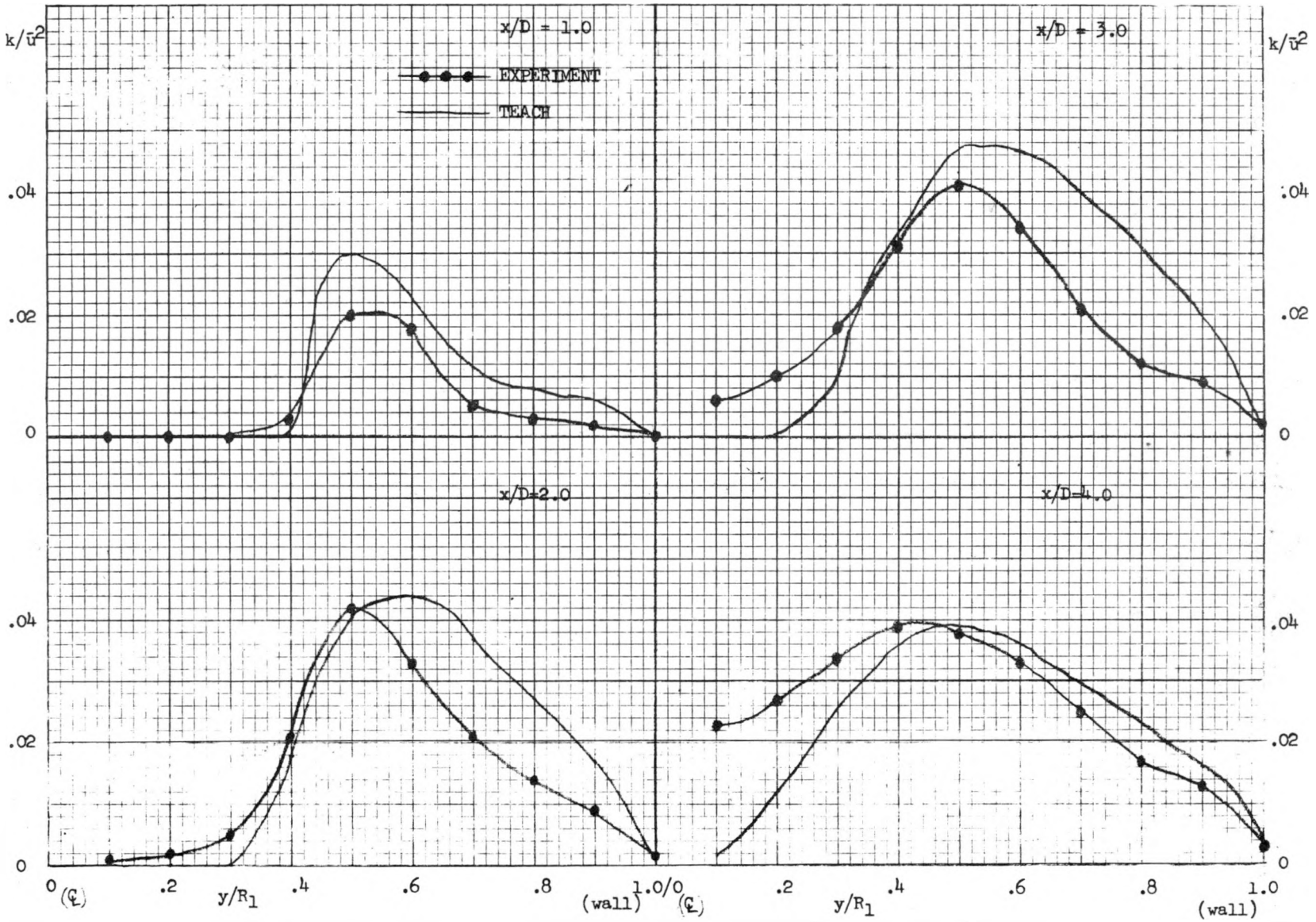

FIGURE 32. Turbulent Kinetic Energy (Chaturvedi). RE = 200,000.
KS-76196

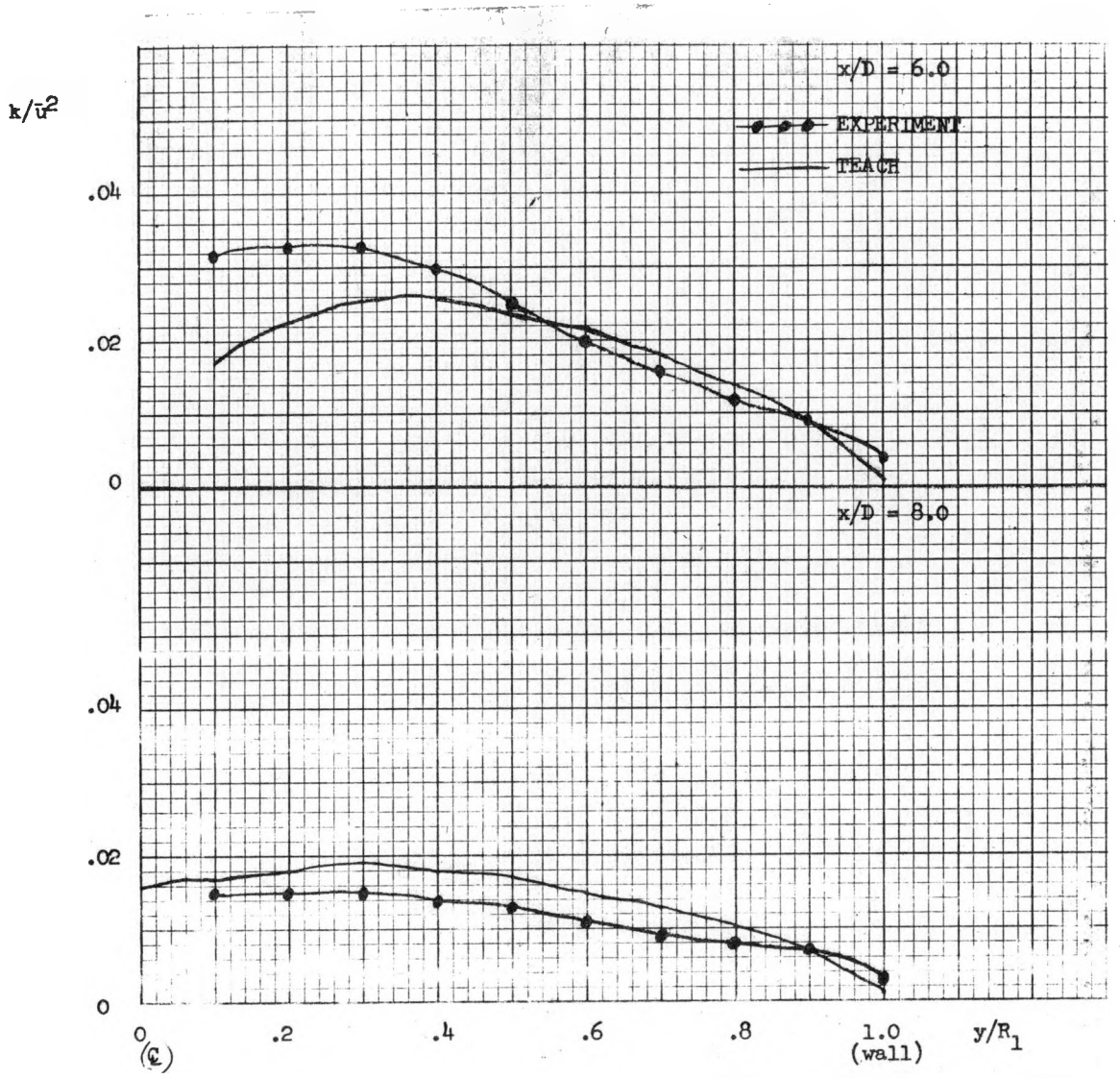

FIGURE 33. Turbulent Kinetic Energy (Chaturvedi). RE = 200,000.
KS-76197

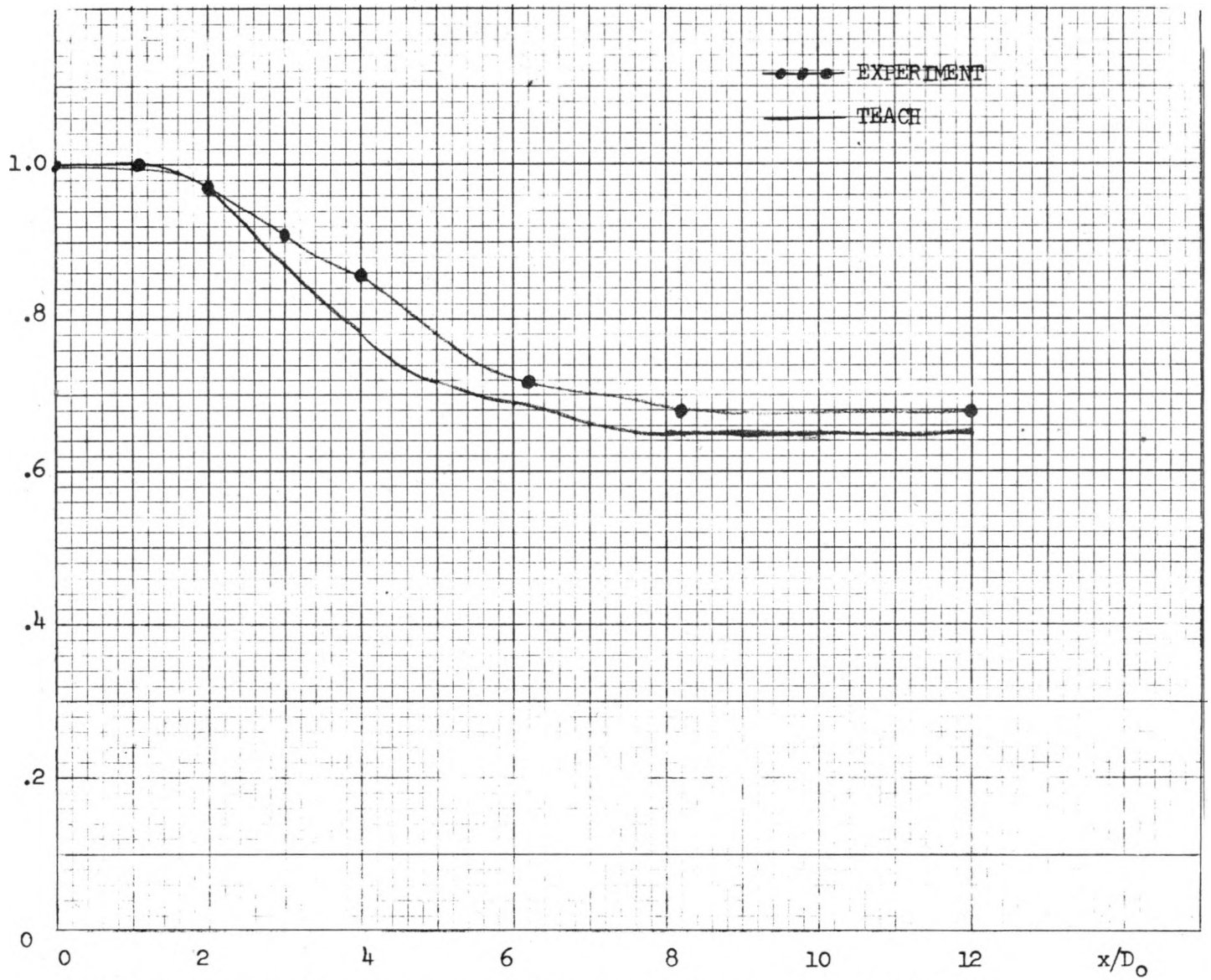

FIGURE 34. Centerline Pressure Profile (Chaturvedi). RE = 200,000.
KS-76198

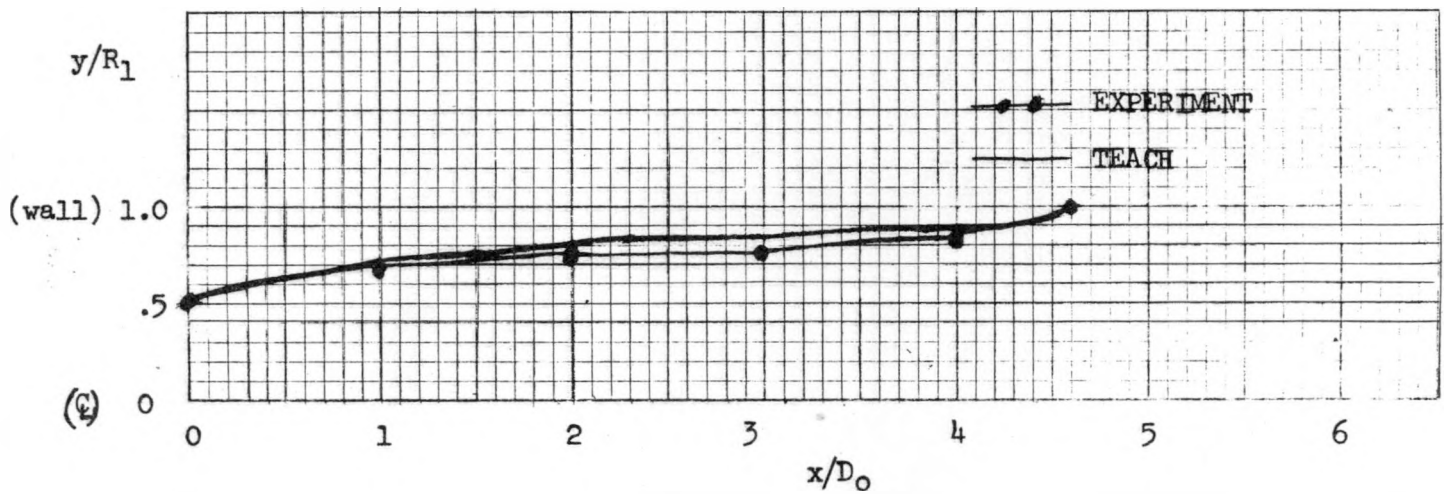

FIGURE 35. Contour of Zero u (Chaturvedi). RE = 200,000.
KS-76199

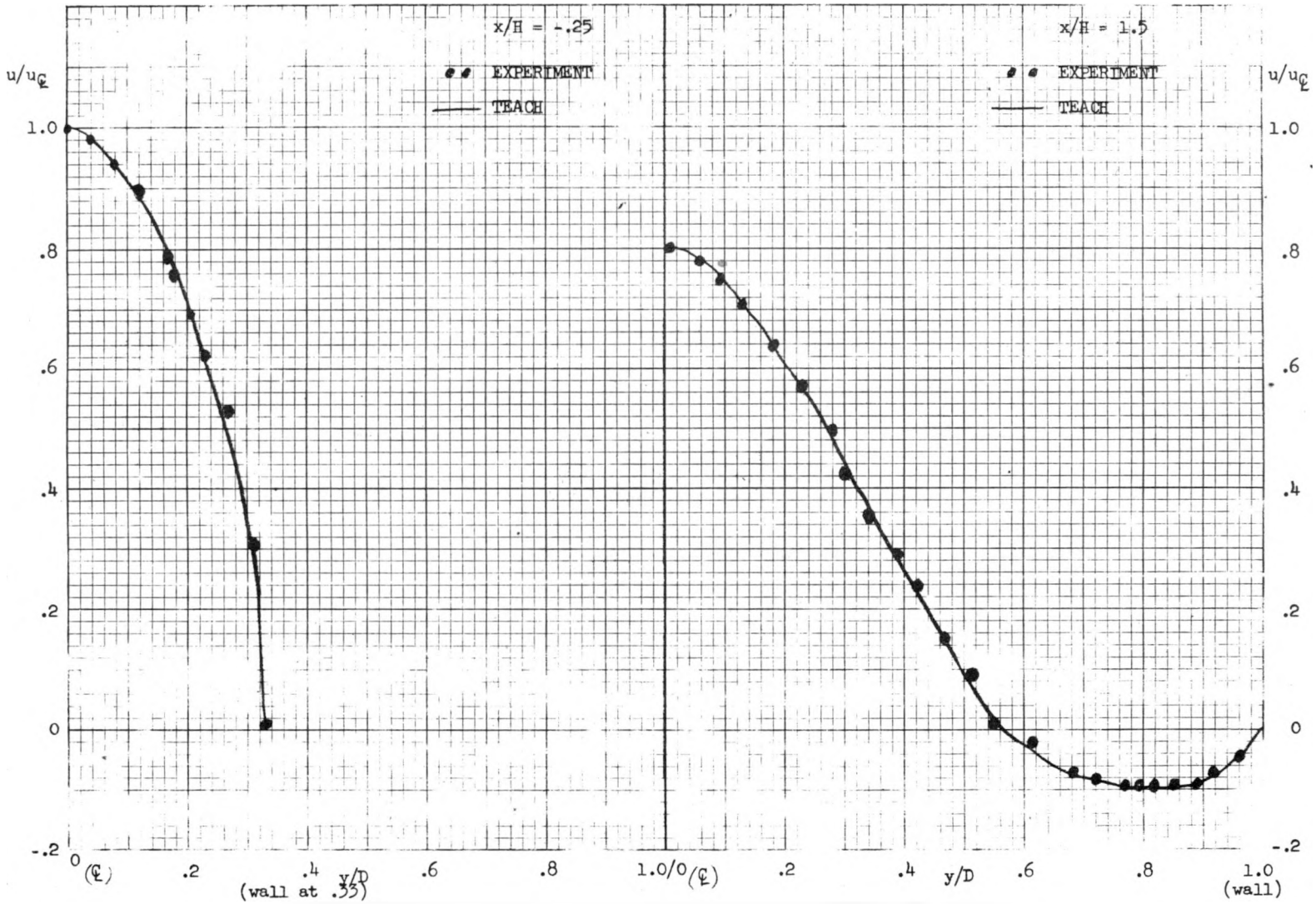

FIGURE 36. Velocity Profile (Durst). RE = 56.
KS-76200

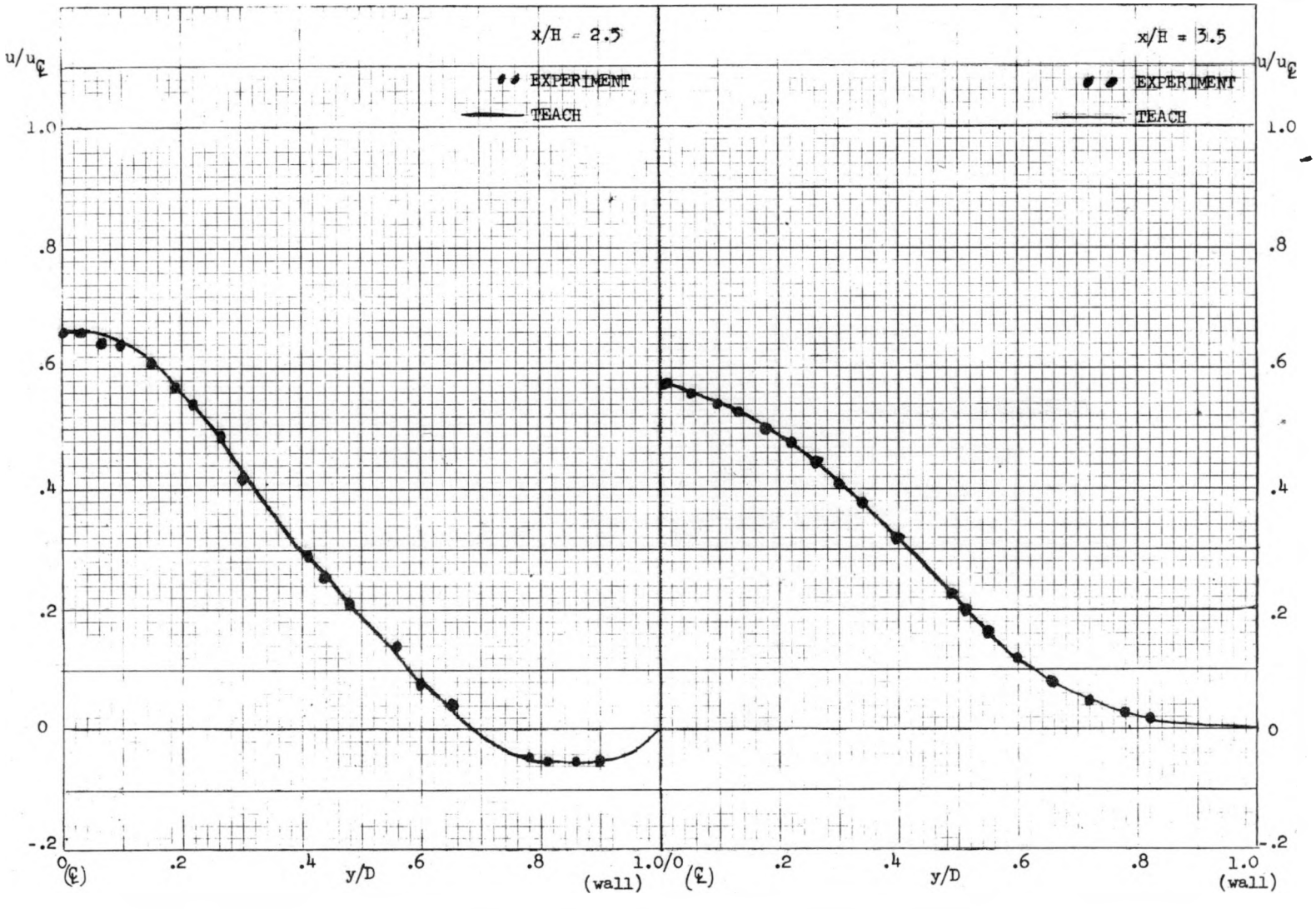

FIGURE 37. Velocity Profile (Durst). RE = 56.
KS-76201

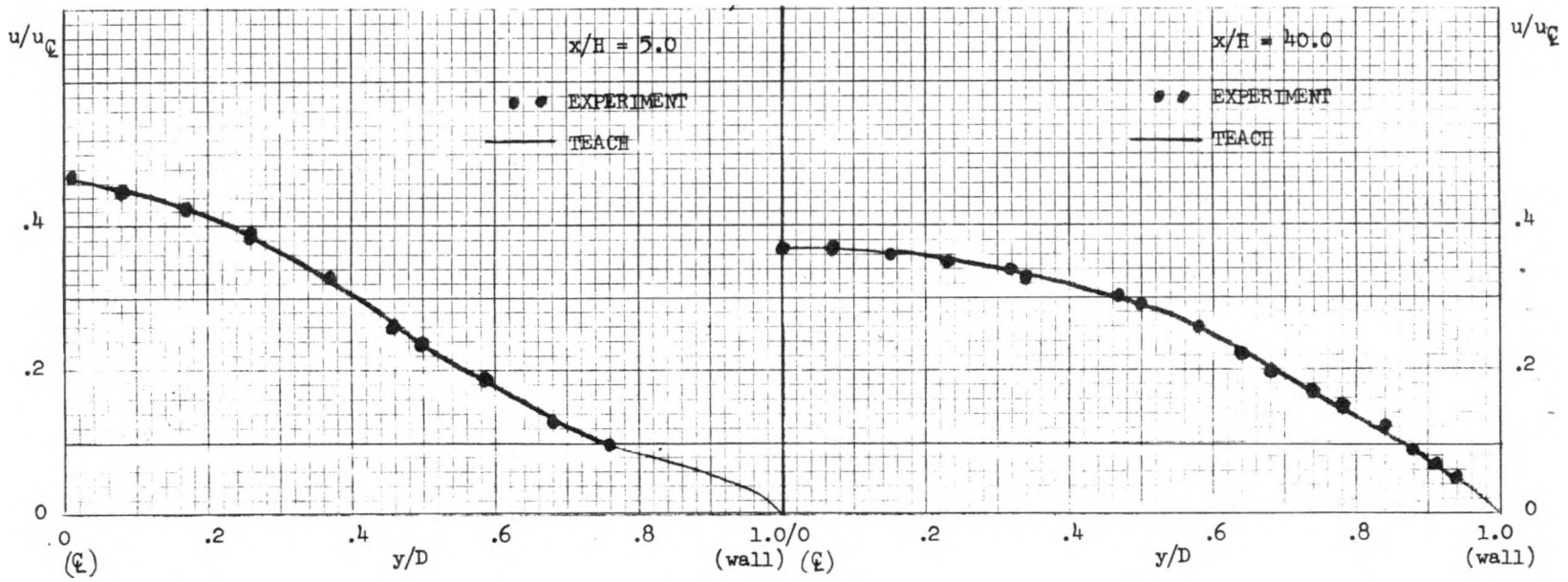

FIGURE 38. Velocity Profile (Durst). RE = 56.
KS-76202

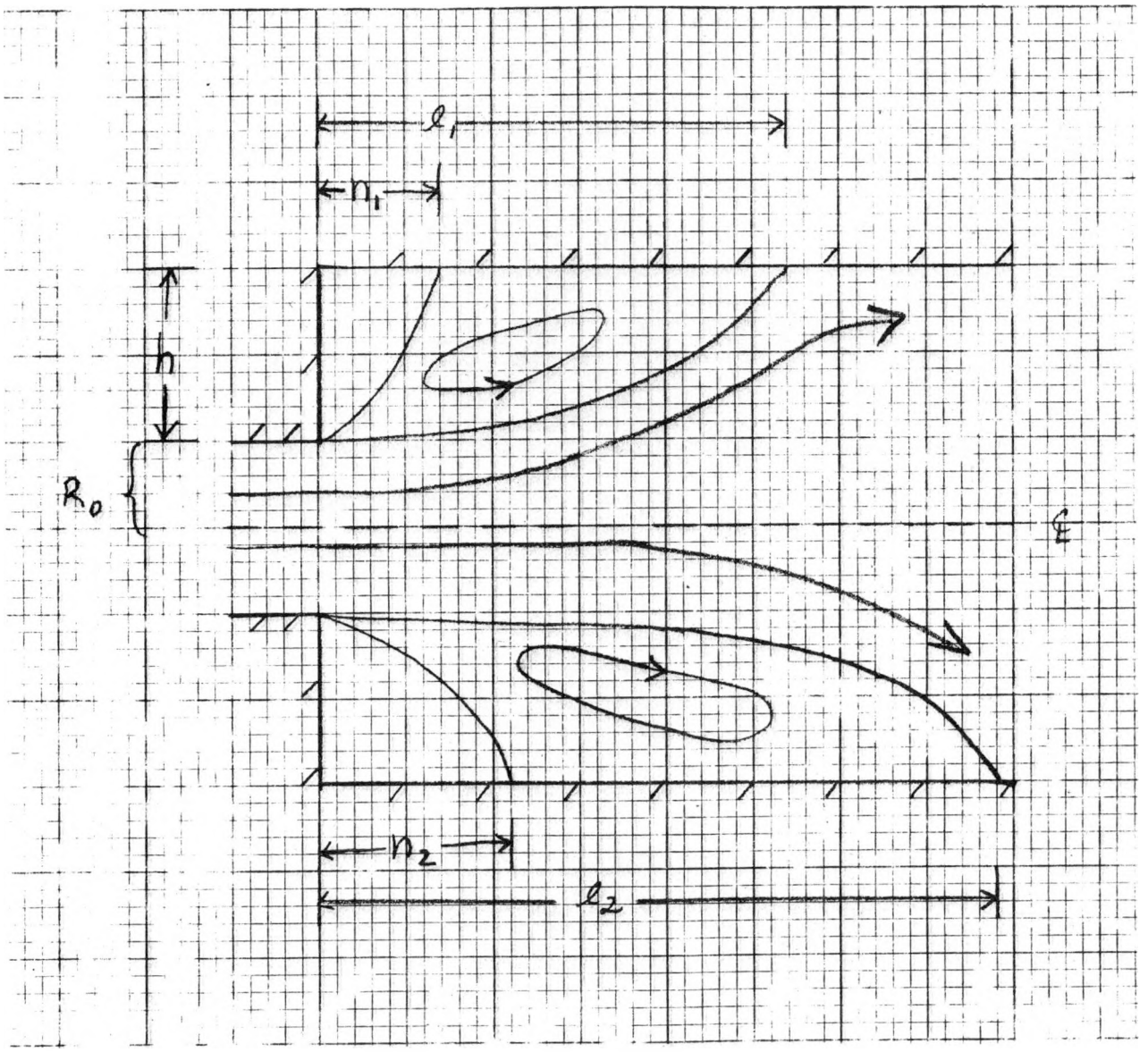

FIGURE 39. Flow Pattern in the Abbott and Kline Experiment.
KS-76203

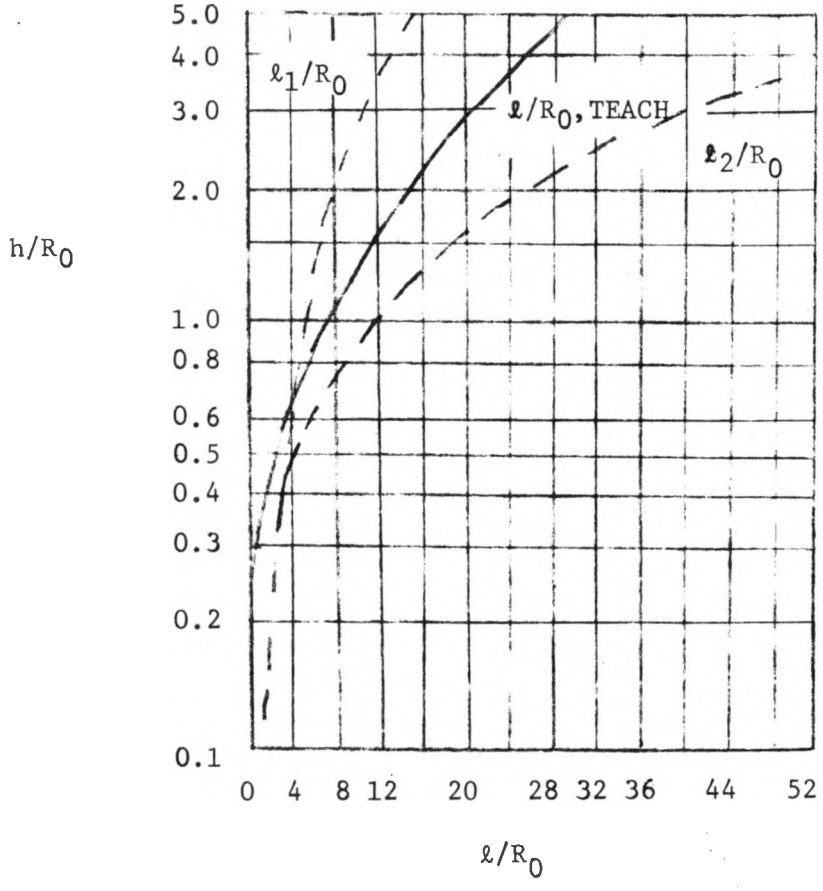

FIGURE 40. Reattachment Lengths.
KS-76204

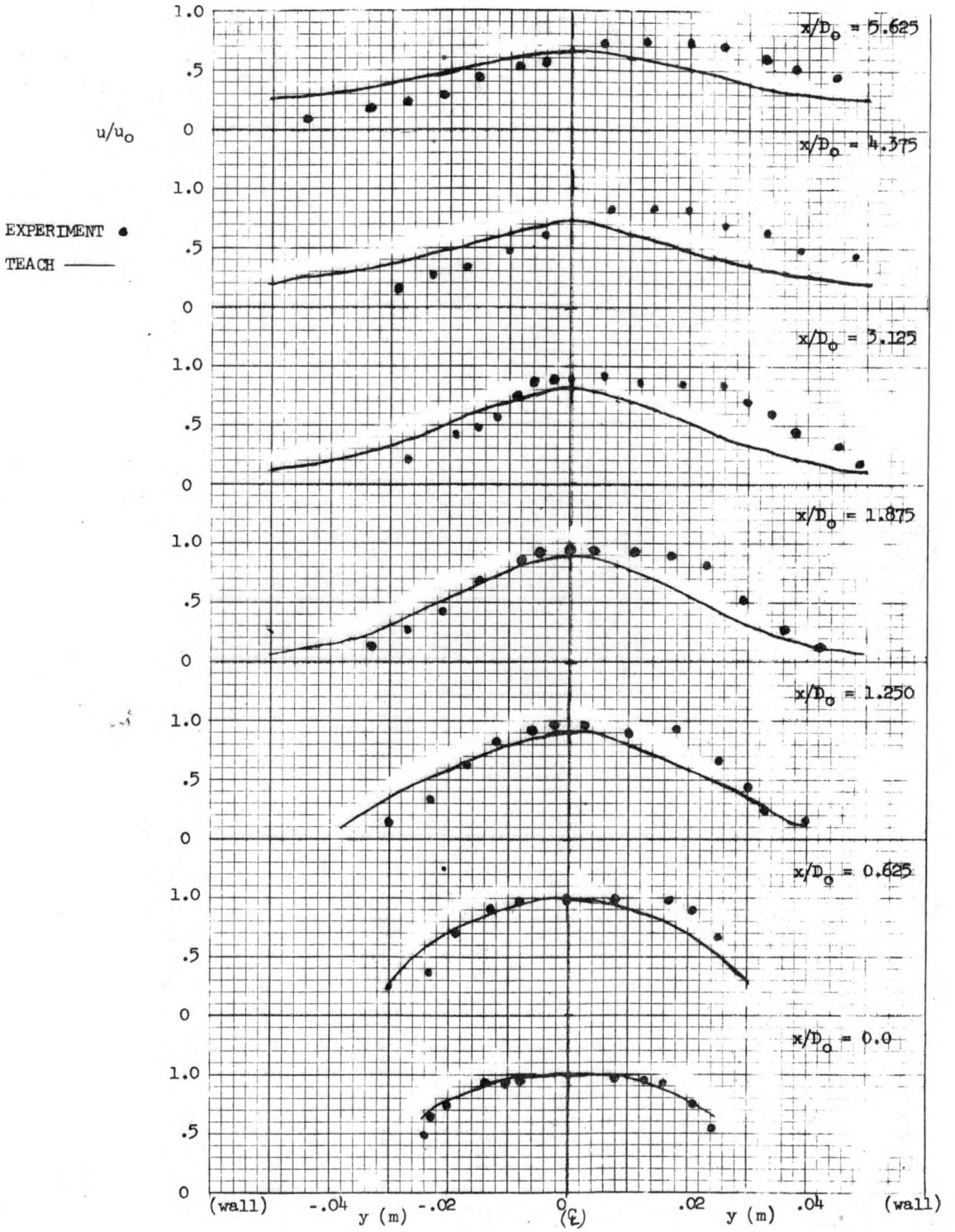

FIGURE 41. Velocity Profile, Double Step (Abbott and Kline). RE = 63,400.
KS-76205

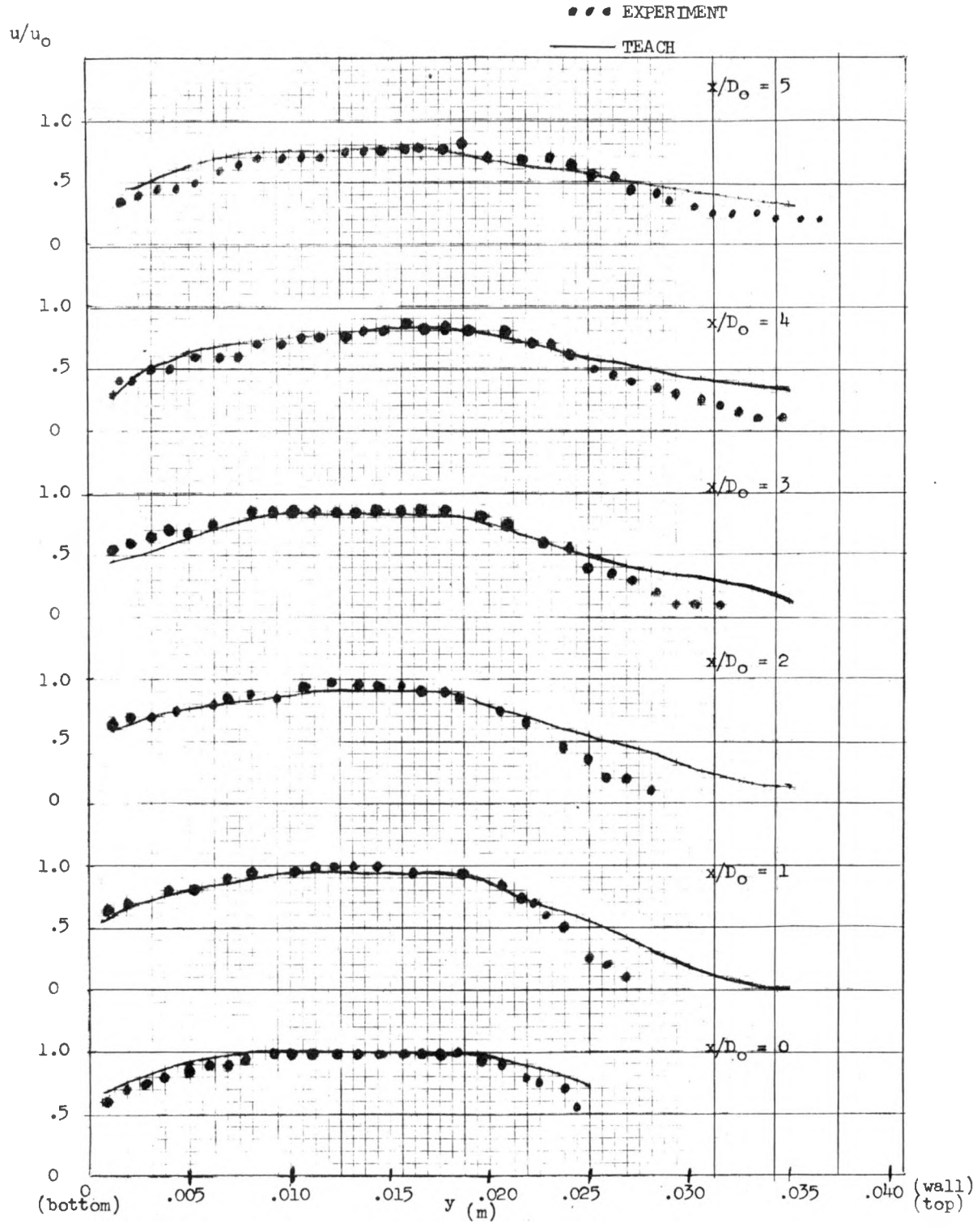

FIGURE 42. Velocity Profile, Single Step (Abbott and Kline). RE = 31,700.
KS-76206

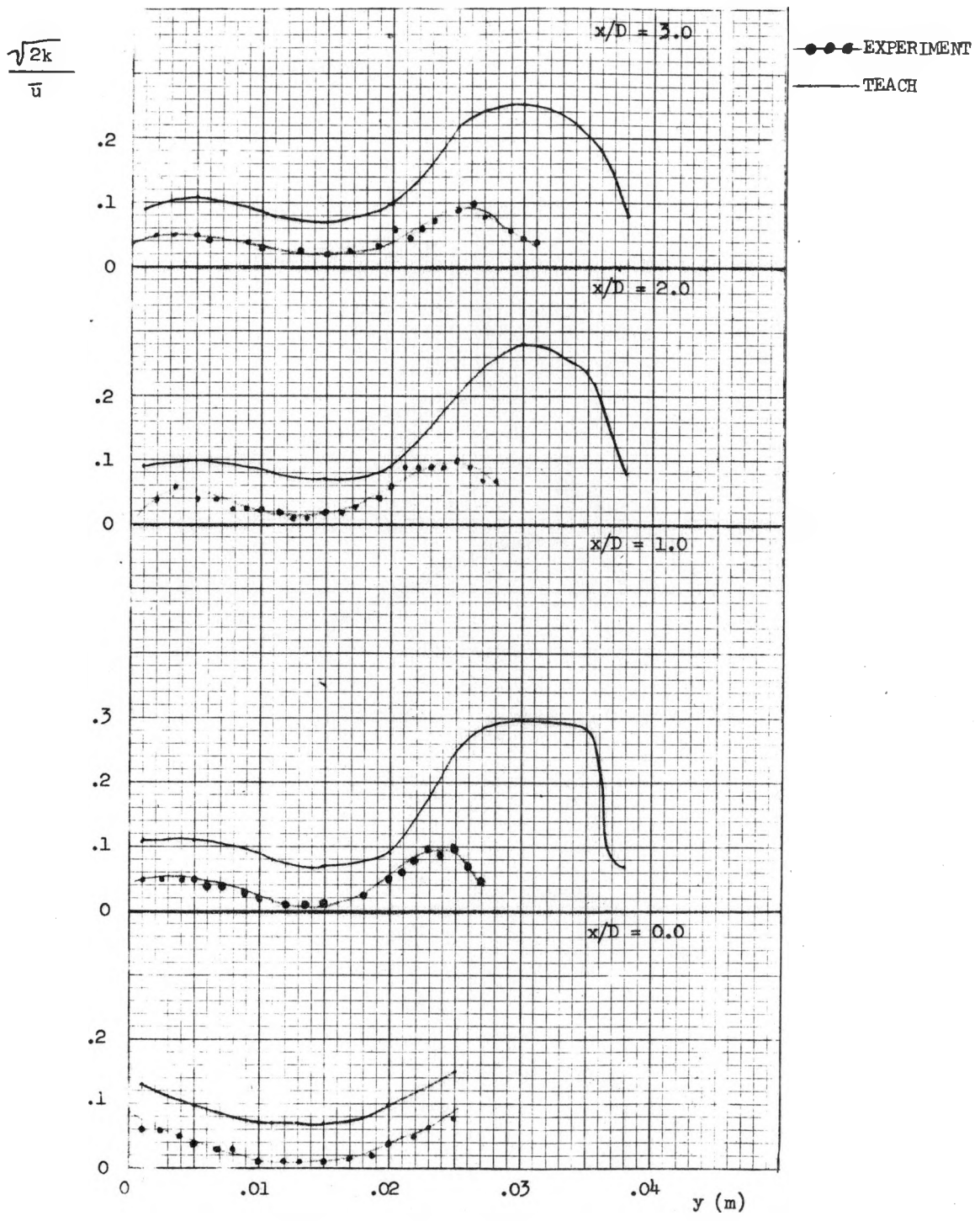

FIGURE 43. Turbulent Kinetic Energy, Single Step (Abbott and Kline). RE = 31,700.

KS-76207

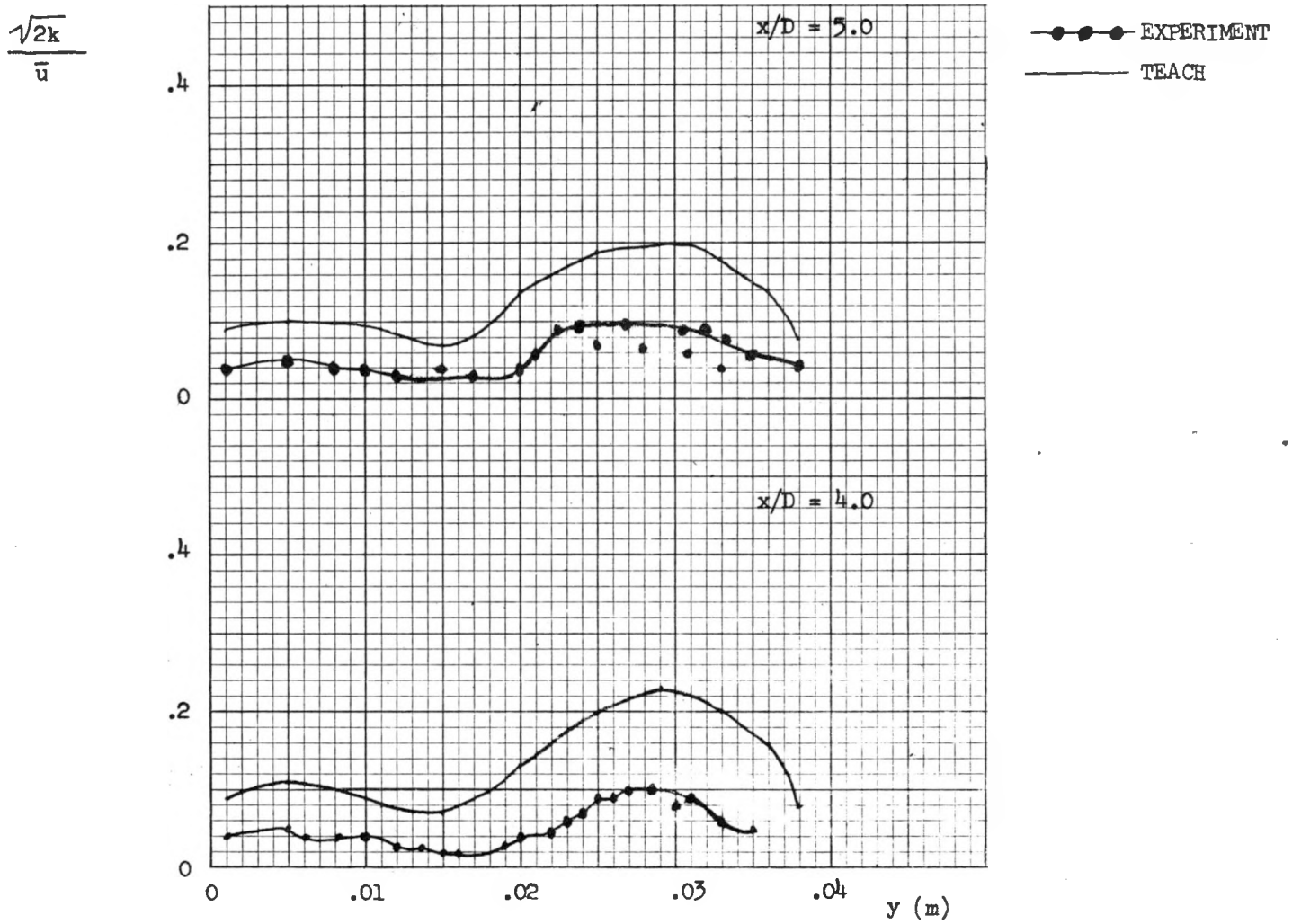

FIGURE 44. Turbulent Kinetic Energy, Single Step (Abbott and Kline). RE = 31,700.
KS-76208

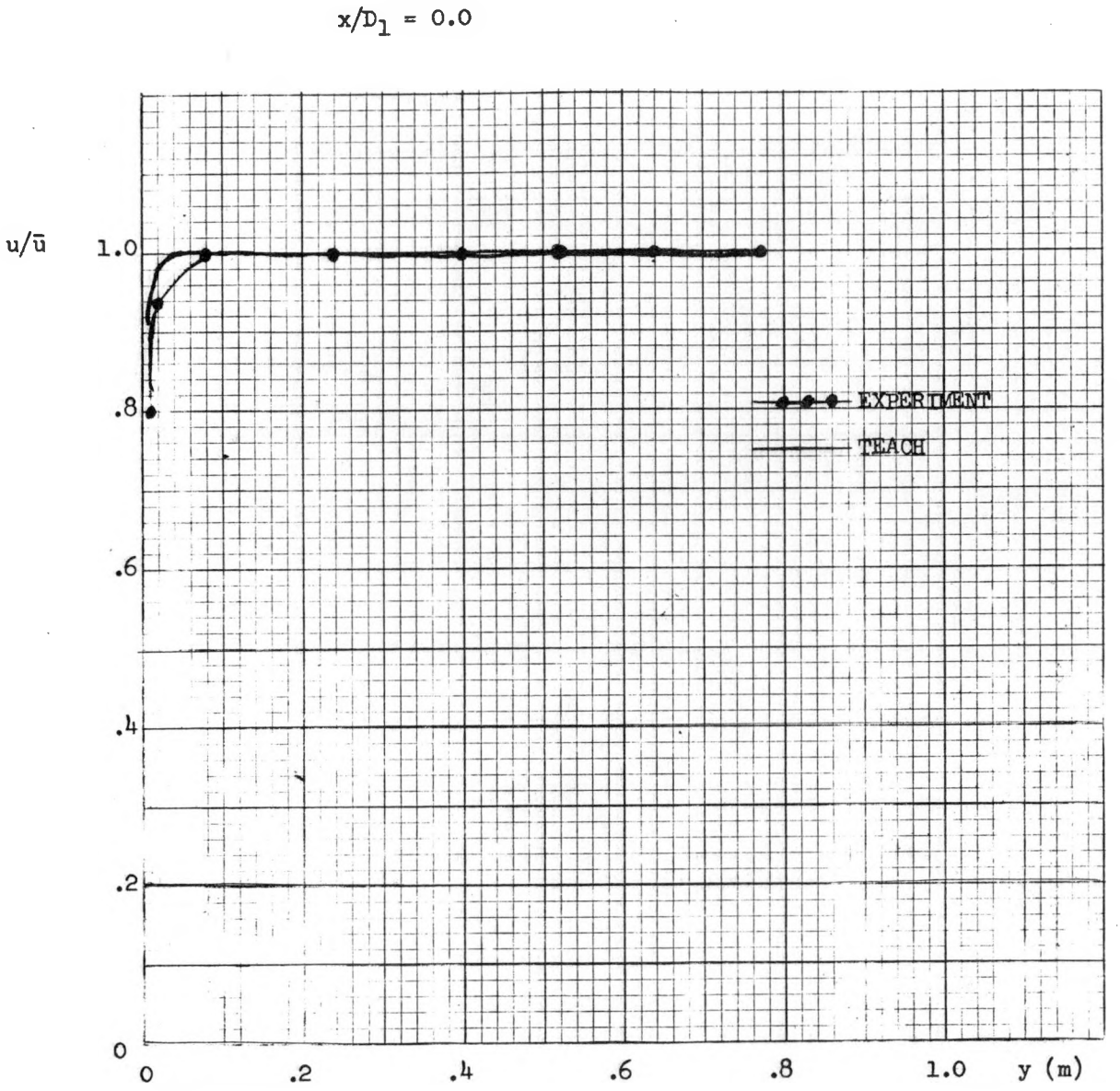

FIGURE 45. Velocity Profile (Hsu). RE = 501,000.
KS-76209

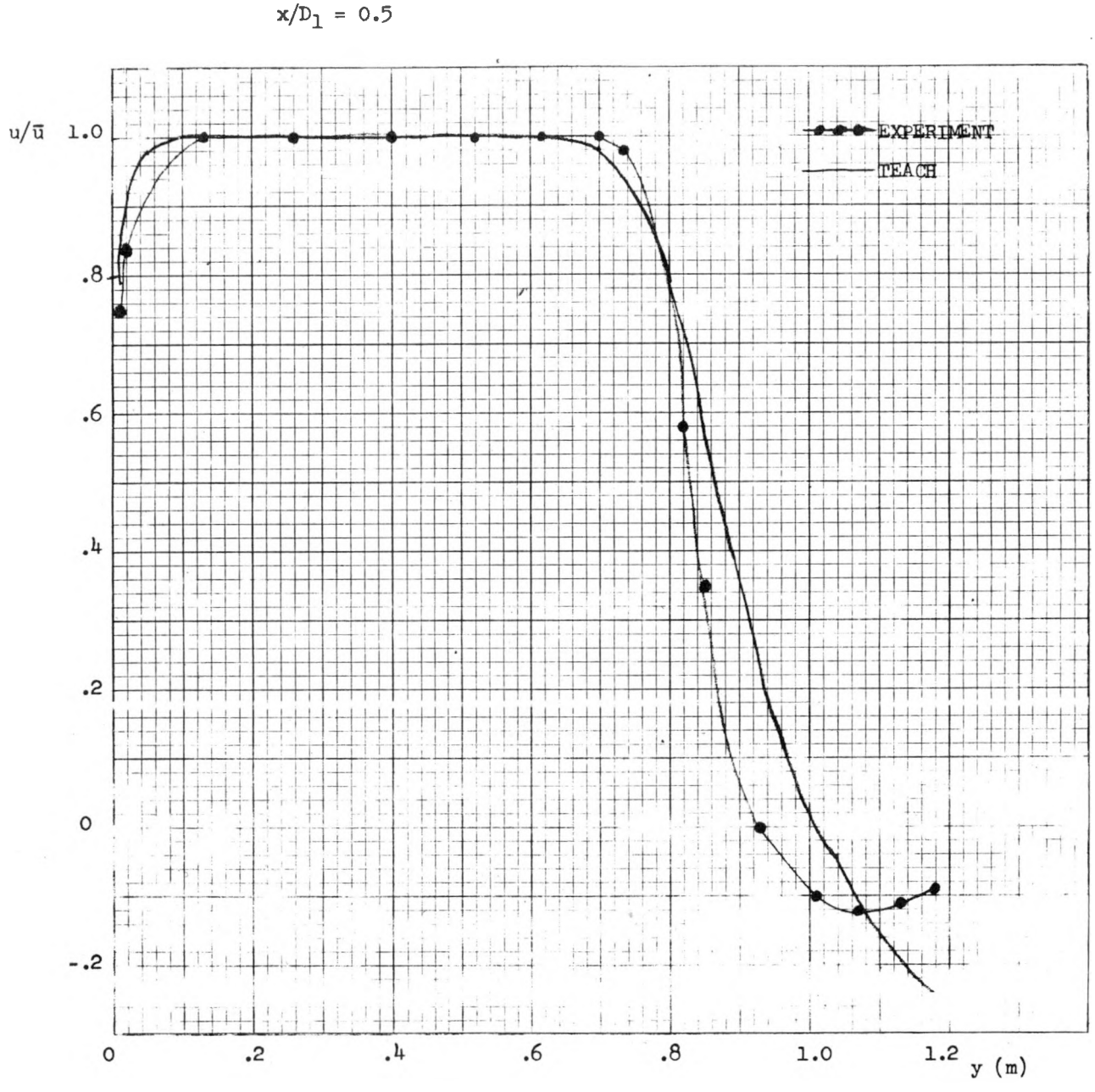

FIGURE 46. Velocity Profile (Hsu). RE = 501,000.
KS-76210

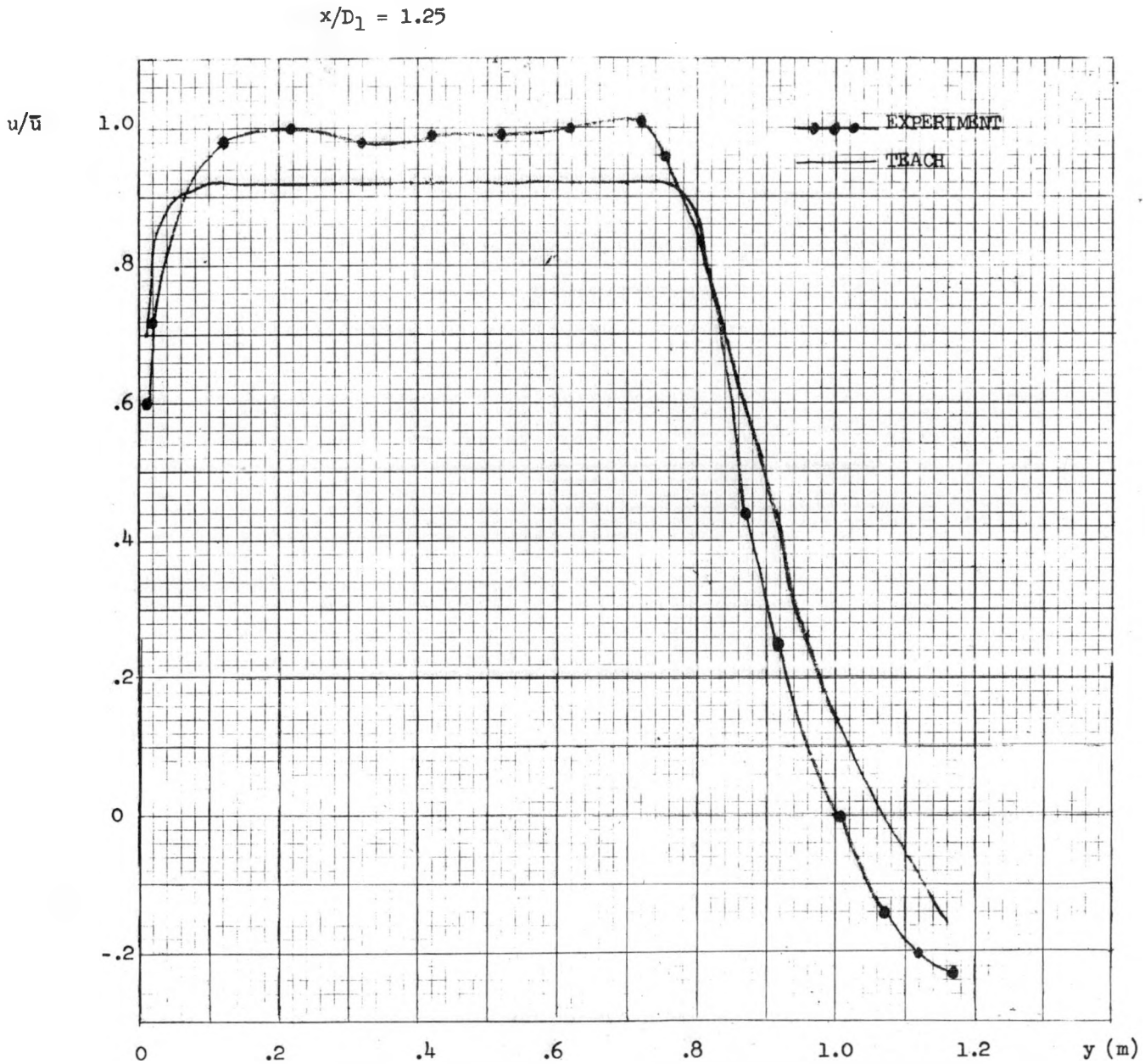

FIGURE 47. Velocity Profile (Hsu). RE = 501,000.
KS-76211

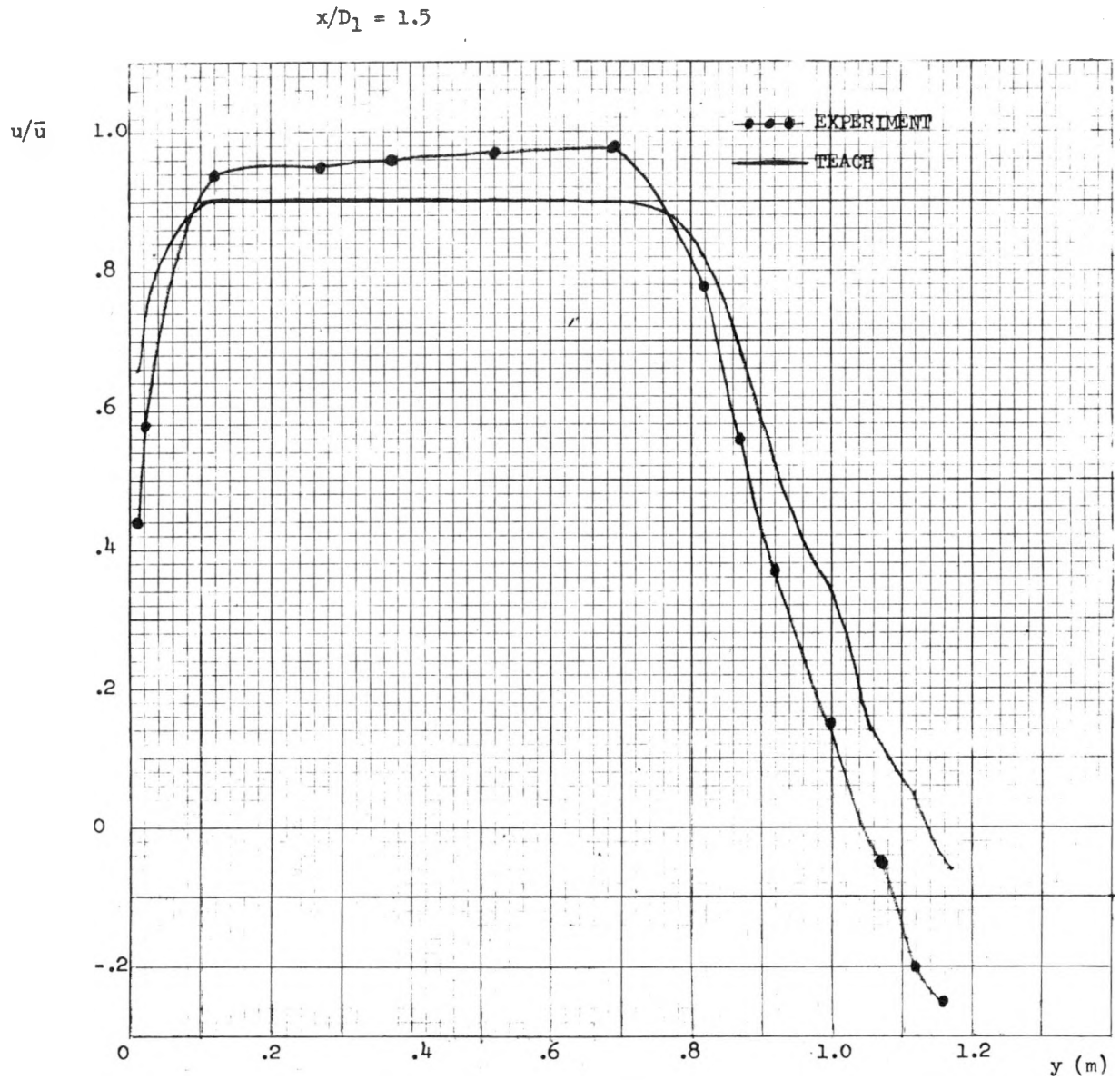

FIGURE 48. Velocity Profile (Hsu). RE = 501,000.
KS-76212

$x/D_1 = 2.0$

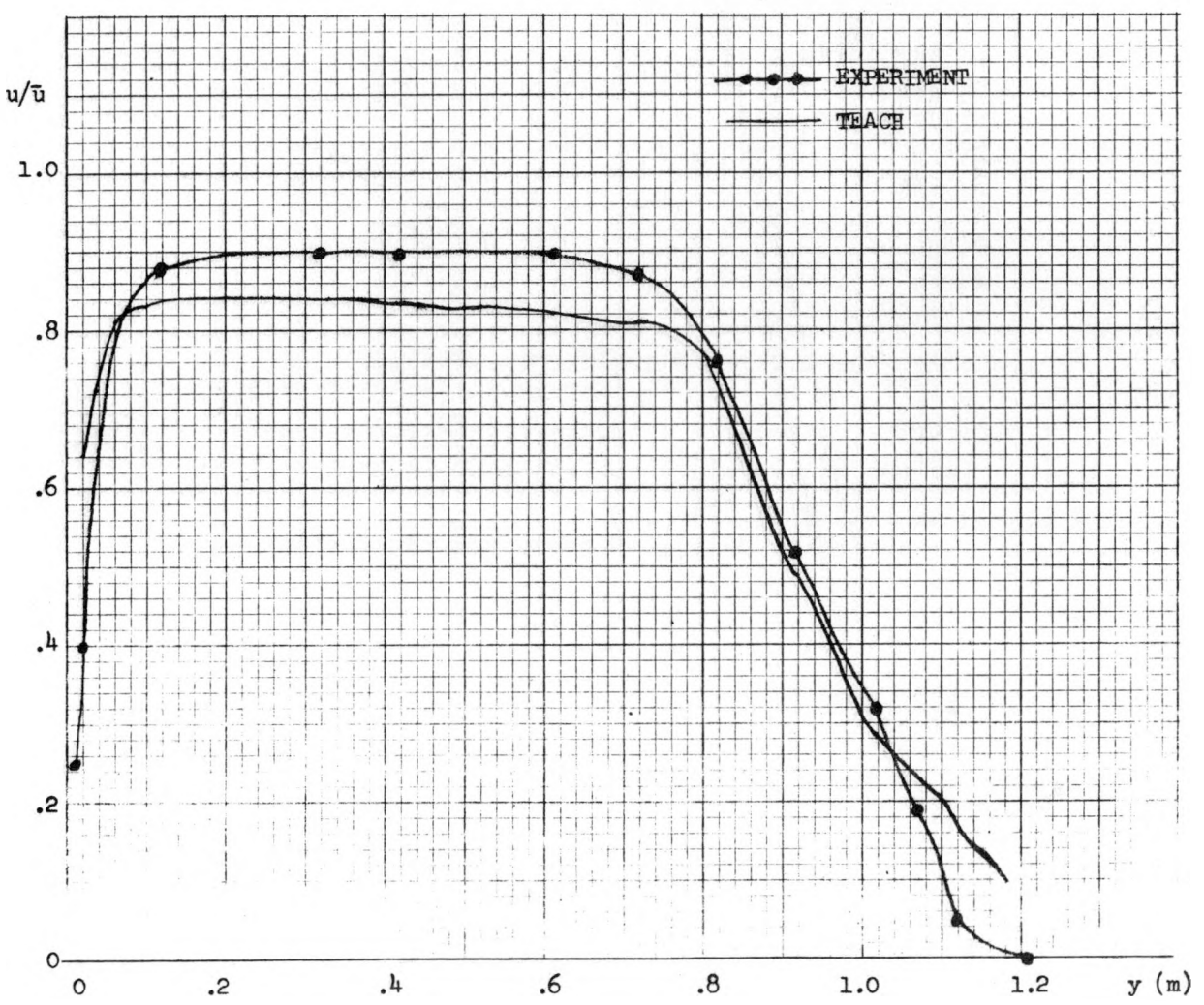

FIGURE 49. Velocity Profile (Hsu). RE = 501,000.
KS-76213

$x/D_1 = 2.5$

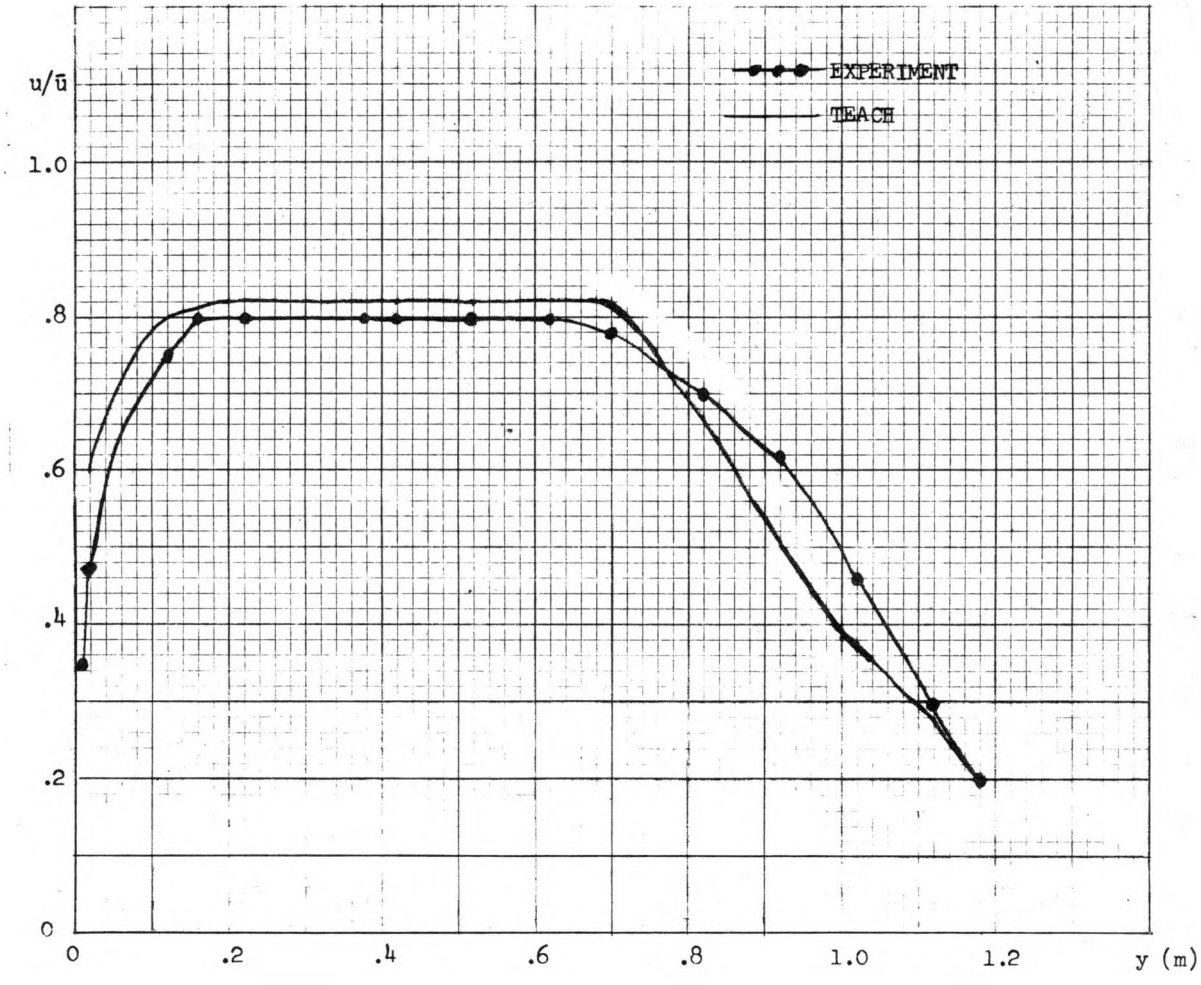

FIGURE 50. Velocity Profile (Hsu). RE = 501,000.
KS-76214

$x/D_1 = 3.0$

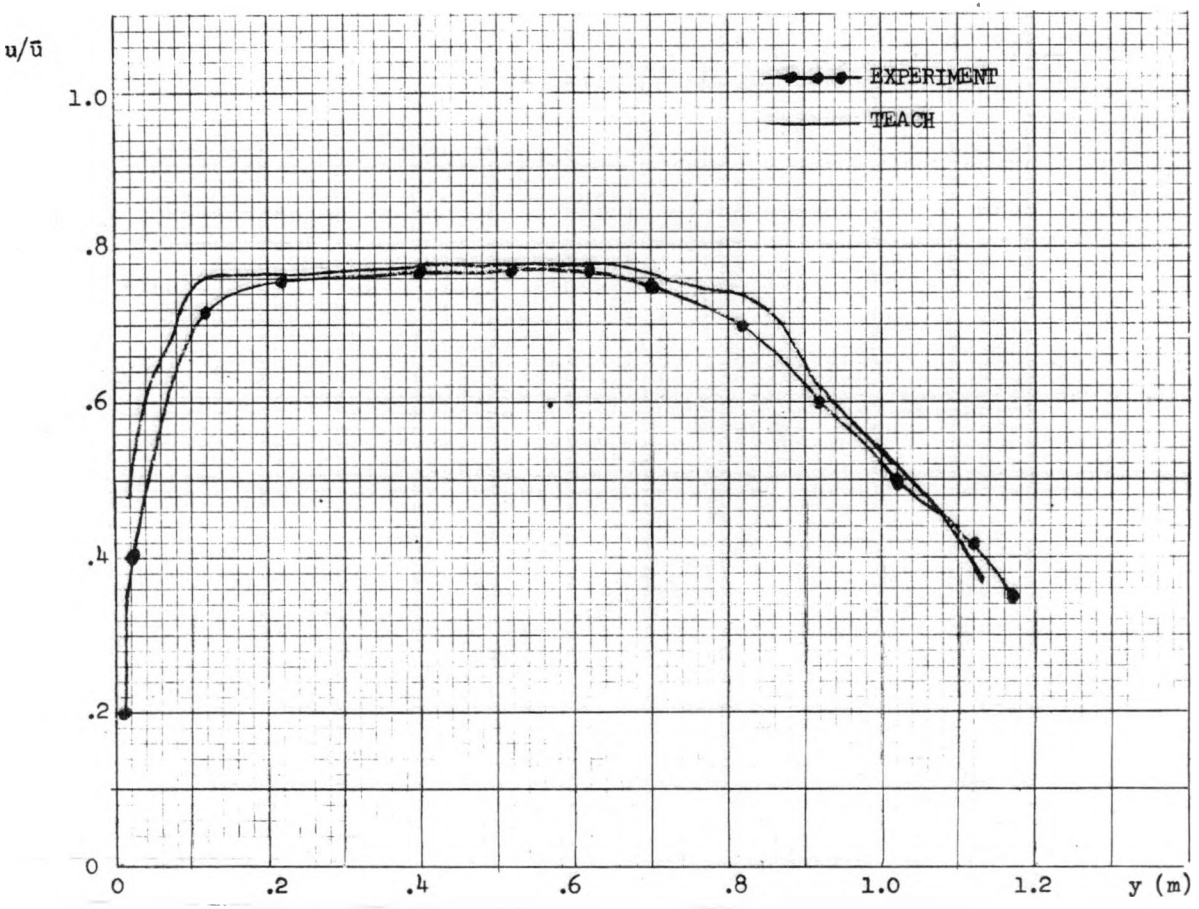

FIGURE 51. Velocity Profile (Hsu). RE = 501,000.
KS-76215

$x/D_1 = 3.5$

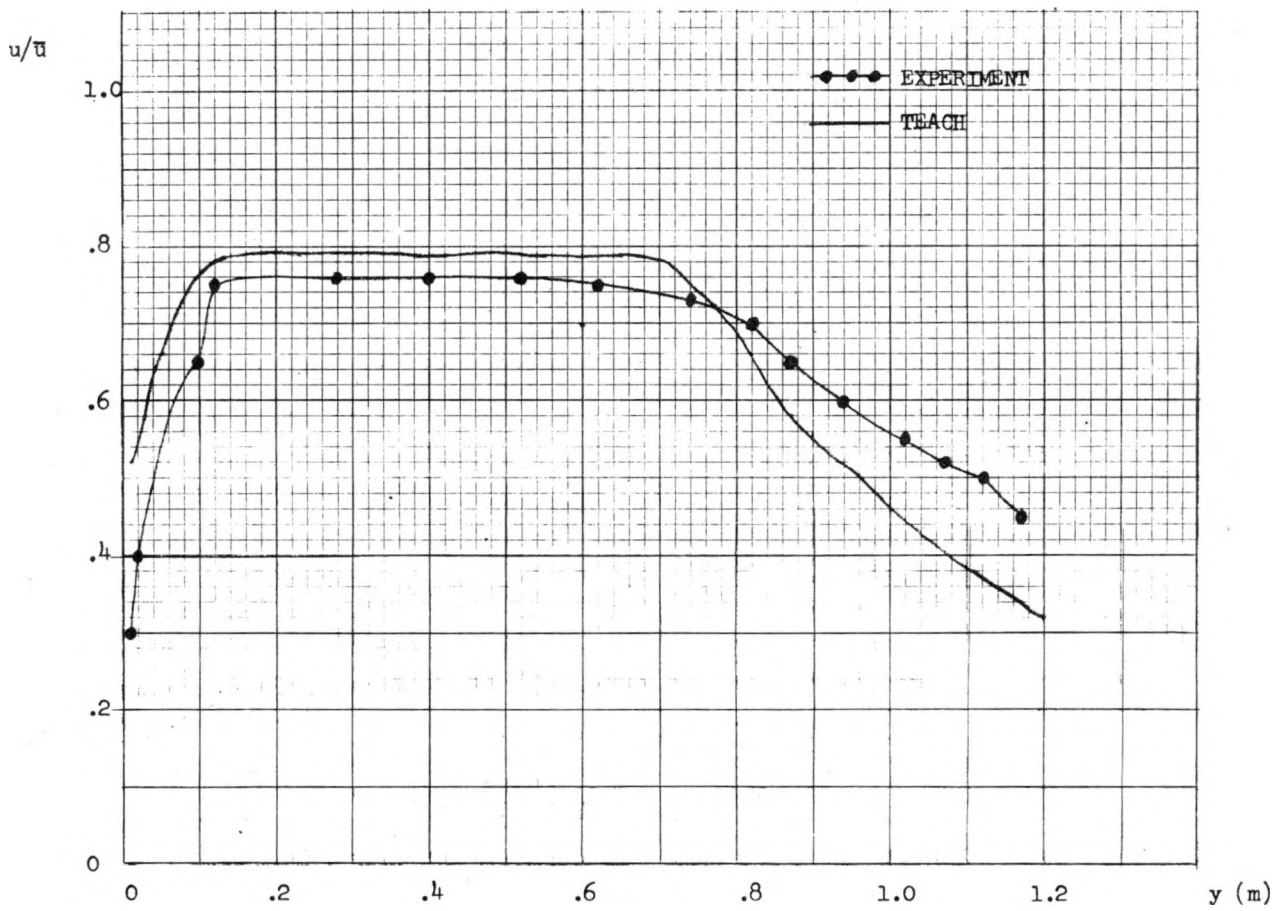

FIGURE 52. Velocity Profile (Hsu). RE = 501,000.
KS-76216

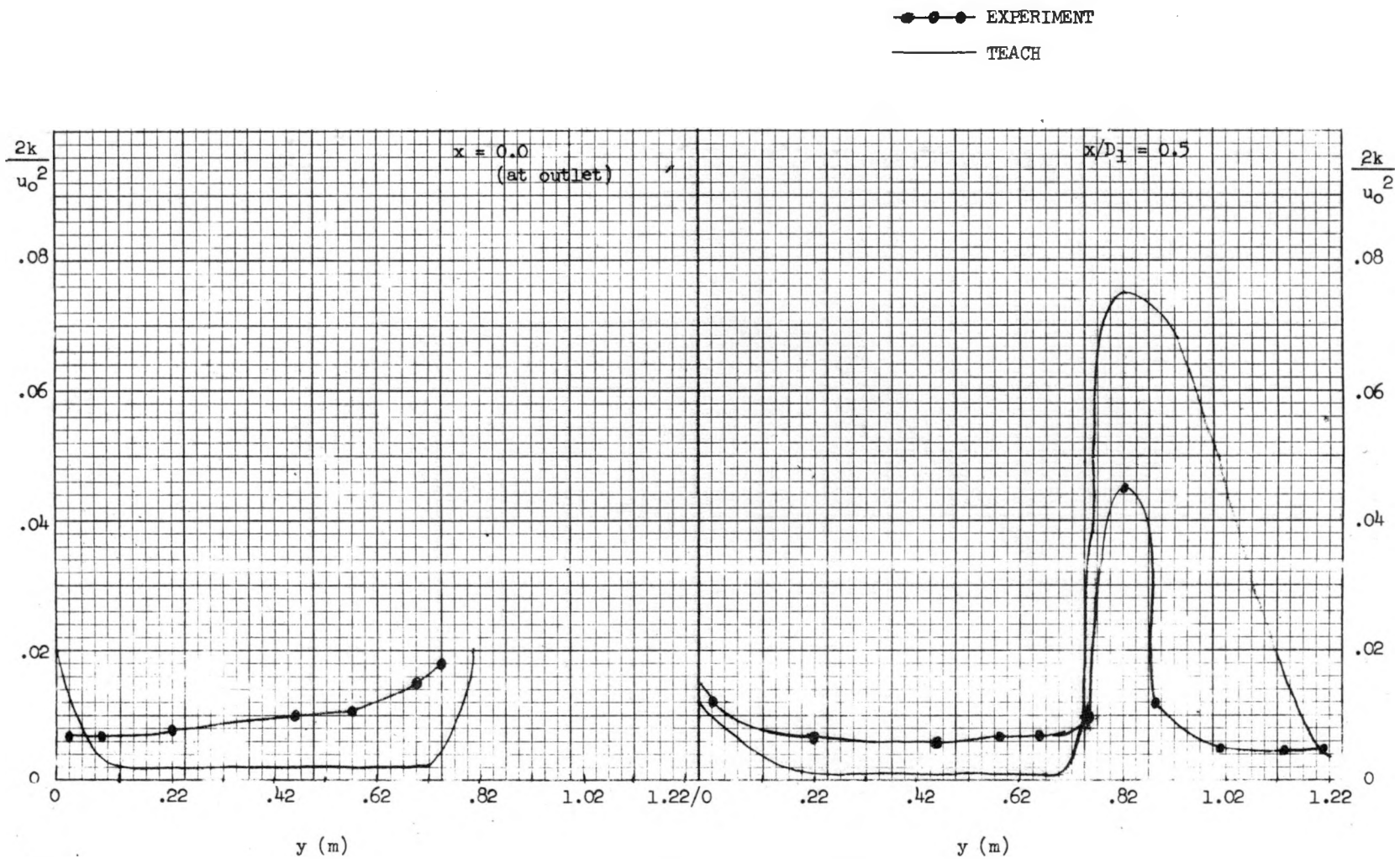

FIGURE 53. Turbulent Kinetic Energy (Hsu). RE = 501,000.
KS-76217

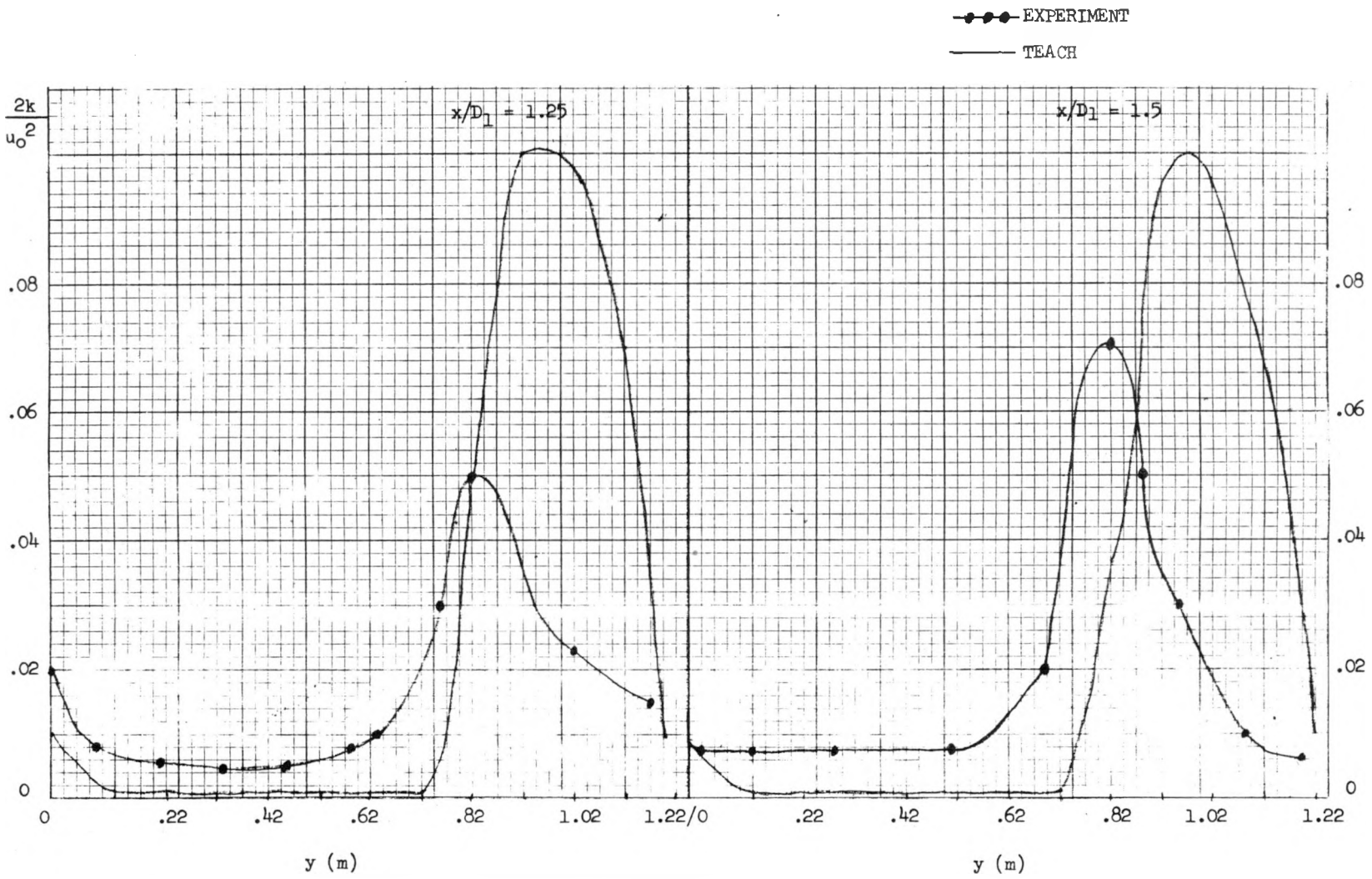

FIGURE 54. Turbulent Kinetic Energy (Hsu). RE = 501,000.
KS-76218

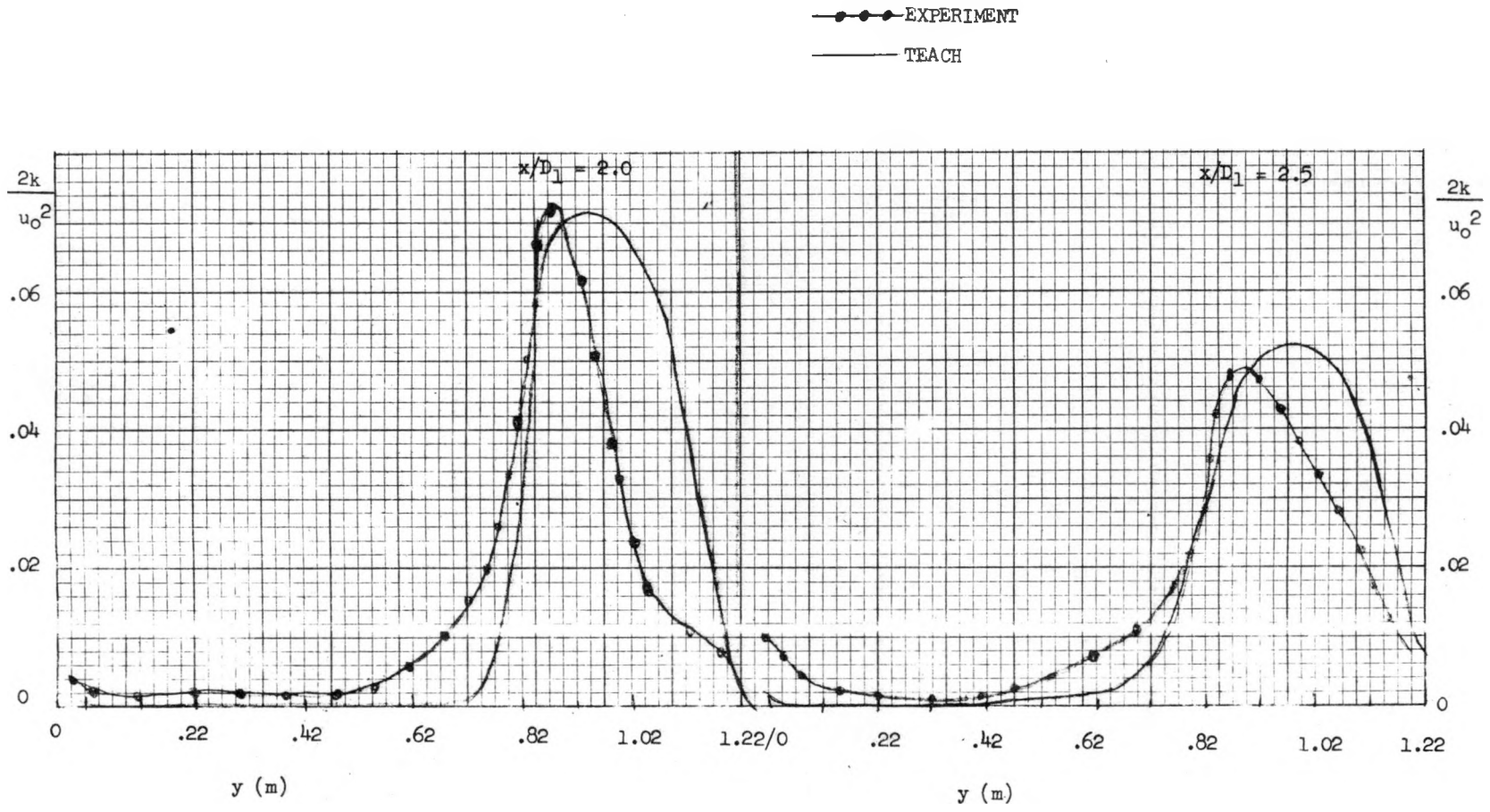

FIGURE 55. Turbulent Kinetic Energy (Hsu). RE = 501,000.
KS-76219

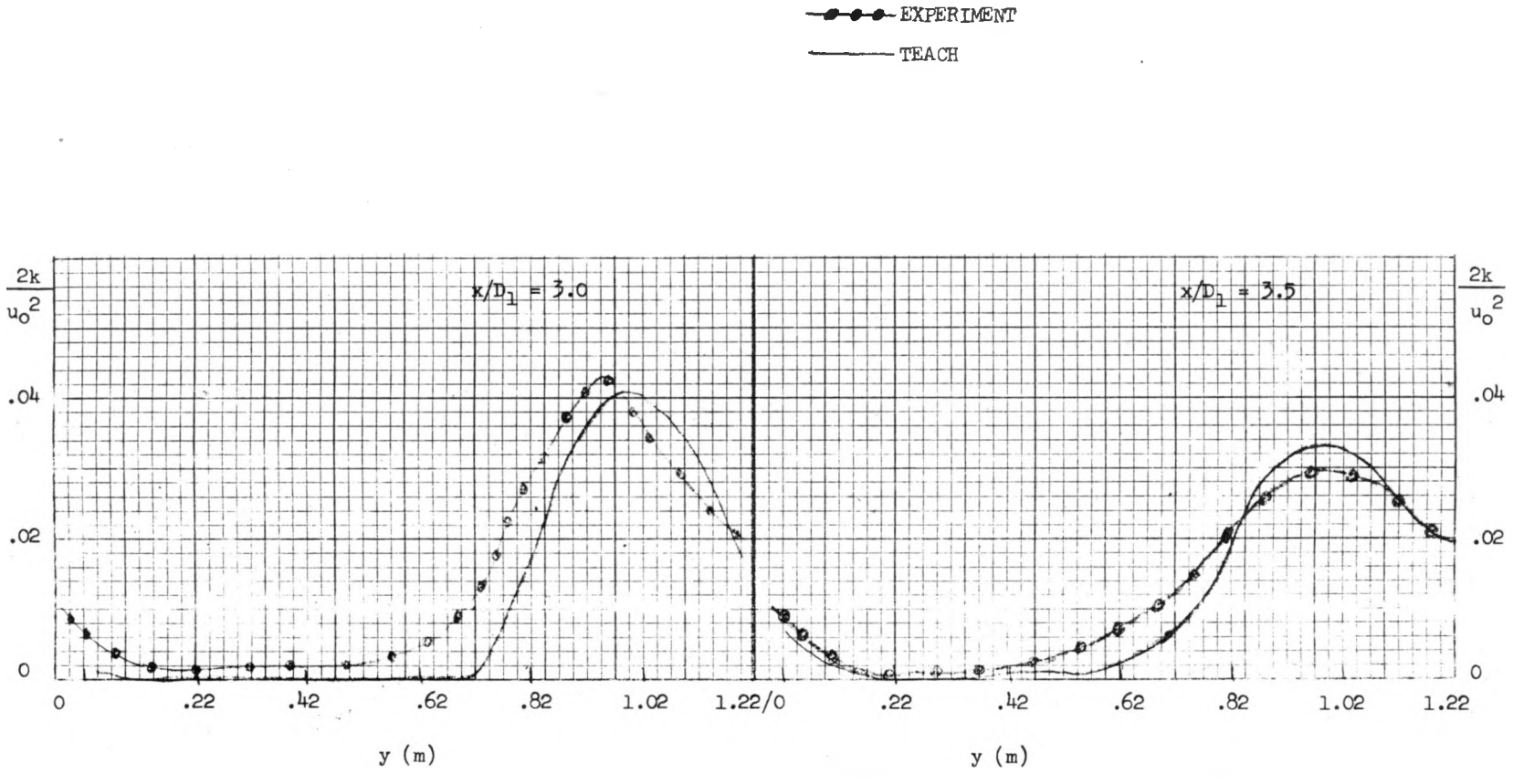

FIGURE 56. Turbulent Kinetic Energy (Hsu). RE = 501,000.
KS-76220

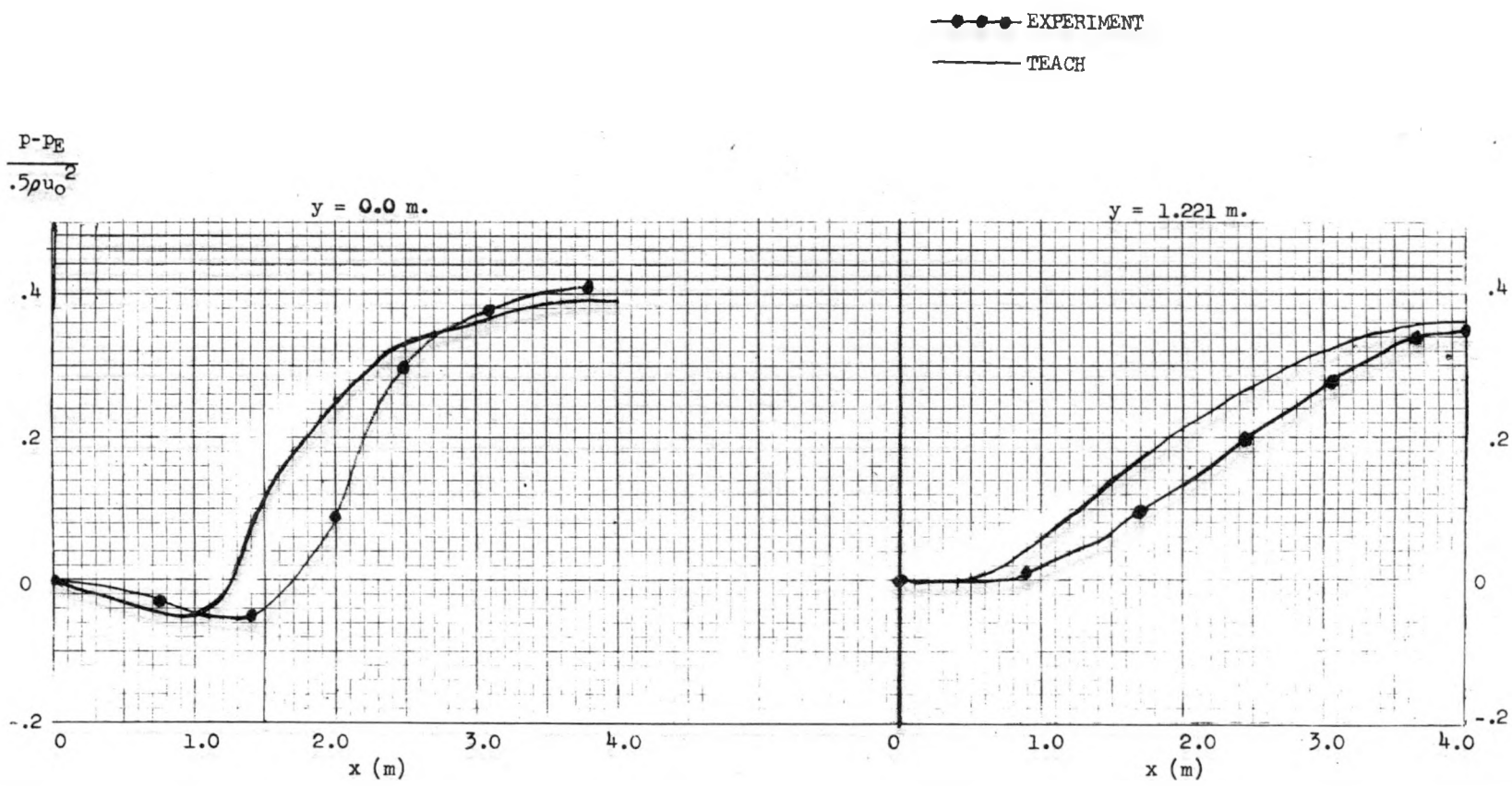

FIGURE 57. Mean Pressure Distribution (Hsu). RE = 501,000.
KS-76221

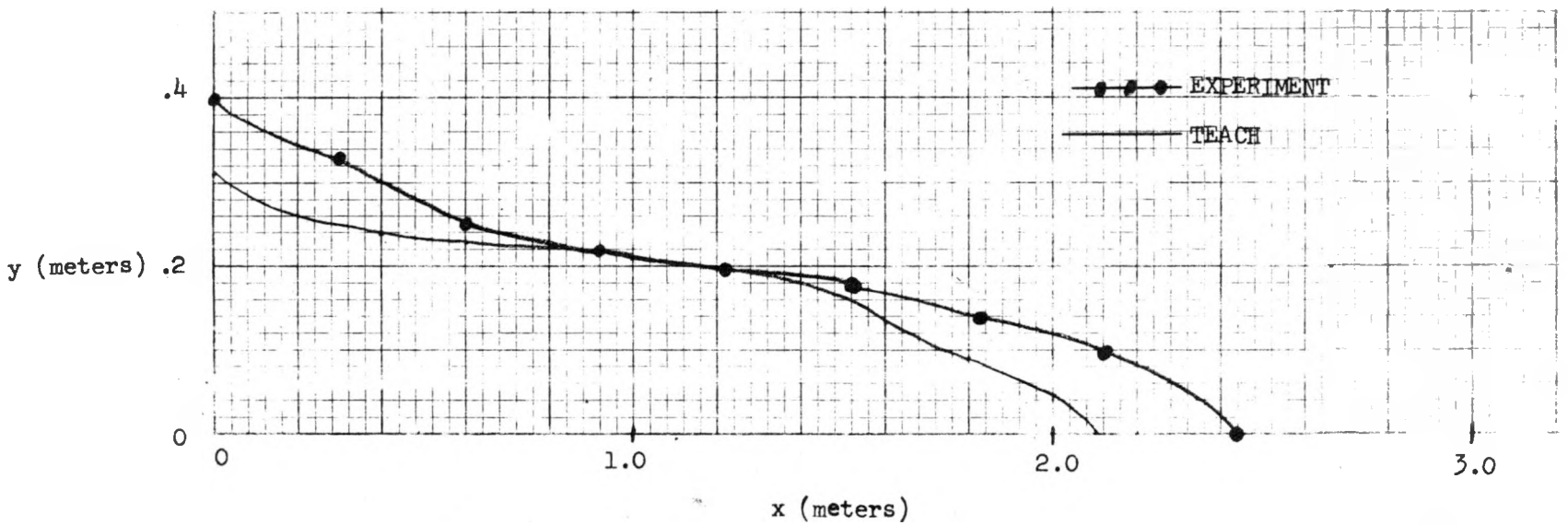

FIGURE 58. Contour of Zero u (Hsu). RE = 501,000.
KS-76222